STUDIA

UNIVERSITATIS BABEŞ-BOLYAI

CHEMIA

2

1989

CLUJ-NAPOCA

Anul XXXIV **1989**

STUDIA

UNIVERSITATIS BABEŞ-BOLYAI

CHEMIA

2

Redacţia: 3400 CLUJ-NAPOCA, str. M. Kogălniceanu, 1 ● Telefon 1 61 01

SUMAR — CONTENTS — INHALT

STUDIA UNIV. BABEŞ—BOLYAI, CHEMIA, XXXIV, 2, 1989

A COMPARATIVE STUDY OF SOME FATTY ACID MONOLAYERS AT THE AIR/WATER INTERFACE

EMIL CHIFU*, JÁNOS ZSAKÓ*, MARIA TOMOAIA-COTIŞEL* and AURORA MOCANU*

Received: 17 December 1988

A parallel study of the compression isotherms (surface pressure π, versus molecular area, A,) of three fatty acid monolayers, viz. oleic (OA), linoleic (LA) and stearic (SA) acids, recorded at the air/water interface is undertaken. The compressibility factor, $z = \pi A/kT$, being plotted against the reduced surface pressure, π/π_c, where π_c stands for collapse pressure, gives a unique curve by taking the metastable collapse pressure of liquid condensed SA monolayer (π_c = = 56.5 mN/m), this value being in accord with experimental results found with high compression speeds. Thereby is inferred the existence of corresponding states of fatty acid monolayers. A state equation proposed by us earlier is tested for the compression of the monolayers to 7 mN/m. It gives a very good description of the isotherms of OA and LA, and the values of the interaction parameters derived are in good agreement with theoretical expectations.

Introduction. In our previous paper [1], compression isotherms, i.e. surface pressure (π) versus mean molecular area (A) curves were reported for three fatty acids, viz. oleic (OA), linoleic (LA) and stearic (SA) acids, spread at the air/water interface. From these isotherms surface characteristics as collapse pressure (π_c), collapse molecular area (A_c), limiting molecular area (A_0) were derived.

The SA monolayer exhibits a condensed liquid to solid phase transition, marked by the intersection of two linear portions, i.e. by a sudden slope change corresponding to the transition point characterized by surface pressure (π_t) and molecular area (A_t).

In order to test different state equations, the compression isotherm of OA was used, and a new semiempirical equation was proposed to describe the experimental π versus A curves [2, 3].

In the present paper a comparative study of the compression isotherms of OA, LA and SA monolayers spread at the air/water interface on acidic aqueous solutions (pH = 2) is made, and a testing of the equation proposed is followed.

Results and discussion. To estimate deviations from perfect gas behaviour of expanded monolayers, expressed by the state equation [4]:

$$\pi A = kT \tag{1}$$

where k and T stand for Boltzmann's constant and absolute temperature, respectively, the plot of the two-dimensional 'compressibility factor' defined as:

$$z = \pi A/kT \tag{2}$$

* *University of Cluj-Napoca, Faculty of Chemical Technology, 3400 Cluj-Napoca, Romania*

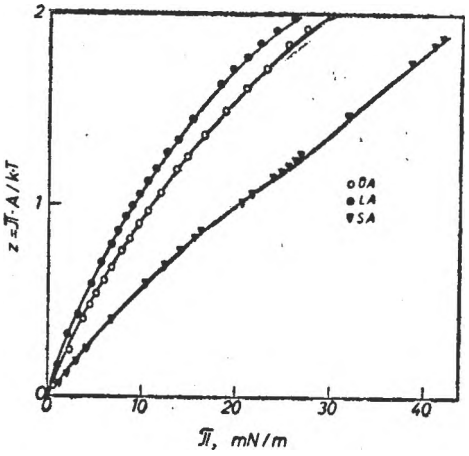

Fig. 1. Surface compressibility factor (z) of fatty acid monolayers as function of surface pressure (π) at the air/water (pH = 2) interface.

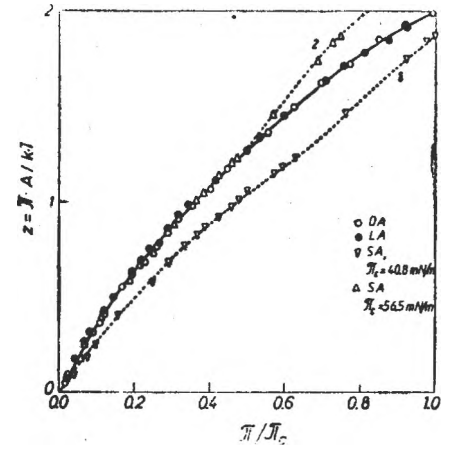

Fig. 2. Surface compressibility factor (z) as function of the „reduced" surface pressure (π/π_c).

versus π has been performed by using our earlier experimental data [1]. Results are visualized in Fig. 1. As seen from this figure, for all the studied acids, at very low π values, z is nearly equal to zero, indicating very large deviations from the perfect gas behaviour ($z = 1$), even at the spreading of the film ($A < 1.00$ nm²/molecule). The curve of SA consists of two distinct portions, the first one corresponding to the liquid expanded (LE) and liquid condensed (LC) states, the second one to the solid (S) state of the monolayer. The curves of OA and of LA are uniform, since these substances remain in the LE state up to the collapse. The curves of unsaturated fatty acids are of similar shape, and they are displayed in the same order as their collapse pressure (π_c) increases. This is obvious on the basis of the surface characteristics of the fatty acids studied (Table 1). This order suggests the idea to plot z versus a kind of "reduced surface pressure", representing the ratio π/π_c. Results are presented in Fig. 2. In this plot the experimental points for both OA and LA are situated on the same full line curve, indicating the existence of a sort of "corresponding states" also in the case of monolayers, at least with uncharged fatty acid films. Presumably, the use of reduced surface pressure entails elimination of the effect of the air phase hydrophobic interactions, and the common "reduced" compressibility curve reflects the interaction of the polar headgroups with each other and with the aqueous subphase, interactions which are the same for all surfactants studied. This hypothesis seems to

Table 1

Surface characteristics of the uncharged fatty acids studied

Surfactant	State	A_0 nm²	A_c nm²	π_c mN/m	ESP mN/m
SA	S	0.20	0.18	40.8	—
	LC	0.255	—	—	—
OA	LE	0.41	0.27	30	33
LA	LE	0.48	0.31	26	29

N.B.: A_0 and A_c are given in nm²/molecule.

be reasonable because the collapse pressure used for the calculation of the reduced surface pressure is mainly determined just by the hydrophobic interactions between the hydrocarbon chains.

In the case of SA, dashed line curve 1 in Fig. 2, has been obtained by using $\pi_c = 40.8$ mN/m, representing the experimental collapse pressure of the solid film. The use of this π_c value shifts the curve of SA nearer to the common curve of OA and LA, as compared to the case in Fig. 1, but it cannot lead to their superposition. This might be a consequence of different state of the SA monolayer as to the unsaturated fatty acids. It is worth mentioning that the π_c value of OA and LA is a little lower than the equilibrium spreading pressure (ESP) of these fatty acids (Table 1), while with SA the experimental π_c value is much greater than the ESP [4, p. 219]. As shown earlier, we presume π_c to characterize a metastable thermodynamic equilibrium between the monolayer phase and the "freshly collapsed" bulk phase, preserving some structural characteristics of the monolayer, i.e. being a mesomorphous state [1]. According to our hypothesis, in the case of a given surfactant the higher the order in this mesomorphous state, the less will be the experimental π_c. Consequently, the π_c of SA in the LC state may be expected to be higher than its π_c value in the S state. This seems to be in agreement with the literature data concerning the influence of compression speed upon collapse pressure. Thus, at very low compression speeds, when the formation of highly ordered mesomorphous phase can be expected, the π_c of SA has been found to have very low values, of about 13 mN/m [5]. At higher compression speeds, values of 40 mN/m [4, p. 187], 44 mN/m [4, p. 220] and of 42 mN/m [6] have been reported, near to the above mentioned value ($\pi_c = 40.8$ mN/m), which was found to be highly reproducible in a relatively large compression speed range [1]. By using very high compression speeds, the π_c value of SA reaches even 60 mN/m [7]. Presumably, the use of high compression speeds allows to avoid the LC to S phase transition, and leads to the collapse of the LC monolayer, similarly to rapid heating of rhombous sulphur, which leads to its melting, thus avoiding rhombous sulphur to monoclinic sulphur phase transition.

On the basis of the above ideas, an attempt was made to calculate the hypothetical π_c value of the liquid SA monolayer ensuring the superposition of compressibility factor curves of the three fatty acids in a z versus π/π_c plot. Our calculations showed that the first portion of curve 1 (Fig. 2) is perfectly superposed onto the full line curve of OA and LA, when taking $\pi_c = 56.5$ mN/m for the hypothetical collapse pressure of the liquid condensed SA monolayer thought to be metastable at $\pi > 26$ mN/m $= \pi_t$, corresponding to the LC → S phase transition. As can be seen in Fig. 2, the experimental points of SA, processed in the way shown above, are situated on the common reduced curve, up to the LC → S phase transition. Further on, they exhibit an increasing deviation (dashed line, curve 2).

Consequently, the existence of corresponding states seems to be real in the case of fatty acid monolayers in their fluid (gaseous and both LE and LC) states.

Concerning the hypothetical $\pi_c = 56.5$ mN/m value for the liquid SA film, it is in rather good agreement with the above cited literature data [7]. Our

experiments showed that, by using compression speeds of 0.16 nm²/molecule min, the well reproducible π_c value reaches 56 mN/m, and the isotherm exhibits no phase transition. These results are in very good agreement with our hypothesis.

State equations of the fatty acids studied. In our previous papers a new semiempirical state equation was derived and tested on OA and LA monolayers [2, 3]. The equation was obtained from the equality of the chemical potential of water in the subphase and in the monolayer, by presuming the latter to be a regular solution or surfactant molecules (head groups only) in water and by using a semiempirical expression for contribution of the hydrocarbon chains of the surfactant to the surface internal pressure. The equation is of the following form:

$$\pi = -\left(\frac{\alpha}{A^{3/2}} + \frac{kT}{A_1}\ln x_1 + \frac{\beta_{12}}{A_1}x_2^2\right) = -\pi_0 + \pi_k + \pi_h \tag{3}$$

In this expression π_k stands for the kinetic surface pressure, corresponding to a monolayer behaving as a perfect solution, without intermolecular interaction; π_h stands for contribution of the interaction of the water molecules and polar head groups of the fatty acids in the monolayer (thought to be a regular solution) to the surface pressure; $\pi_0 = \alpha/A^{3/2} = -\pi_{ch}$, where π_{ch} represents the cohesive surface pressure due to the chain-chain hydrophobic interactions (characterized by the interaction parameter α) in the air phase part of the monolayer. Since in the expanded monolayer these interactions lead to intermolecular attraction, α must have positive values. The interaction parameter, β_{12}, is defined as

$$\beta_{12} = z\left(\varepsilon_{12} - \frac{\varepsilon_{11} + \varepsilon_{hh}}{2}\right)$$

where z stands for the number of contacts of a molecule in the monolayer with neighbouring molecules, ε_{11}, ε_{hh} and ε_{12} stand for potential energy corresponding to the water/water, head group/head group and water/head group interactions, in the monolayer, respectively. Taking into account the structure of the water molecule and of head group COOH, negative values may be expected for β_{12}. In Eq. (3), x_1 and x_2 are the molar fractions of water and of the polar head groups, in the monolayer solution, respectively. A_1 means the cross-section area of the water molecules in the monolayer, π, k and T having their meaning given above. The molar fraction x_2 can be calculated as [8]:

$$x_2 = \frac{A_1}{A - A_2 + A_1} \tag{4}$$

where A_2 stands for the cross-sectional area of the polar head group; A_1 has been approximated as $A_1 = (V^{2/3})/N_A \cong 0.1$ nm²/molecule, where V and N_A stand for the molar volume of liquid water and for Avogadro's constant, respectively.

For the cross-sectional area of the polar head group, in a first approximation, $A_2 = 0.2$ nm²/molecule was taken [2]. By considering A_2 as adjusted parameter, $A_2 = 0.225$ nm²/molecule was obtained [3] from the compression isotherm of OA. In the latter approximation, Eq. (3) contains three adjusted parameters,

viz. α, β_{12} and A_2 (see Eq. (4)). These parameters can be derived from the experimental π versus A curves by means of a triple minimization procedure. For this purpose the theoretical π values are calculated for all experimental A values, by taking a set of α, β_{12} and A_2 values, as well as the standard deviation Δ of the experimental π values from the theoretical ones. Performing a systematic variation of α (β_{12} and A_2 being mentained at a constant value each), an α value is obtained, ensuring the minimum standard deviation, Δ_m. These calculations are repeated for different β_{12} values and the same A_2 value. This double minimization leads to $(\beta_{12})_m$ and a corresponding α_{mm} value, ensuring the standard deviation Δ_{mm}, the latter one representing the minimum of Δ_m values obtained for different β_{12} values presumed. In the final stage all these calculations are repeated for different A_2 values. This triple minimization leads to $(A_2)_m$, $(\beta_{12})_{mm}$ and α_{mmm}, which are taken for the most reasonable values of A_2, β_{12} and α, respectively, allowing the best description of the experimental curve by means of Eq. (3), corresponding to a standard deviation Δ_{mmm}.

This procedure was used for OA, leading to the results given in Table 2 where A_2, α, β_{12} and Δ stand for $(A_2)_m$, α_{mmm}, $\beta_{12})_{mm}$ and Δ_{mmm}, respectively). The compression isotherms of LA and SA were also processed in the above shown way, by using all experimental points up to $\pi = 7$ mN/m, exactly as with OA. The parameters of Eq. (3), derived from the experimental compression isotherms of the fatty acid monolayers by means of triple minization of Δ, are presented in Table 2. The last stage of the procedure used is visualized in Fig. 3, giving the Δ_{mm} value as function of the A_2 value presumed. The arrows indicate the minima of the curves, corresponding to the best A_2 values, presented in Table 2.

Inspection of Table 2 shows that Eq. (3) describes very well the compression isotherms, especially with unsaturated fatty acids; and for these the standard deviation Δ is less than the experimental errors in π measurements.

The A_2 values derived seem to be quite realistic. Practically, they are situated between the A_0 values of SA in its S and LC states, respectively, (see Table 1) and are much lower than the A_0 values of both OA and LA, the latter ones being

Table 2

Parameters of the state equation (3) derived for the fatty acids studied ($\pi \leqslant 7$ mN/m)

Surfactant	A_2 nm²/molec.	$\alpha \cdot 10^{20}$ Nm²	$\beta_{12} \cdot 10^{20}$ Nm	Δ mN/m
OA	0.225	7.714	−1.507	0.087
LA	0.265	6.932	−1.150	0.073
SA	0.207	2.593	+0.513	0.150

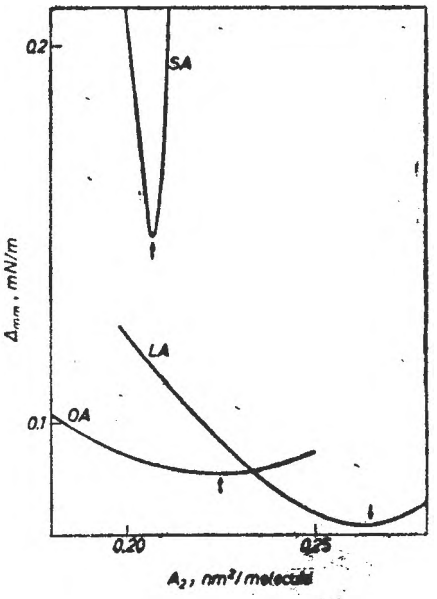

Fig. 3. Deriving of A_2 value by triple minimization.

determined by the geometry of the hydrocarbon chains. Therefore, A_2 characterizes indeed the carboxyl head group. The increase of A_2 in the order SA < OA < LA is not surprising, since at a given π value the monolayers have their molecular areas increasing in the same order [1], which might entail a modification in the head group conformation. Due to the lateral constraints at the compression of the monolayer, near to the collapse of the SA monolayer, the COOH groups are forced to readily accomodate beneath the hydrocarbon chains, i.e. to adopt a vertical orientation corresponding to a cross-sectional area less than 0.18 nm²/molecule. At lower π values, the COOH group may also adopt a horizontal orientation. In this conformation, its area necessity is grater than 0.3 nm²/molecule [1]. Consequently, one may presume the part of the vertical and horizontal orientations to vary, depending on the area available in the monolayer. The A_2 value can be thought to represent the mean value of the cross-sectional area of the carboxyl group; therefore, its variation between 0,18 and 0.3 nm²/molecule is in good agreement with our results.

Concerning the β_{12} values obtained, they seem to be quite reasonable in the case of OA and LA, in both cases expressing strong attraction between the COOH group and water molecules, although their numerical values differ from each other. Anyhow, a certain difference may be expected, since the intermolecular interactions depend also on the conformation of the head group and even an increase of the absolute value seems to be reasonable if the vertical orientation is prevalent, since in the latter case the H- bond formation with subphase water molecules is favoured. This might explain the higher negative valve of β_{12} in the case of OA, as compared to LA. Reversely, the β_{12} value obtained for SA is quite unrealistic, expressing a repulsion which cannot occur.

The α values obtained for OA and A are also very reasonable. They express strong hydrophobic interactions between the hydrocarbon chains, these interactions being stronger with OA as compared to LA, in good agreement with the higher collapse pressure of the former as compared to the latter. The α value derived for SA is unrealistic, again. Although it corresponds to the intermolecular attraction, its value is much too low, taking into account that π_c of SA is even greater than that of OA.

All these results show that Eq. (3) gives a very good description of the π versus A isotherms of OA and LA, up to $\pi = 7$ mN/m, yielding very reasonable A_2, β_{12} and α values. Reversely, in the case of SA, the description is rather poor, Δ depassing experimental errors, and although Eq. (3) yields a reasonable A_2 value, the interaction parameters derived are rather unrealistic.

One may conclude that Eq. (3) is a very good state equation for liqiud expanded monolayers of fatty acids, but it cannot be applied to liquid condensed monolayers of saturated fatty acids.

REFERENCES

1. M. Tomoaia-Cotişel, J. Zsakó, A. Mocanu, M. Lupea, and E. Chifu, *J. Colloid-Interface Sci.*, **117**, 464 (1987).
2. M. Tomoaia-Cotişel, J. Zsakó and E. Chifu, *Studia Univ. Babeş—Bolyai, Chem* **33**, (2), 54 (1988).

3. J. Zsakó, M. Tomoaia-Cotişel, A. Mocanu, and E. Chifu, unpublished results.
4. G. L. Gaines, Jr., „Insoluble Monolayers at Liquid-Gas Interfaces", Interscience, New York, 1966, p. 159.
5. E. F. Porter, *J. Amer. Chem. Soc.*, **59**, 1883 (1937).
6. H. E. Ries, Jr., and H. Swift, *J. Colloid Interface Sci.*, **64**, 111 (1978).
7. P. Joos, *Bull. Soc. Chim. Belge* **80**, 277 (1971).
8. Y. C. Lim and J. C. Berg, *J. Colloid Interface Sci.*, **51**, 162 (1975).

STUDIA UNIV. BABEŞ—BOLYAI, CHEMIA, XXXIV, 2, 1989

ON THE DIOXIMINE COMPLEXES OF TRANSITION METALS

LXXIX[1]. Some New Chelates of Iron with Nioxime and Trioxime

JÁNOS ZSAKÓ*, CSABA VÁRHELYI* and TEODÓRA SÁRVÁRI*

Received: 28 November, 1988

The formation of some iron(II) and (III) complexes with nioxime (1,2-cyclohexane dione dioxime) and trioxime (1.2.3-cyclohexane trione trioxime) was studied on spectrophotometric way. Their composition was established using Job's method. A number of nine complexes of the type $Fe(Niox.H)_3(Am)_3$ (Am — organic amines and tertiary phosphines) have been isolated and characterized by i.r. and electronic spectra. The trioxime forms insoluble macromolecular Fe(II) complexes in analogous experimental conditions.

Introduction. The formation of iron complexes with α — dioximes was mentioned first by Chugaev [1]. In contrast to the Ni, Pd, Pt and Cu derivatives of the $[M(Diox.\ H)_2]$ type, insoluble in water and soluble in polar organic solvents, the red coloured Fe(II) compounds are very easily soluble in water and in solid, crystalline state can be obtained very difficultly [2]. Colour reactions of iron salts can be observed also with — hydroxy — oximes (e.g. salicylaldoxime [3], rezorcylaldoxime [4]) and formaldoxime in alkaline media [5]. These reactions were also recommended for analytical purposes.

If aromatic and heterocyclic organic N-bases or phosphines are present in the iron(II) — α-dioxime system, sparingly soluble, crystalline compounds can be isolated. The diamagnetic properties of these hexacoordinated mixed chelates: $[Fe(Diox.\ H)_2Am_2]^\circ$ (Diox. H_2 = dimethylglyoxime, benzyldioxime) prove the presence of Fe (II) in their composition.

X-ray studies confirm an analogy in the structure of the above complexes with those of the $[M(III)\ (Diox.\ H)_2\ (Am)_2]^+$ and $[M(III)\ (Diox.\ H)_2X_2]^-$ type derivatives (M = Co, Rh, Ir).

The $[Fe(Diox.\ H)_2\ (Am)_2]$ complexes can be extracted from aqueous media with organic solvents (e.g. $CHCl_3$, CCl_4, higher aliphatic alcohols)/[7—9]. In etherical suspension they can be oxidized with Br_2, I_2 to Fe(III) derivatives (e.g. $[Fe(DH)_2\ (Py)_2]X.nHX$ (X = Cl, Br, I))/[10].

The iron (II) dioximines form adducts also with halogens and pseudohalogen: $[Fe(DH)_2X_2]^{2-}$ (X = Cl, Br, I, NCS, NCSe, DH_2 = dimethylglyoxime) [11].

The complex formation of iron(III) with the above mentioned chelating agents is not so characteristic. In aqueous media various Fe(III) -oxime ratios were reported, but the complexes have not been isolated in solid state. Concerning their structure only presumptions were forwarded (e.g. with dimethylglyoxime: $[Fe(DH)_3]$, $[Fe(DH)_2\ (OH)]$, etc. [12—13].

---

[1] Part LXXVIII, Cs. Várhelyi, J. Zsakó, G. Liptay, Z. Finta, *J. Thermal Anal.*, 32, 785 (1987)

* *University of Cluj-Napoca, Faculty of Chemical Technology, 3400 Cluj, Romania*

In the present paper the interaction of nioxime (1,2-cyclohexane dione dioxime) and trioxime (1,2 3- cyclohexane trione trioxime) with Fe(II) and Fe(III) — salts was studied in aqueous solutions under various experimental conditions, and several new [Fe(Niox. $H)_2$ $(Am)_2$] type complexes were synthesized and investigated (Niox. H_2 stands for nioxime, "Am" for organic amines and tertiary phosphines.

Experimental. Electronic spectra were recorded in aqueous solutions and in methanol, respectively, with a Specord spectrophotometer (Carl Zeiss Jena) (conc. 10^{-3} mole/l in visible and 5×10^{-5} mole/l in UV region). The colorimetric measurements were carried out by means of a PEK photocolorimeter.

The IR spectra were recorded in KBr pellets with an UR 20 Carl Zeiss Jena spectrophotometere.

Synthesis of [Fe(Niox .H)$_2$(Am)$_2$]-type complexes. From solutions of 10 mmoles of $Fe(NH_4)_2(SO_4)_2$ $6H_2O$ (4.0 g) in 60—80 ml water and of 20 mmoles nioxime and 30 mmoles amine (phosphine) in 100 ml methanol, respectively, air was removed by bubbling methane for 10 minutes. After mixing of the solutions the removal of air is continued for 5—10 minutes. The separated crystalline products were filtered off, washed with dil. methanol and dried on air.

Analysis. The iron content of the samples (150—200 mg) was determined gravimetrically as Fe_3O_4 after ignition, oxidation of the residue with 4—5 drops conc. HNO_3 followed by calcination at 800—900 °C. Nitrogen content was determined by the micro-Dumas method.

Results and discussions. With aliphatic and alyclic α-dioximes the iron(II) salts (as $Fe(NH_4)_2$ $(SO_4)_2$) give solutions only very weakly coloured in dose. Using trioxime for this purpose, the colouration is more intense. The Job curve, i.e. the extinction (E) vs. X curve, where X stands for the formal molar fraction of the oxime : X = [oxime]/([Fe(II)] + [oxime]), for the Fe(II) — 1, 2, 3- cyclohexane trione trioxime system is dresented in Fig. 1.

Spectrophotometric measurements were carried out 15 minutes after mixing, at 440 nm (22.8 kK) in the presence of Britton-Robinson buffer solution of pH = 1.18.

As seen from this figure, a molar ratio Fe : trioxime = 1 :3 is observed for the complex obtained. This is in contrast with the behaviour of Fe(II) — 1,2-dioxime systems, which give always a molar ratio Fe(II) : dioxime = 1 :2 [14].

The colour of the Fe(II) — dioxime complexes becomes darker and more intense in the presence of ammonia or of aliphatic amines (methylamine, ethylamine, etc), indicating the coordination of the latters by Fe(II) and the formation of Fe(Diox. $H)_2$ $(Am)_2$] type complexes. In the present paper the formation of such a complex was studied in the system Fe(II)-nioxime — NH_3, by using Job's method. The curve shown in Fig. 2. was recorded by mixing Fe(II) salt solutions with equimolecular binary solutions of nioxime and ammonia, at pH = 1.81.

The maximum absorption (at 400 nm) corresponds to a molar ratio 1 :2. This result is in good agreement with the formation of the complex [Fe(Niox. $H)_2$ $(NH_3)_2$].

In analogous experimental conditions, by

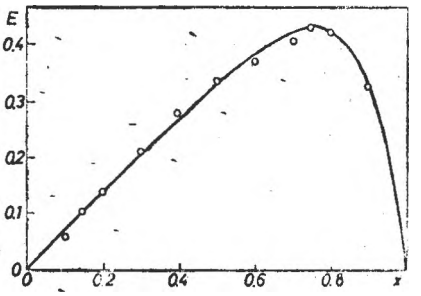

Fig. 1. Job curve of the Fe(II)-trioxime system.
λ = 440 mm; [Fe(II)] + [trioxime] = $= 10^{-3}$ M; pH = 1.81

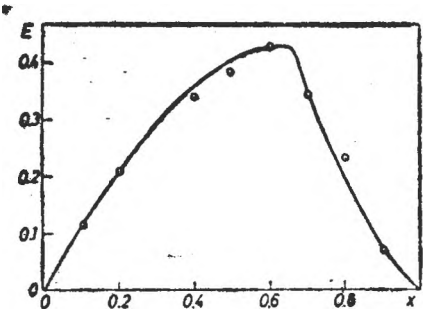

Fig. 2. Job curve of the Fe(II)-nioxime-NH_3 system.
$\lambda = 400$ nm; [Fe(II)] + [nioxime] = $= 10^{-3}$ M; [nioxime]: $[NH_3] = 1:1$; pH = 1.81

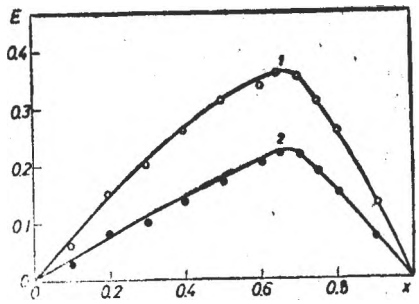

Fig. 3. Job curve of the Fe(II)-trioxime-NH_3 system.
[Fe(II)] + [trioxime] = 10^{-3} M; [trioxime]: $[NH_3] = 1:1$
1 — $\lambda = 580$ nm; 2 — $\lambda = 400$ nm

using trioxime instead of nioxime, a blue violet colouration appears. The Job curves recorded at 580 and 400 nm, respectively, are vizualized in Fig. 3.

Obviously, both curves are of the same shape indicating a molar ratio Fe : trioxime : $NH_3 = 1:2:2$ for the complex obtained.

The formation of Fe(Triox. $H_2)_3$ and Fe(Triox. $H_2)_2(NH_3)_2$ type complexes show that trioxime behaves in these cases as bidentate ligand, although potentially it is a tridentate one. This phenomenon can be easily understood by taking into account the geometry of the trioxime molecule. The hydroaromatic ring and the conjugated π — bond system makes the molecule rigid. Therefore, the three N- atoms are coplanar and their simultaneous co-ordination to the Fe^{2+} ion is not possible.

It is interesting to observe that the colour (blue violet) of the [Fe(Triox. $H_2)_2$ $(NH_3)_2$] complex differs from the colour of the analogous derivatives of alycyclic and aliphatic α-dioximes (red), but is almost the same as in the case of the α-benzyldioxime and α-furyldioxime derivatives [15]. This might be the consequence of the dimension of the delocalized π-bond system in the coplanar moiety of co-ordinated oxime molecules. This π-bond system is larger in the case of trioxime, benzyldioxime and furyldioxime derivatives as compared to the alycyclic and aliphatic dioxime ones. Consequently, the energy of the lowest empty π-type level will be less in the case of the formers as compared to the latters. Since the absorption band in the visible region is assigned to a metal to ligand charge transfer [16—18], it will be shifted by the enlarging of the π-bond system towards lower wave numbers, which is in agreement with the colour of these complexes and the position of the absorption band in the visible region.

It is worth mentioning that a similar effect can be expected by presuming π-bond formation between the co-ordinated oxime molecule and the iron atom. In the formation of these π-bonds the Fe atom participates with its occupied d_{xz} and d_{yz} orbitals and the oxime molecules with their π-type antibonding molecular orbitals (MO), leading to a large delocalized π-bond system comprizing besides the Fe atom all double bonded atoms of both oxime molecules.

In this assumption, the larger the delocalized π-bond system, the nearer will be the energy of the first empty MO to the energy of the last occupied MO, i.e. by presuming the absorption band to be due to a $\pi \rightarrow \pi^*$ transition, its position will be shifted towards lower wave number values in the case of trioxime, benzyldioxime and furyldioxime, as compared to its position with alycyclic and aliphatic oximes. Therefore, this would be an alternative explanation for the effects observed.

Using instead of ammonia aromatic — and especially heterocyclic amines (pyridine bases, imidazole-, benzimidazole derivatives) or tertiary alkyl-aryl-phosphines for the colour reaction, sparingly soluble, crystalline compounds can be separated.

A series of new compounds of the type $[Fe(Niox.\ H)_2\ (Am)_2]$ were obtained n this way and characterized in Table 1.

Table 1

New mixed chelates of the type $[Fe(Niox.\ H)_2\ (Am)_2]$°

No.	Formula	Mol. wt. calcd.	Yield (%)	Appearance	Analysis	Calcd.	Found
1.	$[Fe(Niox.H)_2(3,5\text{-lutidine})_2]$	552.4	75	red short prisms	Fe	10.11	10.25
					N	15.21	15.09
2.	$[Fe(Niox.H)_2(4\text{-ethyl-pyridine})_2]$	552.4	70	red prisms	Fe	10.11	9.90
					N	15.21	15.32
3.	$[Fe(Niox.H)_2(2\text{-methyl-imidazole})_2]$	502.4	75	red, irregular prisms	Fe	11.11	11.26
					N	22.30	23.02
4.	$[Fe(Niox.H)_2(benzimidazole)_2]$	574.4	85	red-brown irregular cryst.	Fe	9.72	9.88
					N	19.51	19.19
5.	$[Fe(Niox.H)_2$(diethyl-phenyl-phosphine)$_2]$	670.5	90	gold-yellow plates	Fe	8.32	8.60
					N	8.35	8.23
6.	$[Fe(Niox.H)_2$(diethyl-p-tolyl-phosphine)$_2]$	696.6	90	gold-yellow prisms	Fe	8.01	8.42
					N	8.04	7.92
7.	$[Fe(Niox.H)_2$(diphenyl-ethyl-phosphine)$_2]$	766.6	95	sparkling gold-yellow long prisms	Fe	7.28	7.62
					N	7.31	7.19
8.	$[Fe(Niox.H)_2$(n-dibutyl-phenyl-phosphine)$_2]$	782.7	85	sparkling dark yellow rhomb. plates	Fe	7.13	7.50
					N	7.16	7.09
9.	$[Fe(Niox.H)_2$(tributyl-phosphine)$_2]$	742.8	80	yellow-brown short prisms	Fe	7.52	7.80
					N	7.55	7.36

$NioxH_2$: nioxime: $C_4H_{10}N_2O_2$

These compounds with non electrolytic character are very sparingly soluble in water. They dissolve in some organic solvents, e.g. $CHCl_3$, CCl_4, DMFA, DMSO, THF, etc.

The triaryl-phosphines (triphenylphosphine, tri- p-tolyl-phosphine), weaker bases as the alkyl-aryl-phosphines are unable for this reaction. In these cases also a steric effect may hinder the complex formation.

It is worth mentioning, that the trioxime forms insoluble macromolecular products in the presence of heterocyclic amines and phosphines, analogously

with the cobalt (III) derivatives: $[(Co(triox.\ H_2)_{1.5}\ (amine)\ X)]_n$. The study of the formation conditions of these complexes will be the subject of a coming paper.

In the *i.r. spectra* of the $[Fe(Niox.\ H)_2\ (Am)_2]$ complexes the ν_{C-H} valence vibrations (2960—70 cm^{-1} (s), 2860—70 cm^{-1} (v.s.) and the δ_{CH_3} deformation vibrations (1340, 1380 cm^{-1} (s) appear as strong bands, not influenced by co-ordination effect, because of the hydroaromatic ring systems. The ν_{O-H} (2300—2400 cm^{-1} (m) and the $\delta_{O-H..O}$ (1660—1750 cm^{-1} (w- m) bands are characteristic for the strong, short intramolecular O—H..O hydrogen bridges, which stabilize the coplanar $Fe(Niox.\ H)_2$ moiety, analogously as with the $[M(Diox.\ H)_2L_2]$ derivatives (M = Co, Rh, Ir, L = amine, Cl, Br, I, etc.) [19]. The co-ordinated oxime frequencies $\nu_{C=N}$ (1550—1560 cm^{-1} (v.s.), ν_{N-OH} (1220—1230 cm^{-1} (v.s.) and $\nu_{NO..}$ (1080—1100 cm^{-1} (v.s.) show strong Fe-N covalent bonds.

The tertiary phosphine frequencies (ν_{C-H}, δ_{CH_3}) are not influenced by co-ordination.

In the *electronic spectra* of the $[Fe(Niox.\ H)_2\ (Am)_2]$ taken in alcohol appears an intensive band in the visible region at 18—20.5 kK (with amines) and a 21—21.5 kK in the case of phosphine derivatives.

As mentioned above this band can be considered as a charge transfer band Fe → Oxime and his position depends especially on the molecular structure of the chelating dioxime [15, 16].

According to our observations made on a series of $[Fe(Diox.\ H)_2\ (amine)_2$ and $[Fe(Diox.\ H)_2\ (phosphine)_2]$ complexes with identical oximes and different amine or phosphine ligands the position of this absorption band is not uniquely determined by the nature of the oxime and depends also on the nature of the axial ligands. Presumably, the strength of the bond between the iron atom and the axial bases slightly modifies the electron energies in the Fe(Diox. H) moiety. Other 2—3 bands appear in the UV-region (25 and 33—34 kK) and presumably correspond to charge transfer from the iron atom to the axial bases.

Further an attempt is made to evidence complex formation of Fe(III) with oximes. For this purpose electronic spectra were recorded in $Fe(NO_3)_3$ — oxime mixtures (aqueous solutions with $Fe^{3+} = 10^{-3}$ M; oxime = 5×10^{-3} M containing Britton-Robinson buffer solutions of different pH values. Spectra data are presented in Table 2.

Table 2

Electronic spectral data concerning the first absorbtion band of some Fe (III)- oxime mixtures as function of the pH — value

pH	1.81	4.1	8.36	9.91	11.82	13.0
nioxime						
$\tilde{\nu}$ kK	22.0_i	21.6_i	—	21.7_i	21.2_i	—
ε	2.9×10^3	2×10^3	—	3.7×10^3	3.25×10^3	
trioxime						
$\tilde{\nu}$ kK	21.6_i	—	21.2_i	—	20.3_i	20.0_i
ε	8×10^3	—	2×10^3	—	2.3×10^3	5.3×10^3

^{i} — inflexion point

Mostly, in the visible region only an inflexion point appears at 20.5—22.5 kK, its position depending on the pH value. At higher pH values this inflexion point is a little shifted towards lower wave number values. The yellow to brown colour of the solutions is stable in basic media, in acidic solutions a fast decolouration occurs.

For the determination of the composition of the iron(III) derivatives of this type recording of Job curves have been tried at various pH values.

These experiments show that at lower oxime : Fe(III) ratios ($r = 0.2—1.0$), $Fe(OH)_3$ precipitates from the solution and the spectrophotometric curves can be recorded only for higher ratios ($r = 1.5—3.0$). As observed, at higher ratios the optical density exhibits a maximum corresponding to a molar ratio comprized between 2.0 and 3.0. On the basis of these results, the formation of Fe(III) $(oxime)_n$ complexes may be taken for granted.

The weak absorbtivity of the Fe(III)-oxime systems did not allow us to determine exactly the molar ratio and it makes this reaction unsuitable for analytical purposes.

REFERENCES

1. L. A. Chugaev, *Z. anorg. Chem.*, **46**, 144 (1905).
2. K. Burger, L. Korecz, I. B. A. Manuaga, P. Mag., *J. Inorg. Nuclear Chem.*, **28**, 1673 (1966).
3. D. Bandyopaghayay, *J. Indian Chem. Soc.*, **33**, 269 (1956).
4. D. E. Howe, M. Mellon, *Ind. Eng. Chem. Analit. Ed.*, **12**, 448 (1940).
5. Z. Marczenko, K. Kasiura, *Chem. Analit. (Warszawa)*, **6**, 37 (1961)
6. C. K. Prout, T. J. Wiseman, *J. Chem. Soc.*, **1964**, 497.
7. S. L. Chien, T. M. Shih, *Fac. Sci. Univ. Tokyo*, **5**, 154 (1937).
8. E. K. Astakhova, V. M. Savostina, V. M. Peshkova, *Zhur. Fiz. Khim.*, **38**, 2299 (1964).
9. B. Egneus, *Talanta*, **19**, 1387 (1972).
10. L. Korecz, A. A. Saghier, Cs. Várhelyi, K. Burger, *Acta Chim. Acad. Sci. Hung.*, **101**, 27 (1979).
11. K. Burger, B. Pintér, *J. Inorg. Nuclear Chem.*, **29**, 1717 (1967).
12. S. S. Braley, F. B. Hobbart, *J. Amer. Chem. Soc.*, **43**, 482 (1921).
13. V. M. Peshkova, V. M. Savostina, E. K. Astakhova-Ivanova, "Solvent Extraction Chemistry", Amsterdam, North-Holland Publ., 1967, p. 66.
14. K. Burger, I. Ruff, *Talanta*, **10**, 329 (1963).
15. P. B. Michelson, A. K. Boriak, L. T. Moskovskaya, *Zhur. analit. Khim.*, **26**, 877 (1971).
16. C. Matsumoto, Y. Yamano, K. Shinra, *J. Chem. Soc. Japan, Ind. Chem.*, **89**, 44 (1968).
17. N. Sanders, P. Day, *J. Chem. Soc.*, **1969** A, 2303.
18. A. K. Babko, P. B. Michelson, *Zhur. neorg. Khim.*, **14**, 1302 (1969).
19. A. Nakahara, *Bull. Chem. Soc. Japan*, **28**, 473 (1955).

STUDIA UNIV. BABEŞ—BOLYAI, CHEMIA, XXXIV, 2, 1989

CALORIMETRIC DETERMINATION OF THE ELECTROCATALYTICAL ACTIVITY

LIVIU ONICIU*, VASILE A. TOPAN*, LIANA MUREŞAN*, IOAN BALDEA* and DAN GHERŢOIU*

Received: 5 January, 1989

The electrocatalytical activity of copper, molybdenum, nickel, palladium (on active coal), silver and tungsten as powders, as well as cobalt-, copper-, manganese-, nickel- and zirconium-borides has been studied in a non-electrochemical way, by recording the variation of temperature versus time in the case of $N_2H_4 - H_2O_2$ redox process, taking place on their surfaces. The catalytical activity was parallel to the electrocatalytical one, observed on electrodes prepared from the same materials.

Introduction. A heterogenous electrochemical process is characterized by electron-transfer at the solid-electrolyte interface, taking place with higher entropy change as compared to homogenous one. In order to minimize this entropy change, the electrodes of electrochemical reactor should display a considerable catalytical activity. This activity can hardly be studied by an usual electrochemical method. Jahnke [1] used the fluidization of the catalyst in a reactant solution flow, the electric contact being provided by a surrounding metallic gauze made of Pt, Au or gold-plated nickel.

The purpose of this paper is to report data on a rapid and simple method of testing catalytic activity of materials to be used in preparation of various electrodes. Focussing the interest on hydrazine, a substance frequently used in fuel-cells, the reaction between hydrazine and hydrogen peroxide has been chosen to take place

$$N_2H_4 + 2\,H_2O_2 \rightarrow N_2 + 4\,H_2O \qquad (1)$$

on the surfaces of studied catalysts. There are data in the literature showing that the reaction rate is zero-order with respect to hydrazine and first-order with respect to hydrogen peroxide, and very sensitive to the presence of impurities [2]. Cobalt boride as well as other metal borides or transitional metals exhibit catalytical activity towards the oxidation of hydrazine [3—8].

A change of the electrode potential ε of an electrode immersed in an appropriate solution induces a change of solution composition, through a current intensity I, taking place, fast or slow, until a new steady-state is reached. The higher the instantaneous current I thus appeared, the larger the catalytical activity of electrode material. In the same way, a change of the free energy of the system induces a corresponding shift of the electric field intensity. A dispersed electrocatalyst in contact with a redox couple dissolved in an appropriate medium displays some activity towards both the oxidation and the reduc-

* *University of Cluj-Napoca, Faculty of Chemical Technology, 3400 Cluj-Napoca Romania*

tion charge-transfer processes, as depicted schematically in Fig. 1, where I and II represents the fraction of the surface occupied by anodic and cathodic sites, respectively. The two charge-transfer processes will be influenced to a different degree by the presence of the electrocatalyst, without any possibility of discriminating the particular effect of the electrocatalyst on the two components of the overall process

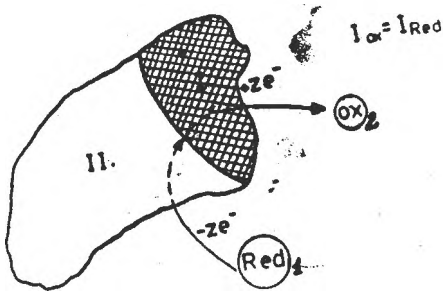

Fig. 1. Redox process on the catalyst grain.

$$Red_1 + Ox_2 \rightarrow Ox_1 + Red_2 \qquad (2)$$

Therefore, a good catalyst acting on the oxidation process may appear unsatisfactory because of activity towards the "Ox" species. This difficulty could be avoided by using two catalytical species.

In order to compare different catalysts for the same process (*e. g.* oxidation), the thermal effect generated by the reaction between hydrazine and hydrogen peroxide taking place on their surface has been recorded using different amount of studied catalyst in the presence of the same amount of reduction catalyst. The contact between the catalyst grains has been provided by a vigorous stirring, so that the shape of kinetic recordings has not been dependent upon the stirring rate. When two different grains of catalyst were in contact, a mixed potential has appeared. The position of this potential towards the equilibrium one of a singular grain depends upon both the value of exchange current density (i_0) and the surface ratio of the two grain species, as schematically is depicted in Fig. 2. Some complications may arise in the cases when ε reaches positive values that exceed those of corrosion potential of the oxidation catalyst (see Fig. 2 c). To avoid such a situation, experimental conditions were chosen as to eliminate corrosion effects.

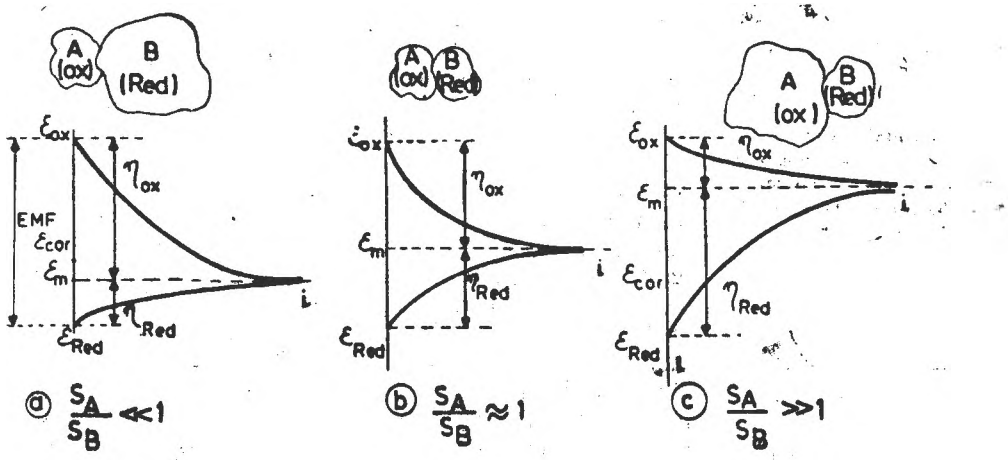

Fig. 2. Mixed potentials of systems with two different catalysts at three real surface ratios.

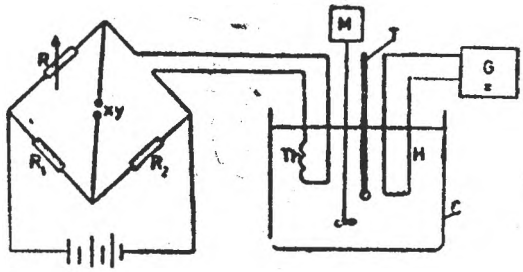

Fig. 3. Experimental arrangement for calorimetric testing of electrocatalysts.

Experimental. The experimental device used in the study is presented in Fig. 3, and consists of a calorimeter, C, provided with a stirrer, M, and a heater, H, connected to a stabilized voltage source, and a thermistor, Th, connected to a Wheatstone bridge. The temperature — time curves were recorded on an Endim 620.02 XY recorder. The calibrated heater compensates the heat losses. The small temperature variation given by the progress of reaction was directly recorded for various experimental conditions. A known quantity of distilled water, previously heated at the desired temperature, and a known amount of catalyst powder were introduced into calorimeter and maintained as a suspension by means of a glass stirrer. The voltage of heater was properly adjusted as to obtain a steady temperature. Known aliquots of hydrazine of 0.14% and hydrogen peroxide of 0.1 % solutions were then added and temperature — time curve were recorded. A small excess of hydrazine was used.

The catalysts were obtained either from commercial sources or prepared in the laboratory. The metal-borides were prepared by the reduction of metal oxides with boron, using a 50% excess (noted with I), or 100 % excess (noted with II) of boron. They were ground and passed on fine-mesh sieves, and a granulosity fraction was then used as catalysts. The surface area per gram of catalyst was determined by BET method with kripton at liquid nitrogen temperature.

Results and discussions. The small temperature increase (0.6—1 degrees) during the process is directly correlated to the number of moles reacted, so that, for the first-order dependence the integrated rate law is:

$$\ln \frac{C^\circ}{C} = \ln \frac{T_\infty - T_\circ}{T_\infty - T} = k_{app} \cdot t \qquad (3)$$

where C° and C represent the initial and actual concentration of reference chemical species, respectively, $T_\circ$, T and T_∞ represent the initial, the actual and the value at total conversion temperature, respectively. The plots of $\ln (T_\infty - T)$ versus time were linear for more than 90% of completion, proving the first-order kinetics. The slopes of the plots gave apparent first-order rate constants k_{app}. When T_∞ values were not precisely obtained, Guggenheim method [9] was used to determine the apparent first-order rate constant. The temperature values were corrected to allow for the contribution of homogenous reaction.

Table 1

Experimental first-oder rate constants for homogenous reaction between hydrazine and hydrogen peroxide in neutral media

Temp (°C)	$10^4 k_{app}$ (s^{-1})
44	1.63
52	2.99
63	5.67
66	10.90
76	20.80

Table 1 contains kinetic data for the homogenous reaction as determined by our method. The reaction on the catalyst surface, and the temperature increase due to homogenous process was subtracted from the values obtained when catalysts were present. From the data in Table 1 an experimental activation energy of 18.1 kcal/mole (75.7 kJ/mole) was calculated, in agreement with the literature data. Table 2 summarizes the data obtained in the presence of a single catalyst species. Each value in the table is a mean of 2—3 individual runs. An increasing effect of one to three orders of magnitude on first-order rate constants as compared to the

Tabelle 2

Kinetic data on the reduction of hydrogen peroxide by hydrazine in the presence of a solid catalyst

Catalyst	Amount m(g)	Temp. (°C)	k_{app} (s^{-1})	$k' = \frac{k_{app}}{m}$ ($s^{-1}g^{-1}$)
Ag	0.25	59	1.08×10^{-2}	4.32×10^{-2}
Cu	0.50	63	3.13×10^{-2}	6.26×10^{-2}
Mo	0.50	63	2.40×10^{-2}	4.80×10^{-2}
Ni (Raney)	0.50	63	3.10×10^{-2}	6.20×10^{-2}
Pd (on coal)	0.20	63	1.70×10^{-1}	8.50×10^{-1}
W	0.50	63	1.65×10^{-2}	3.30×10^{-2}
Co_2B(I)	0.25	59	3.31×10^{-2}	1.32×10^{-2}
	0.50	63	3.8×10^{-2}	7.60×10^{-2}
Co_2B(II)	1.00	60	8.53×10^{-2}	8.53×10^{-2}
		50	5.80×10^{-2}	5.80×10^{-2}
Cu_2B(I)	0.20	63	2.41×10^{-1}	1.21
Mn_2B(I)	1.00	50	4.80×10^{-2}	4.80×10^{-2}
		52	5.18×10^{-2}	5.18×10^{-2}
Ni_2B(I)	0.25	59	0.80×10^{-2}	3.20×10^{-2}
Ni_2B(II)	0.25	59	1.66×10^{-2}	6.64×10^{-2}
Zr_2B(I)	1.00	50	6.60×10^{-2}	6.60×10^{-2}
		52	7.60×10^{-2}	7.60×10^{-2}

homogenous reaction has been observed. Last column of the table contains the rate constants raported to unit mass of catalyst. Best results were obtained with copper boride, but important effects gave Co_2B(II) and Ni_2B(II). An Arrhenius activation energy of reaction in the presence of Co_2B(II) of 8.2 kcal/mole (34.5 kJ/mole) has been estimated within a relatively narrow range of temperature of 10°C. This value is far below the one for homogenous reaction.

The data in Table 2 were obtained using different catalysts prepared in the laboratory or obtained from commercial sources, having various surfaces per unit mass, and the comparison between their performances in enhancing the rate of hydrazine-hydrogen peroxide reaction is only a qualitative one. All these materials can be used to prepare electrodes for fuel-cells.

Table 3 contains data raported to the unit area of catalyst. Cobalt boride and two sorts of nickel boride as oxidation catalysts for N_2H_4 and silver powder as reduction catalyst for H_2O_2 were tested. Although Co_2 B(I) displays a surface

Table 3

Kinetic data related to surface area per gram of catalyst, at 59°C

Catalyst	S_g (m^2/g)	Amount of catalyst m (g)	k_{app} (s^{-1})	$k'' = \frac{k_{app}}{m \cdot S_g}$ ($s^{-1}m^{-2}$)
Co_2B(I)	0.44	0.25	3.31×10^{-2}	3.00×10^{-2}
Ni_2B(I)	18.3	0.25	0.80×10^{-2}	1.75×10^{-4}
Ni_2B(II)	90.0	0.25	1.66×10^{-2}	7.37×10^{-5}
Ag	8.2	0.25	1.08×10^{-2}	5.20×10^{-3}

area per gram of material of only 0.44 m^2/g, its catalytic activity is characterized by $k'' = k_{app}/m \cdot S_g = 3.0 \times 10^{-2}\ m^{-2}s^{-1}$, higher than that for silver.

On the basis of preliminary tests, the amount of 0.25 g of silver powder and various amounts of cobalt and nickel boride were used together to enhance both the oxidation and the reduction processes. To avoid corrosion effects, the mixed potential ε_m should be close to the rest potential $\varepsilon_{N_2H_4}$, and global area of anodic catalyst should be correlated with the exhange current density. Since the ratio $i_{0\,Ag}/i_{0\,M_xB}$ is about 10^4, it was necessary to have $S_{g\,Ag}/S_{g\,M_xB} \leqslant \leqslant 10^4$; our experiments were performed at surface ratios between 0.09 and 150. Table 4 reports data in the presence of anodic and cathodic catalysts used together. Last column contains differences between apparent rate constants obtained with both anodic and cathodic catalysts and first-order rate constant obtained with only one of them, taken in constant amount, divided by the area of the second catalyst. This ratio decreases with the increasing amount of the second catalyst added, showing that cathodic and anodic fraction areas of catalysts change. More and more anodic sites on silver surface change their character as the anodic surface presented by metal borides increases.

Table 4

Kinetic data in the presence of anodic and cathodic catalysts at 59°C

Silver catalyst for "Ox" species amount m (g)	area (m^2)	Catalyst for "Red" species	amount m(g)	area (m^2)	k_{app} (s^{-1})	$\Delta k_{app}/m \cdot S_g$ ($s^{-1} \cdot m^{-2}$)
0.1	0.82	—	—	—	5.92×10^{-3}	—
		Co_2B	0.5	0.22	1.87×10^{-2}	5.8×10^{-2}
			1.5	0.66	2.43×10^{-2}	2.78×10^{-2}
0.25	2.05	—	—	—	1.08×10^{-2}	—
		Co_2B	0.05	0.022	1.32×10^{-2}	1.09×10^{-1}
			0.1	0.044	1.49×10^{-2}	9.32×10^{-2}
			0.5	0.22	3.13×10^{-2}	9.32×10^{-2}
			1.0	0.44	4.49×10^{-2}	7.75×10^{-2}
			2.0	0.88	7.38×10^{-2}	7.16×10^{-2}
—	—	Co_2B	0.25	0.11	3.31×10^{-3}	—
0.25	2.05				3.38×10^{-2}	1.48×10^{-2}
0.5	4.10				4.58×10^{-2}	1.04×10^{-2}
1.0	8.20				8.33×10^{-2}	9.75×10^{-3}
2.0	16.40				1.23×10^{-1}	7.3×10^{-3}
0.25	2.05	Ni_2B(I)	0.25	4.57	1.38×10^{-2}	6.56×10^{-4}
		Ni_2B(II)	0.25	22.50	1.60×10^{-2}	2.31×10^{-4}

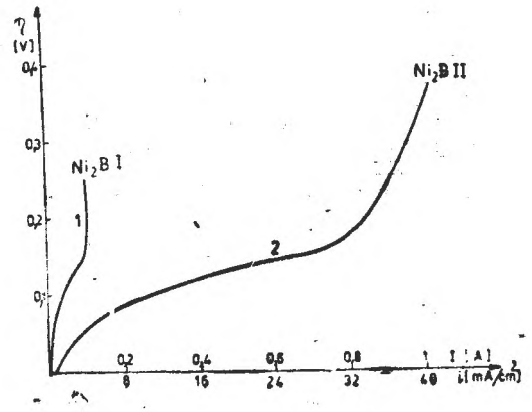

Fig. 4. Polarization curves of hydrazine electrodes prepared of Ni_2B I(1) and Ni_2B II(2).

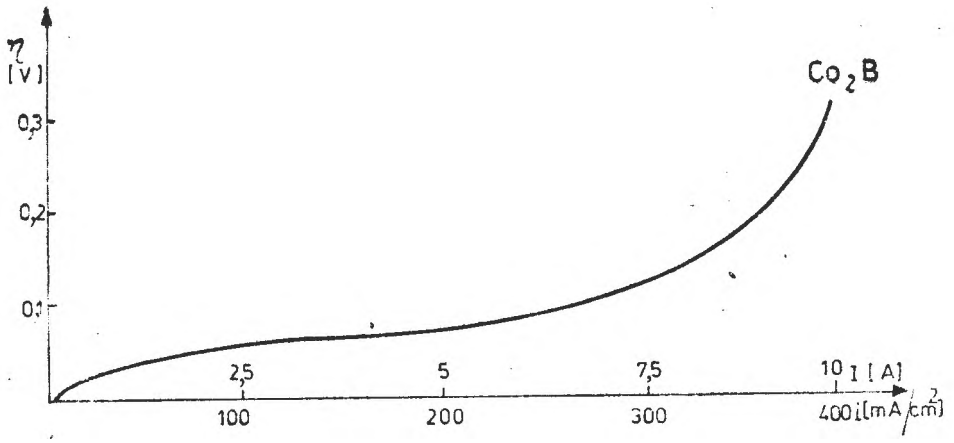

Fig. 5. Polarization curve of hydrazine electrode prepared of Co_2B.

The efficiency of the electrocatalysts tested is in the order : $Zr_2B < Mn_2B < Ni_2B(I) < Ni_2B(II) < Co_2B(I) < Co_2B(II) < Cu_2B$. These results were compared to those obtained in an electrochemical investigation using electrodes prepared from some of these materials and having equal apparent surface areas. The polarization curves are presented in Fig. 4 and 5. The behaviour deduced from electrochemical tests shows the same order of activity increase, thus confirming the validity of estimations made by the more rapid calorimetric method described in this paper.

REFERENCES

1. H. Jahnke, M. Schönborn, „Proceedings of the Third Symposium of Fuel Cells" Brussels, 1969, p. 60.
2. L. P. Kuhn, C. Wellman, *US Nat. Tech. Inform. Serv.*, AD Rep. No. 746956, 1972.
3. G. Bliznakov, P. Peşhev, G. Gyurov, *Dokl. Bolg Akad. Nauk.*, **25**, 1209 (1972).

4. S. G. Meibuhr, R. F. Paluch, *J. Electrochem. Soc.*, **122**, 164 (1975).
5. A. N. Sofronkov, S. D. Korolenko, I. S. Mezeutsev, *Zhur. fiz. Khim.*, **47**, 2036 (1973).
6. A. N. Sofronkov, Yu. Tkach, S. D. Korolenko, *Zhur. priklad. Khim.* **49**, 220 (1976).
7. A. N. Sofronkov, L. D. Skrylev, Deposited Doc. VINITI, 1351 (1977).
8. E. J. Zeitmer, M. E. Wheatley, R. R. Witherspoon, S. G. Meibuhr, *US Pat.* 3,772,086 (1973).
9. E. A. Guggenheim, *Philos. Mag.*, **2**, 538 (1926).

STUDIA UNIV. BABEŞ—BOLYAI, CHEMIA, XXXIV, 2, 1989

MULTI-ELEMENT DETERMINATION IN THE LAVA FROM BERCA MUD VOLCANOES (ROMANIA) BY NEUTRON ACTIVATION ANALYSIS

CONSTANTIN COSMA*, CĂLIN ZNAMIROVSCHI**, MARIA SĂLĂGEAN***, ANA PANTELICĂ***

Received: December 6 1988

The neutron activation analysis for detection and determination of minor and trace elements in the lava from Berca mud volcanoes (Buzău county) was applied. Because by usual chemical methods only a few elements were detected, in our paper the multielemental analysis by neutron activation method was used. Neutron activation analysis, having some desirable attributes as non-destructiveness, a very high sensitivity and ability to determine several elements simultaneously, offers good possibilities for rapid and precise determination of a wide range of elements, in a broad spectrum of matrices. Besides major elements (Al, Ca, Cl, Fe, Na) the minor and trace elements (As, Ba, Br, Ce, Co, Cr, Cs, Dy, Eu, Hf, La, Lu, Mn, Nd, Rb, Sb, Sc, Sm, Sr, Th, U, V, Yb, Zn) in the lava from Berca mud volcanoes were determined.

1. **Introduction.** The mud volcanoes are situated within the area of Berca village, Buzău county, on the left bank of the Berca river. They represent fluid mud eruptions and emerge as a result of natural gas (methane) eruption, post-volcanic emanations and seismic movements. In its way to the surface, the gas carries fresh or salt water, which softens and weathers the encountered rocks, bringing them to the surface along minimal resistance lines.

The mud is deposed arround the eruption-point and formed hillocks shaped as pointed or flattened cones (frustum of a cone) with an aperture at the top which is the crater. The cones dimension and from depend by the mud composition and viscosity [1].

Pîclele Mari and Pîclele Mici are the names of the mud volcanoes groups which made the subject of this work.

Mud volcanoes in Pîclele Mari are placed in the central part of the Berca depression, at an altitude of 322 m and they are formed by active cones, not higher then 3 metters and by fossil cones, more higher (6—8 metters). Generally, in Pîclele Mari prevail volcanoes discharging viscous mud with oil traces. There are, however, puddles, 4—6 m in diameter, discharging fluid mud and especially boiling mud.

Mud volcanoes in Pîclele Mici are situated in the central area of the Berca depression, at an altitude of 341 m. In this group, volcanoes are smaller and fewer and the eruption mud is less viscous.

By the chemical analysis accomplished up to the present, showed that the mud contains, besides water and liquid hydrocarbons, calcium, magnesium, sodium, potassium and chlorine. The total mineralization is greater (70880.7 mg/l)

* *University of Cluj-Napoca, Faculty of Mathematics and Physics.*
** *University of Cluj-Napoca, Faculty of Chemical Technology.*
*** *Institute for Physics and Nuclear Engineering, Bucharest*

in Pîclele Mari that in Pîclele Mici (54226.0 mg/l). Also, the alkalization differs: pH (20°C) is 6.90 in Pîclele Mari and 8.10 in Pîclele Mici [1].

Because by usual chemical methods only a few elements were detected, in this paper we used the multielemental analysis of the mud by neutron activation analysis, which is able to provide information on a large number of elements, simultaneously, in a single analytical procedure.

This method is utilised in a large number of fields, for the analysis of ores, meteorites, lunar rocks, medical, chemical, biological samples and high purity materials. [2—5]

2. **Experimental.** The applied method is based on the nuclear reaction (n, γ) induced by thermal neutrons in their interaction with the nuclei of the chemical elements. The study of the characteristic gamma radiations, emitted by these nuclei, gives information about the elemental composition of the sample. [6]

Owing to the high sensitivity of this method, it exceeds all others: gravimetry, colorimetry, optic spectroscopy and mass spectrometry. Also, the sensitivity of the method increases with the neutron flux. [7, 8]

In this work, the utilised neutron source was the VVR-S reactor of the Institute for Physics and Nuclear Engineering from Bucharest. The choice of thermal neutrons for the activation is relied on the high cross section for the

Table 1

Nuclear data for the identified elements

Element	Isotope	Half-life	Gamma-ray energy (keV)
Al	^{28}Al	2.3 m	1779
As	^{76}As	1.097 d	559
Ba	^{131}Ba	11.7 d	496
Ca	^{47}Sc	3.4 d	160
Ce	^{141}Ce	32.5 d	145
Co	^{60}Co	5.271 y	1172; 1332
Cr	^{51}Cr	27.704 d	320
Cs	^{134}Cs	2.06 y	605; 796
Dy	^{165}Dy	2.35 h	95; 362
Eu	^{152}Eu	13.33 y	344; 1408
Fe	^{59}Fe	44.496 d	1099; 1292
Hf	^{181}Hf	42.4 d	133; 482
La	^{140}La	40.2 h	487; 1596
Lu	^{177}Lu	6.71 d	208
Mn	^{56}Mn	2.5785 d	847
Na	^{24}Na	15.03 h	1368
Nd	^{147}Nd	11.1 d	91; 531
Rb	^{86}Rb	18.65 d	1078
Sb	^{122}Sb	2.72 d	564
Sc	^{46}Sc	83.83 d	889; 1120
Sm	^{153}Sm	46.8 h	70; 103
Sr	^{85}Sr	64.8 d	514
Th	^{233}Pa	27.0 d	312
U	^{239} Np	2.355 d	106; 278
V	^{52}V	3.76 m	1434
Yb	^{175}Yb	4.21 d	283; 396
Zn	^{65}Zn	244.1 d	1116

most of chemical elements. The irradiation was made at short time and long time for cover a wide range of elements.

The samples alongside with SL-1 and Soil-5 standards from IAEA Vienna, were irradiated for 29 hours in a thermal flux of 2×10^{11} n/cm^2 · s, for the long-lived isotopes detection. A measuring time of 30 min.—2 hours, after 5—30 days cooling time have been used.

For the short-time determination, the samples with the same standards, using the pneumatic transfer system, were irradiated for 15 seconds in a flux of 2×10^{12} n/cm^2 · s. The measuring time was 10 minutes, after a cooling time of 2—20 minutes.

The measurements have been performed by aid of a Ge(Li) gamma detector having a resolution of 2 keV for 1332 keV (^{60}Co). The detector was coupled to a Canberra multichannel analyser.

By calibration, each channel corresponds to a well determined energy. The establishment of each element was made using the nuclear properties of the isotopes (Table 1). The listed gamma-ray energies were taken from the published data. [9, 10]

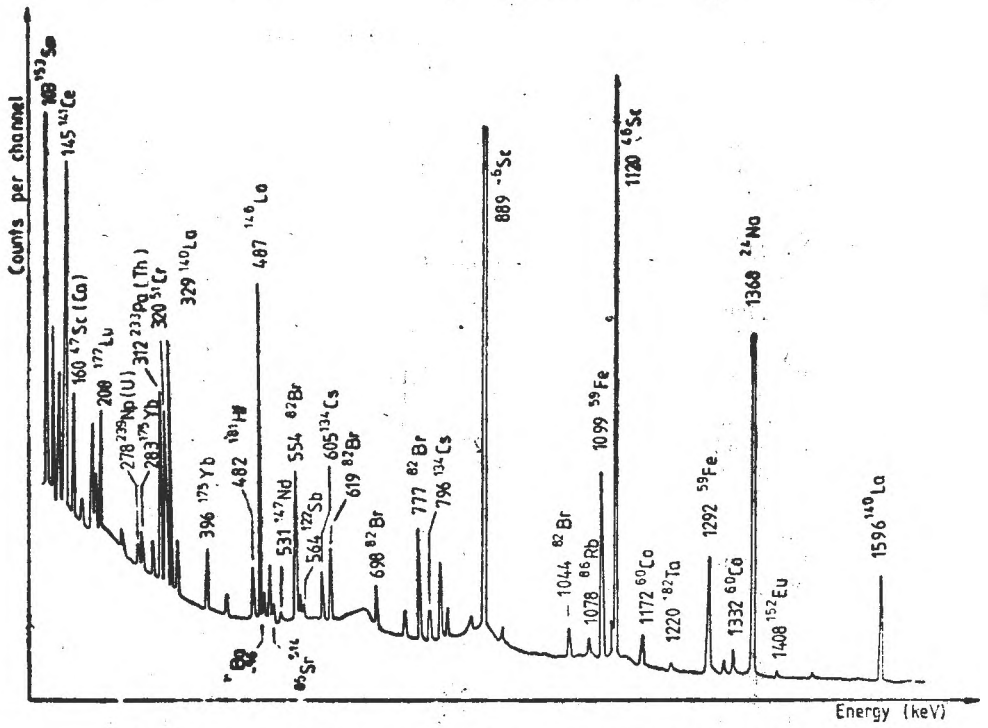

Fig. 1The gamma-ray spectrum of the lava sample from Piclele Mari

For the quantitative analysis, the samples and the standards were weighted and packaged in quartz tubes, for the long time irradiation or in polyethylene vials for the short time irradiation.

3. **Results.** By using the gamma-ray spectra (Fig. 1) and the nuclear characteristics, as the energy and the half-life (Table 1), the peaks of elements were identified.

For the determination of the abundance of each element was used the proportionality between the peak area and the elemental concentration. The background correction was applied to all the samples and standards.

On this way, the abundances of 29 elements were determined. The results are shown in Table 2.

It were determined 5 major elements (Al, Ca, Cl, Fe, Na) and 24 minor and trace elements (As, Ba, Br, Ce, Co, Cr, Cs, Dy, Eu, Hf, La, Lu, Mn, Nd, Rb, Sb, Sc, Sm, Sr, Th, U, V, Yb, Zn).

Among these, the presence of some rare earth elements (Dy, Eu, Hf, La, Lu, Sm, Yb), uranium (1—2 ppm) and thorium (10 ppm) may be remarked.

Comparing the obtained results, we noticed the presence of the same elements, both in Pîclele Mari and in Pîclele Mici. There are insignifiant diffe-

Table 2

The elemental concentration in the lava samples

Element (units)	Concentration ± uncertainty	
	Piclele Mici	Piclele Mari
Al (%)	4.85 ± 0.19	6.72 ± 0.27
As (ppm)	10 ± 2	11 ± 2
Ba (ppm)	1181 ± 175	276 ± 68
Br (ppm)	57 ± 3	30 ± 2
Ca (%)	3.26 ± 0.32	3.48 ± 0.33
Ce (ppm)	55 ± 3	60 ± 3
Cl (%)	10.43 ± 0.52	2.21 ± 0.18
Co (ppm)	13.2 ± 1.2	14.0 ± 1.2
Cr (ppm)	88 ± 10	83 ± 9
Cs (ppm)	7.5 ± 0.6	6.0 ± 0.5
Dy (ppm)	2.5 ± 0.7	4.4 ± 0.8
Eu (ppm)	0.75 ± 0.10	0.78 ± 0.11
Fe (%)	2.70 ± 0.16	2.95 ± 0.15
Hf (ppm)	4.5 ± 0.5	4.7 ± 0.5
La (ppm)	27 ± 2	31 ± 2
Lu (ppm)	0.33 ± 0.05	0.36 ± 0.05
Mn (ppm)	606 ± 12	750 ± 15
Na (%)	4.97 ± 0.29	3.18 ± 0.19
Nd (ppm)	22 ± 10	28 ± 11
Rb (ppm)	94 ± 20	94 ± 16
Sb (ppm)	0.95 ± 0.22	1.3 ± 0.3
Sc (ppm)	10.7 ± 0.5	12.3 ± 0.6
Sm (ppm)	443 ± 75	121 ± 69
Th (ppm)	9.9 ± 0.8	11.6 ± 0.9
U (ppm)	1.4 ± 0.4	1.9 ± 0.4
V (ppm)	48 ± 10	112 ± 17
Yb (ppm)	1.9 ± 0.3	1.7 ± 0.3
Zn (ppm)	74 ± 6	65 ± 5

rences between the elemental concentrations, excepting a few elements as Al, Ba, Cl, Dy, Na, Sr, V. For all that, these can't point out a different origin of the lava from the both volcanoes formations which were studied.

REFERENCES

1. V. Sencu, „Vulcanii noroioşi de la Berca", Ed. Sport-Turism, Bucureşti, 1985.
2. S. Apostolescu, Proc. of the First Balkan Conference on Activation Analysis, Varna, May 6—8, 1985, p. 5.
3. R. M. Parr, *J. Radioanal. Nucl. Chem.*, **123** (1), 259 (1988).
4. M. de Bruin, P. M. van Wijk, *J. Radioanal. Nucl. Chem.*, **123** (1), 227 (1988).
5. R. A. Nadkarni, *Radiochem. Radioanal. Lett.*, **30** (5—6), 329 (1977).
6. T. Năşcuţiu, „Metode radiometrice de analiză", Ed. Acad. R.S.R., Bucureşti, 1971.
7. G. E. Baiulescu, T. Năşcuţiu, „Metode fizice de analiză a urmelor", Ed. Tehnică, Bucureşti, 1974.
8. W. R. Corliss, „Neutron Activation Analysis", U. S. Atomic Energy Commision, 1968.
9. R. H. Filby, A. J. Davis et al., „Gamma Ray Energy Tables for Neutron Activation Analysis", U.S.A., 1969.
10. G. Erdtmann, W. Soyka, „The Gamma-Rays of the Radionuclides", Verlag Chemie Weinheim, 1979.

STUDIA UNIV. BABEŞ—BOLYAI, CHEMIA, XXXIV, 2, 1989

XANTHOPHYLLS

V. Dynamics of Xanthophyll Monolayers at the Liquid/Air Interface

E. CHIFU*, MARIA TOMOAIA-COTIŞEL*, M. SĂLĂJAN*, ALEXANDRA CHIFU** and J. ZSAKÓ*

Received: April 25 1989

Experimental data with respect to time variation of the molecular area (recorded at constant surface pressure values) and to time dependency of the surface pressure (recorded at constant molecular areas) are presented for monolayers of xanthophylls, viz. astaxanthin ÷ 3,3′-dihydroxy-4,4′ dioxo-β-carotene and zeaxanthin ÷ 3,3′-dihydroxy-β-carotene, spread at the air/water interface. Varied relaxation mechanisms are proposed, using the Prout-Tompkins equation adapted to the dynamics of the monolayers at fluid interfaces.

In monolayers of insoluble surfactants spread at the air/water interface frequently relaxation phenomena may occur, consisting e.g. of a surface pressure decay at constant area. Such phenomena are observed especially if at the working temperature the surfactant is in solid state. In this case the monolayer can be compressed to surface pressures which overpass by far the equilibrium spreading pressure (ESP). Consequently, the monolayer at $\pi > \mathrm{ESP}$ will be in a metastable equilibrium, allowing the development of different relaxation phenomena, leading to the diminution of π and eventually a thermodynamic equilibrium is reached.

Many attempts were made to derive kinetic equations and to clear up the processes occuring at the molecular level.

Kinetic equations used. To describe relaxation phenomena in monolayers frequently was used the Prout-Tompkins equation of the form:

$$\log B_1 \equiv \log \frac{\alpha}{1-\alpha} = K_1 \log t + C_1 \tag{1}$$

where α stands for the collapsed monolayer fraction.

In conditions when the molecular area is maintained constant, Eq. (1) becomes [1, 2]:

$$\log B_2 \equiv \log \frac{\pi_0 - \pi_t}{\pi_t} = K_2 \log t + C_2 \tag{2}$$

where π_0 is the surface pressure recorded at $t = 0$, and π_t is recorded at a certain time t.

By using the condition $A = \text{const.}$ the film no longer needs to be compressed, but the unaltered portion of the monolayer does not remain under the same physical conditions, since the surface pressure descreases continuously.

* *Physical Chemistry Department, University of Cluj-Napoca 3400 Cluj, Romania*
** *Institute of Isotopic and Molecular Technology, 3400 Cluj-Napoca, Romania*

If π is maintained at constant value, the physical conditions are not changed, but a gradual compression of the film is needed.

For π = const. the following three mechanisms were proposed [3, 4]:

Mechanism 1. Relaxation is considered to consist in the formation of compact islets, which is described by

$$\log B_3 \equiv \log \frac{A_0 - A_t}{A_t - A_e} = K_3 \log t + C_3 \quad (3)$$

where A_0 stands for the molecular area at $t = 0$, A_t is the molecular area at a certain t, while A_c is the collapse area.

Mechanism 2. Formation of trilayers is viewed, which is described by:

$$\log B_4 \equiv \log \frac{A_0 - A_t}{A_t - A_c/3} = K_4 \log t + C_4 \quad (4)$$

Mechanism 3. A collapsed bulk phase is supposed to form, and this is described by

$$\log B_5 \equiv \log \frac{A_0 - A_t}{A_t} = K_5 \log t + C_5 \quad (5)$$

It is worthwhile to note that under the proposed conditions K_i and C_i are dimensionless constants. K_i does not depend on the time scale used, representing the slope of a straight line, but C_i does depend on the time units used since it is the ordinate intercept of the linear $\log B_i$ vs. $\log t$ plots.

At π = const, the relaxation may occur, depending on the surface pressure range, either in accordance with one single mechanism, or following a sequence of mechanisms, as observed in the case of apocarotenoids [3, 5] and of fatty acid [4] monolayers.

In the present paper we have investigated the relaxation of the monolayer of two xanthophylls, namely zeaxanthin and astaxanthin.

Experimental Part and Methods. The surfactants used were: zeaxanthin (3,3'-dihydroxy-β-carotene (ZX)) and astaxanthin (3,3'-dihydroxy-4,4'-dioxo-β-carotene (AX)), both of all-trans configuration synthetic commercial products (Hoffmann la Roche) of chromatographic purity.

Solutions used for the spreading were: benzene containing 2—3%(v/v) absolute ethanol in the case of ZX, and benzene with 4—8% (v/v) content of chlorophorm for AX. The solvents were of p.a. purity (Reactivul). The subphase consisted of double-distilled water.

Methods. Working temperature was of 20°C. Xanthophylls were spread at the air/water interface by a micropipet. Waiting time was between 5 to 15 min, allowing for complete evaporation of the spreading solvents and establishment of the internal equilibrium of the expanded film. Relaxation phenomena were followed, after compression to a certain π and A, in two ways:

— The surface pressure was maintained constant, and the variation of the molecular area with time was recorded;

— The molecular area was maintained constant, and the alteration of the surface pressure with time was recorded.

Table 1

The monolayer characteristics of ZX and AX

Parameters / Xanthophylls	A_0^*	A_c^*	π_c^{**}	C_{so}^{-1**}
ZX	0.49	0.30	40.0	103
AX	0.46	0.25	45.0	99

* in nm²/molec.;
** in mN/m

Film compression was effected discontinuously. To determine the surface tension the Wilhelmy method was used, for both types of experiments.

The experimental curves were processed by methods of linear and nonlinear regression, using computation programs in BASIC run on a "a-MIC" computer.

Results and Discussion. *Monolayer Characteristics of the Xanthophylls Used.* The compression isotherms of ZX and AX and their monolayer characteristics were studied elsewhere [6]. The latters are given in Table 1.

Relaxation of Xanthophyll Monolayers at A = const. Measurements were performed at several constant areas for both astaxanthin and zeaxanthin. The experimental curves $\pi = f(t)$ for ZX are plotted in Fig. 1.

Experimental data were processed according to Eq. (2). The such proces sed $\pi = f(t)$ isotherms linearize satisfactorily with all the cases studied, and for AX they are given in Fig. 2. As can be seen, the plots present two linear portions each, the first portion having a more accentuated slope than the second. Table 2 exhibits the kinetic parameters obtained by processing the $\pi = f(t)$

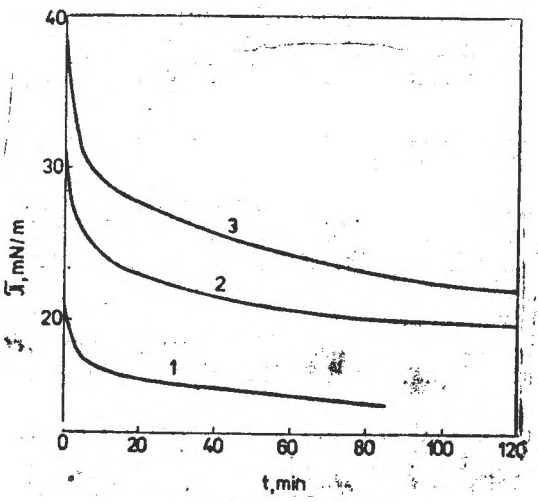

Fig. 1. Kinetic curves $\pi = f(t)$ at A = const. Curve (1) — A = 0.40 nm²/molec; (2) — A = = 0.34 nm²/molec; (3) — A = 0.305 nm/molec.

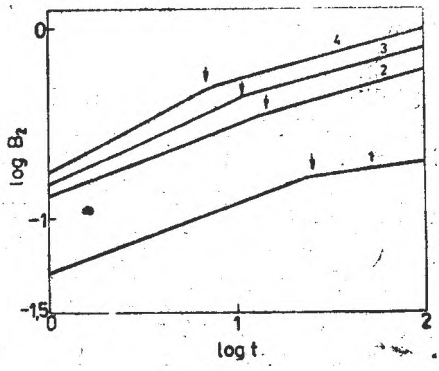

Fig. 2. Prout-Tompkins linearizations according to Eq. (2) for the monolayers of AX. Curve (1) — A = 0.38 nm²/molec; (2) — A = 0.32 nm²/molec; (3) — A = =0.27 nm²/molec; (4) — A=0.25 nm²/molec. Downward arrows (↓) indicate the slope change in the linearizations performed.

Table 2

The kinetic parameters obtained by processing curves $\pi = f(t)$ at A = const., according to Eq. (2)

Compound	A const nm²/molec	K_2'	t_2' min	ρ_2'	K_2''	t_{exp} min	ρ_2''
AX	0.38	0.3581	25	0.9986	0.1225	60	0.9895
	0.32	0.3816	15	0.9983	0.1790	70	0.9989
	0.27	0.4463	11	0.9993	0.2605	120	0.9989
	0.25	0.5277	7	0.9980	0.2549	120	0.9974
ZX	0.40	0.4186	15	0.9981	0.1816	85	0.9931
	0.34	0.4420	15	0.9972	0.3177	120	0.9991
	0.305	0.6582	5	0.9975	0.3253	120	0.9964

curves, and together with the slopes of the two linear portions (K_2' and K_2'') also gives the linear correlation coefficients (ρ_2' and ρ_2''), t_2' which indicates the slope change moment and t_{ex} which stands for the duration of the experiment evolvement since the instant ($t = 0$) when the area is maintained constant. Inspection of the linear correlation coefficients indicates a very good linearization, their values raising above 0.989. Existence of the two linear portions is indicative of the presence of two stages in the relaxation processes that emerge in the monolayer. The first, which is more rapid, can be assigned to a process of nucleation. The second, which is slower, could be considered as a growth process of the nuclei. This is plausible since the velocities of both processes increase with decreasing constant maintained area, i.e. with increasing initial pressure. On the same account, the time when the slope change is recorded — i.e. the time when transition from the nucleation stage to the growth of nuclei in the newly formed phase occurs — decreases when the area, maintained at constant value decreases.

The experimental data presented render the complexity of the processes emergent in the case of relaxation of monolayers, which implies processes of nucleation followed by an increase of the newly formed phase nuclei. Also, it is to be noted that these processes occur even at pressures far below the collapse pressure.

Relaxation Phenomena at π = const. In the case of ZX monolayers the relaxation phenomenon was pursued also under conditions when surface pressure, π, was maintained at a constant value. At small surface pressure, $\pi < 5$ mN/m, π is practically constant in time if the area is not modified, while at greater ones it can be maintained constant only if the area available for the monolayer decreases. Fig. 3 gives the plots of kinetic curves A as function of t for several constant maintained surface pressures. The pairs of experimental points (A_i and t_i) were processed by methods of non-linear regression following a third order polynomial, which describes satisfactorily the curves $A = f(t)$. The values of the coefficients of third order polynomials are given in Table 3.

We mention that these coefficients were derived by expressing the time in minutes.

Table 3

Values of the coefficients of polynomials $A = f(t) = a \cdot t^3 + b \cdot t^2 + c \cdot t + d$

π_{const}, mN/m	a	b	c	d
9.71	-2.71871×10^{-5}	4.08649×10^{-3}	−0.20123	51.2459
14.86	-5.01610×10^{-6}	1.28894×10^{-3}	−0.11482	43.0622
23.97	-3.97069×10^{-6}	9.86099×10^{-4}	−0.10165	39.7961
24.92	-7.90357×10^{-5}	9.54818×10^{-4}	−0.28320	40.1196
27.06	-1.21872×10^{-5}	2.13226×10^{-3}	−0.14298	35.3707
33.10	-6.70412×10^{-6}	1.50048×10^{-3}	−0.15148	29.5140
35.78	-9.80589×10^{-6}	2.13801×10^{-3}	−0.15884	28.4805

Table 4

Kinetic parameters derived by linearization of curves

π_{const}	A Å²/molec	K_3	C_3	t_3 min	ρ_3	A_4 Å²/molec	K_4	C_4	t_4 min	ρ_4	t_{exp} min
9.71	51.06 (51.25)	0.9118	−2.0880	12↓	0.9996	—	—	—	—	—	200
14.86	43.55 (43.06)	0.9623	−2.1872	20↓	0.9997	—	—	—	—	—	120
23.97	40.50 (39.80)	0.9689	−2.1487	30−40↓	0.9998	—	—	—	—	—	140
24.92	40.44 (39.62)	0.9500	−2.1130	16↓	0.9991	—	—	—	—	—	195
27.06	36.05 (35.37)	0.9506	−1.8305	30↓	0.9994	—	—	—	—	—	105
33.10	30.31 (29.51)	1.1980	−1.5455	16↑	0.9987	25.43	0.9704	−2.2756	50↓	0.9995	120
35.78	29.81 (28.48)	1.1552	−1.3646	8↑	0.9995	27.34	0.9248	−2.1546	30↓	0.9989	117

N.B. In parantheses the value of polynomial $A = f(t)$ at $t = 0$.

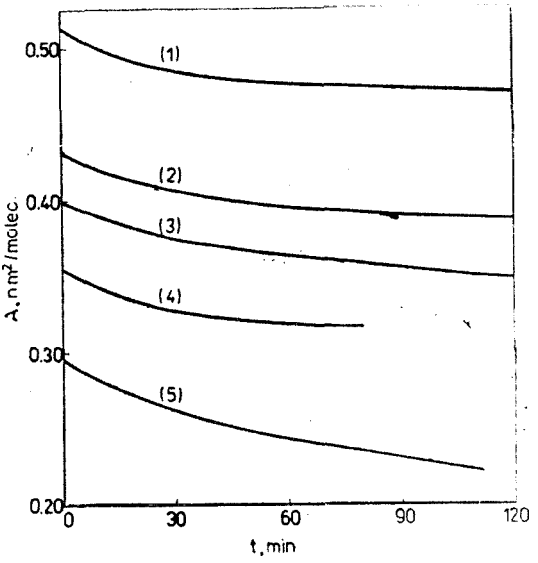

Fig. 3. Kinetic curves A = f(t) at π = const. for the monolayers of ZX. Curve (1) — π = 9.71 mN/m; (2) — π = 14.86 mN/m; (3) — π = 23.97 mN/m; (4) — π = 27.08 mN/m; (5) — π = 33.10 mN/m.

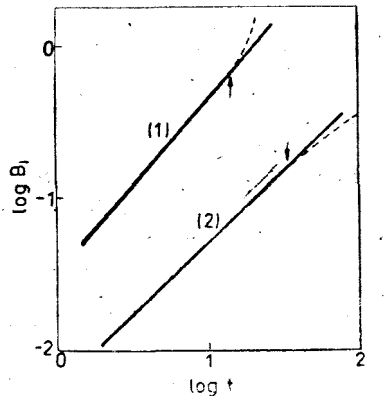

Fig. 4. Prout-Tompkins linearizations with ZX, at π = 33.10 mN/m. Curve (1) obeying Eq (3); (2) obeying Eq. (4).

The $A = f(t)$ type curves were linearized by the Prout-Tompkins equations proposed. Fig. 4 gives the plot of the linearization obtained for π = 33.10 mN/m. The linear portions of these plots were processed by the least squares method and the values are given in Table 4. It tabulates the constant pressure (π) for which the measurement was performed, the area at $t = 0$ (A) when the phenomenon starts — the rate constant (K_i), ordinate intercepts (C_i) corresponding to the linear portions obtained by means of Eq. (i), i.e. by presuming the mechanism (i—2); the time t_i, up to which equation (i) gives a good linearization, and the all-along experiment time (t_{exp}). C_i values given in Table 4 were derived by expressing the time in minutes. The values of the linear correlation coefficients (ρ_i) indicate a very good linearization of the curves $A = f(t)$ by means of Eq. (i).

Upon inspection of the data given in Table 4, one finds that at small and mean pressures the linearization is possible by applying Eq.(3), relaxation of the monolayer following mechanism 1, viz. formation of islets. Negative deviations from the straight line are found after time t_3, which is indicative of ceasation in the action of the mechanism i.e. an equilibration tendency in the system. This instance is indicated by downward arrows (↓) in Table 4. At high surface pressures ($\pi > 30$ mN/m), positive deviations from linearity (marked in Fig. 4 and Table 4 by upward arrows (↑)) are found after time t_3, which signifies a shift in the relaxation mechanism. Further on, linearization can be effected according to Eq.(4), the relaxation obeying mechanism 2 by forma-

tion of trilayers. We mention that the validity of Eq(4) in the second part of the experiment was performed by taking t_3 for the origin of the time scale and A_3 for A_0, i.e. a plot of log $\frac{A_3 - A_t}{A_t - A_c}$[13] vs. log $(t - t_3)$ has been performed. Then, after some other time negative deviations ($\downarrow$) are found, indicating that the action of the mechanism has ceased. Relaxation mechanism 3, which implies formation of a collapsed bulk phase, was not found with surface pressures within the present experiment.

Comparing the values of the linear portion slopes given in Table 4, only a slight increase of these is found with the increase of the surface pressure. In contrast to this behaviour, with the ordinate intercepts an accentuated increase is found in these, particularly at high surface pressures. Upon the shift from mechanism 1 to mechanism 2 no significant variation is found in the rate constant k of the process but the integration constant C_i becomes much less. The general picture is similar to that observed with apocarotenoids [3, 5] and fatty-acids [4]. As shown earlier [5], the parameter C_i seems to be related mainly to the nucleation rate. Consequently, its important increase with increasing working surface pressure is quite reasonable. Also, its decrease may be expected when the relaxation mechanism is changed and experimental results agree with this expectation (see Table 4). The rate constant K seems to be related to the ratio between the rate of growth and the rate of nucleation. This parameter was found to silghtly increase with increasing π, but to be determined mainly by the molecular structure of the film forming substance and not to be modified essentially by the shift of the relaxation mechanism [5].

We can conclude that the Prout-Tompkins type equations describe rather satisfactorily the relaxation phenomena emergent in xanthophyll monolayers, and the values of the kinetic parameters obtained show a similar dependence on working conditions and relaxation mechanisms as observed with other substances.

REFERENCES

1. Baglioni, P., Gabrielli, G., and Guarini, G. T., *J. Colloid Interface Sci.*, **78**, 347 (1980)
2. Tomoaia-Cotişel, M., Sen, A. and Quinn, P. J., *J. Colloid Interface Sci.*, **94**, 390 (1983)
3. Tomoaia-Cotişel, M., Zsakó, J., Chifu, E., Cadenhead, D. A. and Ries, H. E., Jr., „Progress in Photosynthesis Research" (J. Briggins, Ed.), Martinus Nijhoff Publishers, Dordrecht, Vol. II, 1987, p. 333
4. Tomoaia-Cotişel, M., Zsakó, J., Mocanu, A., Albu, I. and Chifu, E., *Studia Univ. Babeş—Bolyai, Chem.*, **32** (1), 58 (1987)
5. Tomoaia-Cotişel, M., Zsakó, J., Chifu, E. and Cadenhead, D. A., *Langmuir* (in press)
6. Chifu, E., Zsakó, J., Tomoaia-Cotişel, M., Sălăjan, M. and Albu, I., *J. Colloid Interface Sci.*, **112** (1), 241 (1986)

STUDIA UNIV. BABEŞ—BOLYAI, CHEMIA, XXXIV, 2, 1989

A NEW SEPARATION AND IDENTIFICATION METHOD OF NAPHAZOLINE HYDROCHLORIDE

CONSTANTIN MĂRUŢOIU*, IONEL HOPÂRTEAN**, LIDIA GHEBAN*** and MIRCEA VLASSA*

Received: February 24 1989

The results obtained by a new detection method of naphazoline hydrochloride 2-(1-naphtylmethyl)-imidazoline hydrochloride using 0.01% solution of 9-hydrazinoacridine in ethanol as visualizing agent are reported.

Kex-words: imidazole, thin-layer chromatography, acridine reagent.

Introduction. Naphazoline hydrochloride 2—(1-naphtylmethyl)-imidazoline hydrochloride is a sympathomimetic vasoconstrictory of nose mucous membrane, used as drug. This compound was prepared by different procedures [1—4]. The purification of raw material is troublesome and is achieved by repeated extractions.

The purity of the product was checked-up by paper [5—7], column [8] or thin layer chromatography [9—10]. The last method makes use of precoated plates with silica gel G as the stationary phase and cyclohexane : benzene : diethylamine (75 : 15 : 10) or benzene : acetone : ammonia (20 : 75 : 5) as the mobile phase. The spots were visualized by spraying with Dragendorff reagent or 5% ferric chloride solution [6], bromophenol blue or potassium permenganate [7], 5% sodium nitrite solution or iodoplatinate [9] and mercuric nitrite or sulfuric acid [10].

The present work reports on the results obtained by using 9-hydrazinoacridine as the spraying reagent for detection of naphazalene hydrochloride.

Experimental. Glass plates 20 × 20 cm covered with 0.3 mm thin layer of silica gel R containing a 1 : 1 starch : agar-agar mixture as binder were used. Ascending development over a distance of 10 cm. was done in a normal chromatographic chamber with benzene : acetone : 25% ammonia (30 : 65 : 5). 0.1% acetone or methanolic solution of naphtylacetonitrile, water solution of purified naphazoline hydrochloride, ethylenediamine or naphazoline hydrochloride obained at the first extraction, were applied to the plates by a micropipete.

After development the plates were dried for 5 min., and finally sprayed with a 0.01% solution of 9-hydrazinoacridine in ethanol and examined in ultraviolet light of 254 nm wave lengh.

Results and discussion. The experimental results are shown in Fig. 1. From his data we can conclude that one extraction is not enough for naphazoline hydrochloride purification. The first extract contains naphtylacetonitrile, naphazoline hydrochloride and other five compunds. Among these unreacted ethylenediamine, piperazine formed from ethylenediamine at 250°C, and other secon-

* *Institute of Chemistry Cluj-Napoca, 3400 Cluj-Napoca, Romania*
** *University of Cluj-Napoca, Faculty of Chemical Technology, Organic Chemistry Department, 3400 Cluj-Napoca, Romania*
*** *Terapia Drugs Factory, 3400 Cluj-Napoca, Romania*

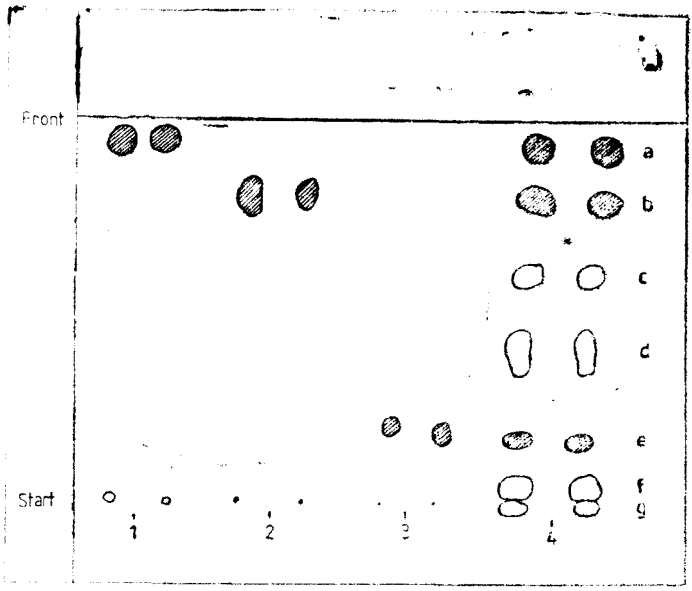

Fig. 1. Chrombtogram of the mixture separated on silica gel R with benzene: acetone:25% ammonia(30:65:5). 1=nitrile; 2=naphazoline hydrocloride; 3=ethylenediamine; 4=first estraction of raw naphazoline hydrohloride (a=nitrile; b=naphazoline hidrochloride; c=d=f=g=unknown compounds; e=ethylenediamine).

dary products which appeared as a result of the condensation reactions of naphtylacetonitrile with ethylenediamine were identified.

Conclusions. This method is suitable for check-up the purity of naphazoline hydrochloride. The spraying reagent (0.01% ethanolic solution of 9-hydrazinoacridine) allows the detection of the above mentioned compound with a detection limit of 0.01—0.05 μg/spot at 254 and 366 nm wavelengths.

REFERENCES

1. Swiss Pat. 221, 216 (1942); *Chem Abstr.* 43, 692 (1949).
2. Z. Bankowska, J. Deles, J. Wolinski, Prezemyl Chem, **9**, 463, (1953); *Chem. Abstr.*, **49**, 11627, (1955).
3. Brit. Pat., 608, 295 (1948); *Chem. Abstr.*, **43**, 5048, (1949).
4. V. Zotta, „Chimie farmceutică", Ed. Medicală, București, 1985.
5. E. Vidic, J. Schnette, Arch. Pharm., **295**, 342 (1962); *Chem. Abstr.*, **57**, 7388, (1962).
6. W. Seydel, K. Gereck, *Arzneimittelstandardisierung*, **6**, 38, (1965); *Chem. Abstr.*, **65** 16790 (1966).
7. E. Pawelczyk, Z. Platkowiakowa, *Dissertationes Pharm.* **17**, 75 (1965) *Chem. Abstr.*, **63**, 6793 (1965)
8. J. Molina, R. D. Poe, *J. Pharm. Pharmacol.*, **20**, 481 (1908); *Chem. Abstr.*, **69**, 30161 (1968).
9. J. Sunshine, W. W. Fike, H. Landesman, *J. Forensic. Sci.*, **11**, 428 (1966); *Chem. Abstr.*, **66**, 16972 (1967).
10. S. Goenechev, *J. Chromatogr.* **36**, 375 (1968).

STUDIA UNIV. BABEŞ—BOLYAI, CHEMIA, XXXIV, 2, 1989

THE RECOVERY OF SULFUR DIOXIDE FROM INDUSTRIAL GASES

J. VODNÁR

Received: March 20 1989

The paper presents a lot of experimental results obtained by studying the absorption of sulfur dioxide from different industrial gases, using as an absorbant N-methyl-pyrrolidone in a permanent recycling [1]. The apparatus used [2] enables the absorption either in an ascending turbulent liquid film or in a pelliclizing-bubbling system. It assures a uniform and self distribution of the absorbent and the gas in the contacting tubes. The absorbent and the sulfurous gas was used in a counter current, but the pelliclizing or the pelliclizing-bubbling of the absorbant took place in a common tide. The apparatus was a Vodnár type column, having three contacting plates and was equipped with pelliclizing tubes of which total length was 1,73 m, inner diameter 27,5 mm and the inner surface, where the absorption takes place, was 0,149385 m².

The paper presents and discusses the experimental results obtained by studying the absorption of sulfur dioxide from different gases, using as an absorbent N-methyl-pyrrolidone in a permanent recycling [1]. The apparatus used was a Vodnár type column with three contacting plates where the absorbent and sulfurous gas was contacted in a counter current, but the pelliclizing phenomenon took place in a common tide [2]. It assures a uniform and self distribution of the liquid and the gas in the contacting tubes which had a total length of 1,73 m, inner diameter of 27,5 mm and an inner surface where the absorption takes place equal 0,149385 m².

Experimental. Experiments were made in a micropilot apparatus of column type. The ascending liquid pellicle (film) on the inner surface of the pelliclizing-bubbling tubes, in a continuous tide was formed. The absorbent (N-methyl-pyrrolidone = NMP) was used in a continuous tide and it was introduced with an adaquate pump. The recycling and mixing of the absorbent were self induced and continouus. The necessary sulfur dioxide was taken from a steel cylinder vessel and the air was ensured by an adequate compressor.

Sulfur dioxide content of the gas mixture was determined iodometrically and the absorbed sulfur dioxide by acid-base titration, too. Temperature was mentained at 18,85 °C. NMP was introduced continuously in the upper plate of the column and the solution resulted by absorption was eliminated on the same way, from the lower plate.

Gas flow varied between 3,5 and 12,3 m³/h, and that of the absorbent between 2 and 9,8 l/h. Sulfur dioxide content of the gas mixture was mentained on a constant value of 0,5 vol%. in every experiments.

The absorption of sulfur dioxide in NMP can be presented by the following physical process:

• *University of Cluj-Napoca, Faculty of Economic Sciences, 3400 Cluj-Napoca, Romania*

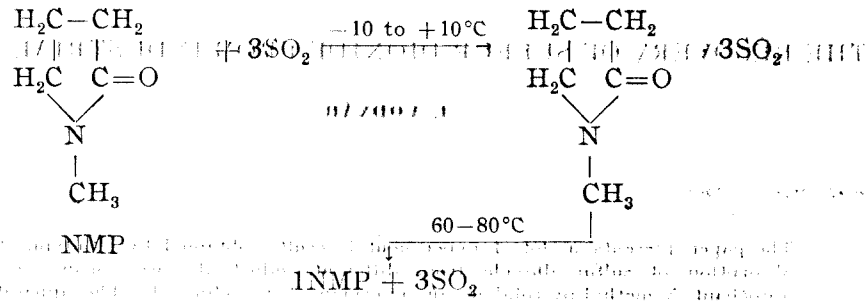

Results and discussion. In the first series of experiments the dependence of the absorption degree (g_a [%]), versus the gas flow (Q_g [l/h]) was studied. The results obtained was illustrated in figure 1. The flow of the absorbent was mentained on a constant value of 5,2 l/h. We can see that in the used conditions of work, the absorption degree attains 96%, if the gas flow decreases from 12,3 to 6 m³/h.

In the second series of experiments the dependence of the absorption degree, versus the absorbent flow (Q_a [l/h]) was studied The results obtained was illustrated in figure 2.

Figure 2 shows that using a constant gas flow of 12,3 m³/h, the absorption degree attains 98%, if the absorbant flow increases to 8 l/h. This result demonstrates that NMP is a very good absorbent of sulfur dioxide.

If the NMP—SO_2 solution resulted by the absorption of SO_2 is heated to 60—80°C, sulfur dioxide is desorbed and can be recycled in the industrial installation, or can be liquified and used for different chemical purposes [3, 4].

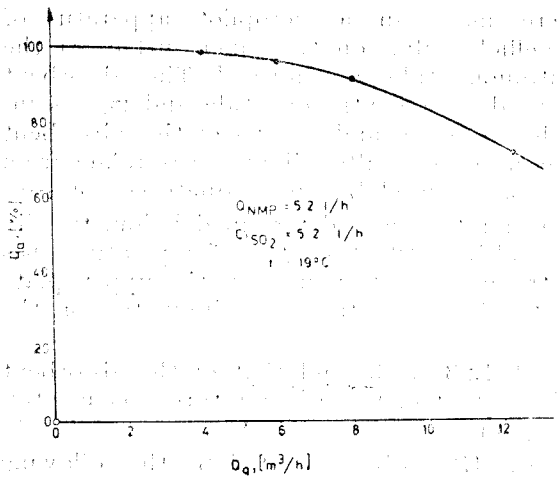

Fig. 1. The dependence of the absorption degree (g [%]), versus the gas flow (Q_g [m³/h]).

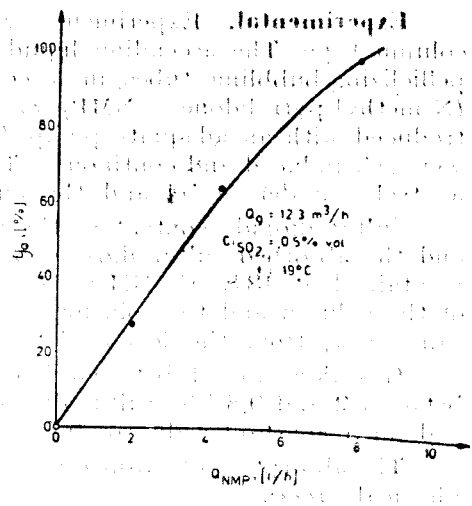

Fig. 2. The dependence of the absorption degree, versus the absorbent flow (Q_a [l/h]).

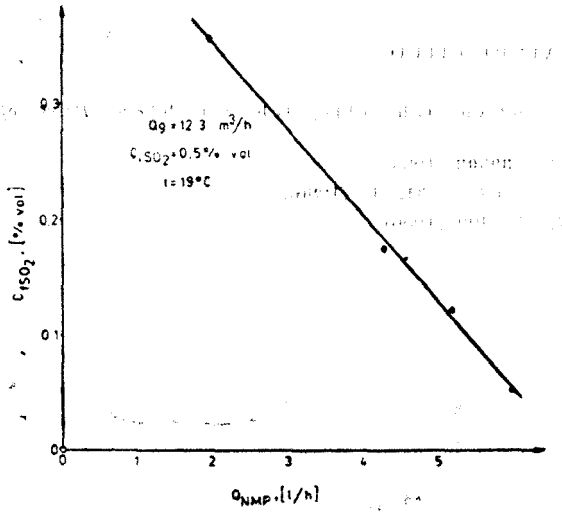

Fig. 3. Sulfur dioxide content of the purified gas (vol. %), versus the absorbent flow.

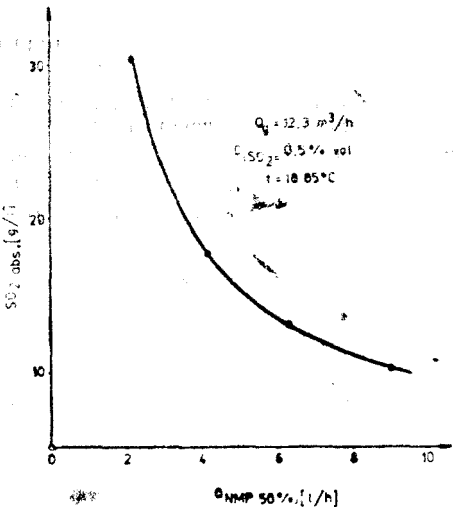

Fig. 4. Variation of the quantity of absorbed sulfur dioxide ($gSO_2/l.h$), versus the absorbent flow.

In figure 3 is illustrated the influence of the absorbent flow, versus the sulfur dioxide content of the purified gas. As we can see, this content can be reduced from 0,5 vol.% to 0,05 vol.%, if the absorbent flow increases from 2 to 6 l/h.

On the base of the presented and discussed experimental results we can state, that the decreasing of the specific consumption of the absorbent is equal 18,36% (mentaining the degree of absorption on 98%), in comparison with the case when the absorbent is not recycled.

In the 4th series of the experiments was studied the variation of the quantity of absorbed sulfur dioxide ($gSO_2/l \cdot h$), versus the absorbent flow (l/h), which in this case was a water solution of NMP having a concentration of 50 vol%. The used temperature was 18,85°C, the gas flow 12,3 m^3/h and the absorbent flow 2,19 l/h (water solution of NMP, 50 vol.%). But the absorption degree in such conditions is not higher than 38%. Inspite of this, when the gas flow is lower than 2 m^3/h, the absorption degree increases to 98%.

The value of the coefficient of total mass transfer (K_g) was calculated, using the following experimental data: initial SO_2 content of gas 0,5 vol.% = = 14,2793 g/m^3; total gas flow 12,3 m^3/h; total initial pressure 769,129 Hgmm; degree of absorption 98,55%; absorbed quantity of SO_2 0,1730885 kg/h; initial partial pressure of SO_2 3,8456 Hgmm; final partial pressure of SO_2 0,05576 Hgmm motive power of the absorption 0,89618 Hgmm; surface area of absorption 0,149385 m^2.

$$K_g = \frac{0,1730885}{0,149385 \ (0,89618/760)} = 982,603 \, [\text{kg } SO_2/m^2 \cdot h \cdot \text{atm}] =$$

$$= 15,3531 \ [\text{kmole } SO_2/m^2 \cdot h \cdot \text{atm}].$$

LITERATURE CITED

1. J. Vodnár, C. Tohătan, V. Bozîntan, Gh. Ilie, Gh. Grebleş, *Patent oj R. S. Romania* Nr. **82661** (1983).
2. J. Vodnár, *Patent of R. S. Romania* Nr. **89508** (1985).
3. J. Vodnár, *Stud. Univ. „Babeş—Bolyai" Chem.* **31,** 37 (1986).
4. J. Vodnár, *Rev. Chim.,* Bucureşti, **37,** (2), 499 (1986).

STUDIA UNIV. BABEŞ—BOLYAI, CHEMIA, XXXIV, 2, 1989

MOLECULAR STRUCTURE MODELATION BY USING A BASIC LINE FORMULA INTERPRETER

D. HORVATH* and I. SILAGHI-DUMITRESCU*

Received: May 10, 1989

A computer program has been written in BASIC, for COMMODORE 64 which automatically generates the tridimensional structure of a molecule from its line formula. The output may be used in molecular orbital, molecular mechanics or QSAR studies.

Introduction. One of the preparatory steps in quantum mechanical or molecular mechanics treatment of molecules is the input of the initial structures, usually, in the form of cartesian atomic coordinates. For this, often some additional computing is needed, just to transform the known or assumed structural data (bond lengths, bond angles, dihedral angles) into coordinates of atoms. This problem is also connected to the storage and retrieval of structural information for QSAR studies [1]. Various solutions proposed include atomic and bond numbering [2] or sophisticated hard dependent systems [3—5].

In this paper, a simple chemical formula interpreter is developed. Its task is a) to identify and to count the atoms of chemical formula; b) to convert the atomic sequence into a topological matrix — the adjacency matrix- which contains information about all neighbours of a given atom and c) to calculate the atomic coordinates for a certain conformation and given bond lenghts, bond angles and dihedral angles.

Line Formula. Interpeter (LFI). Our LFI is written in Basic and operates on linear formulae of molecules. These are graph theory based unambigous representation of molecular topology [6,7.] In Basic, a linear formula is a string X$ consisted of a sequence of valid symbols. These may be the usual chemical symbols of elements or special ones, like "—", "=", "#" (for single, double or triple bonds), "(",")", "", "", indicating side chains or repetitions of elements included. The extremly simple way of encoding can be shown in the following examples:

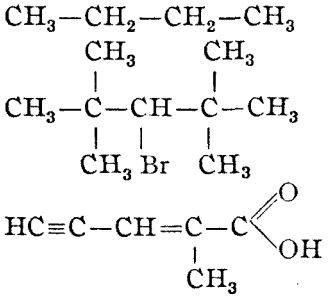

H[C(H2)]4H

HC[(C(CH3)3)]2BR

HC#CC(H)=C(CH3)C(=O)OH

* *Chemistry Departament, University of Cluj, R—3400 Cluj, Romania*

At this point we note that for a molecule, many linear formulae may be se up, differing in the sequence (numbering of atoms), but, eventually the adja cency matrices describe essentially the same structure. If some additional rule are observed in writting LF (i.o. IUPAC rules), the adjacency matrix coul unequivocally be related to a specified molecular geometry. From this poir of view, our LFI may also be of interest in fragment recognition for QSA studies.

Line formula analysis. As a result of encoding, all atoms of a molecu are divided in two sets: a) atoms not included in parenthesis — first orde or main chain atoms and, b) those enclosed in parenthesis — or side chain For example, if K$ = "HC(H2)C(CH3)CC(H2)CH3", the first order chai contains six atoms: HCCCCH. Side chains may be concatenated. Thus, th n-th order chain starts with an atom belonging to the (n−1)-th order chai and ends with a monovalent atom.

The program accepts as many concatenated side chains as are necesary t describe any complex structures. In the above example C_2—C—H, C_3—C—H C_3 —C—C—H are second order chains. Once K$ entered, the computer look for pairs of brackets "[...]" and extends K$ with the content of each pa according to its multiplicity:

H[C(H2)]4H H—CH_2—CH_2—CH_2—CH_2—H

In the next step, the conjugation of parenthesis is analysed. For this, K$ read from left to right, searching for ")" and "(" symbols. Each time, the firs opened parenthesis found, pairs the last unclosed one:

HC(H_2)C(CH_3)(C(H_2)CH_3)C(H_2)CH_2H

After parenthesis and brackets have been located and paired, the identificatio of chemical symbols follows. For each curent chemical symbol, left side an right side neighbours are searched, until the complete set of neighbours established and, hence, the adjacency matrix is known.

Molecular geometry. In order to compute the cartesian coordinates atoms, first, a planar formula of the compound is "written". The main cha is put on the Ox axis, the first, monov lent atom, being located at the origi Second order chains lay perpendicular the Ox axis (on Oy) and start each tin with an atom on Ox. Third order chai are perpendicular to Oy (parallel to O and so on. The bond lengths are take from SGEOM file. As starting points, the bond lengths may be taken as the sum covalent radii of atoms.

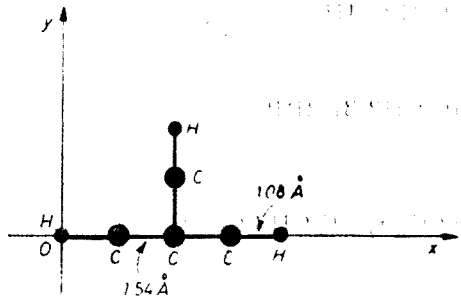

Fig. 1 The planor groph of 2-methyl-propane

Such a planar graph for 2-methy propane is shown in figure 1

Now rotations should be applied

each atom till all bond angles reach the values taken from SGEOM file. In the example of fig. 1 the rotations are done to make tetrahedral angles. (Figure 2)

It is necessary, also to get the correct orientation of higher order chains so that dihedral angles reach the desired values. The direction of the rotation axis is obtained as a double vectorial product $\bar{m} \times (\bar{r}_1 \times \bar{r}_2)$ (figure 3).

where $\bar{m}$ is a unitary vector bisecting ($\bar{r}_1$' $\bar{r}_2$) angle.

All these geometrical transformations are performed by FROTATE subroutine which rotates a set of points along a rotation axis having specified its directory cosines. The points to be rotated are selected by subroutine FSEL. This procedure uses the topological matrix and fragments the molecule in a fixed and a mobil part, respectively. The first atom of the mobil fragment is identified and the mobil fragment includes all atoms which have at least one path connecting them with the first atom.

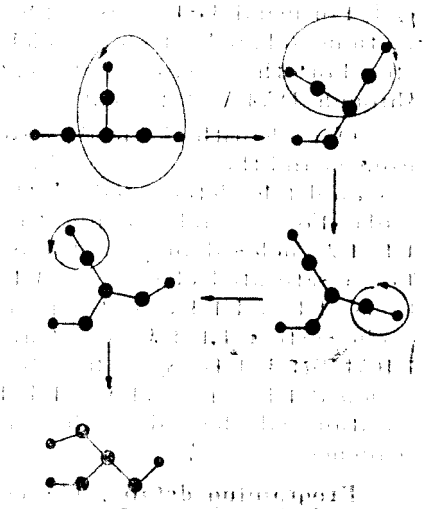

Fig. 2. Rotations applied to the planar structure of fig. 1 to get tetrahedral bond augles

After all higher order chain rotations have been complished, missing monovalent (terminal) atoms are added if necessary. The standard geometrical parameters from SGEOM file affords the staggered conformation of molecule to be computed.

Cyclic systems. From topological point of view, the cyclization is assured by elimination of two monovalent atoms from the molecular graph. The adjency matrix and the list of ligands bound to each atom are, consequently, rearran-

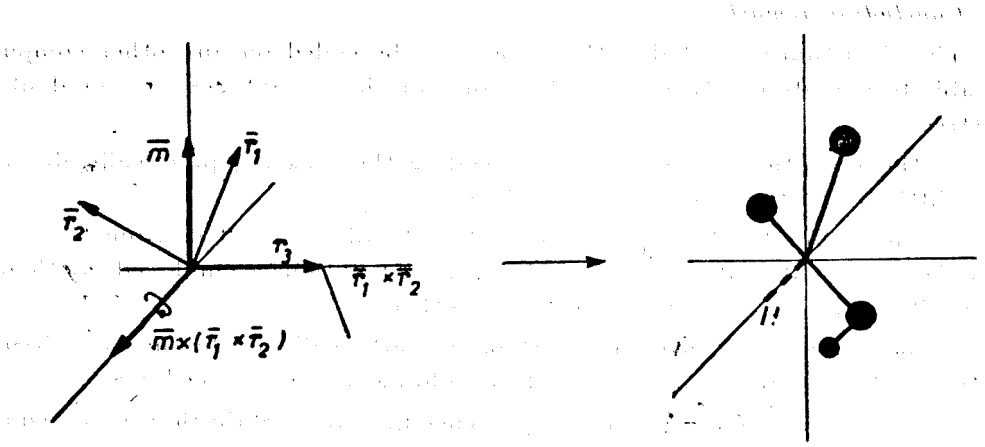

Fig. 3. Setting up a relation oxis around a „methylene" group

ged. For usual 3, 4, 5, 6 and 8-atomic cycles SGEOM enables standard confor mations (chair-boat for cyclehexane, chari-chair, chair-boat for cyclooctan etc.) For other desired conformations, geometrical parameters should be provide through DATA statements.

Our algorithm affords also a direct correlation of a configuration (steri isomer) and the way of encoding the structural formula. Thus, the configuratio is completely determined by the relative positions of ligands in the linear for mula. For example, in unsaturated compounds —C(L1)=C(L2)—, the ligand L1, L2 enclosed in paranthesis are disposed in the same part of the π bond For a saturated chain ...C(L1)(L2)C(L3)(L4) ..., L1 and L3 are in *treo* posi tions; L1 and L4 in eritro positions respectively. If this is a fragment from cyclic system, L1, L3 are in trans, and L1, L4 in cis. For a chiral carbon ator L1C(L2)(L3)(L4), according to the usual rules [8], we assume an R configu ration if $L1 < L2 < L3 < L4$. For other arrangements of ligands, the configu guration will depend on the number of permutations which lead to the abov sequence.

Programing detalis. The computer program was written for a COMMO DORE 64 with BASIC extension which supports high resolution graphics. decoded structure may be visualized through usual ball and stick models o by spacefilling. It can be rotated in space in any direction (Newmann projec tion may result in this way), or translated at will. Also copies on to a graphi printer are available. A special interactive routine have been devised to mo dify and control the geometrical parameters. As the longest string accepted b the C-64 system may not exceed 80, and, on the other hand, long line for mulae are not easy to input, a file — FRFILE — containing the most com mon molecular fragments have been created. Making use of this file, com plex structures may be constructed from their simpler fragments, by indica ting the positions where these fragments should be appended to the mai chain of molecule. The flow chart of the program is shown in the Appen dix.

Concluding remarks

The algorithm presented in this paper may be coded on any other compu ter able to operate on string variables. Some of the advantages we would lik to stress are:

— the operation is very easy, as coding the formula, practically differ very little from the usual chemical language.

— Chemical structures may be automatically generated from the lin formula, or semiatomatically, when the fragment option is employed. Both o these alternatives, however, support each other.

— The program is modular, most of its parts call merely the same basi routines. It may be easily extended by adding up new procedures.

— the observation of some simple encodig rules establishes a univoqu line formula- structure relation.

APPENDIX

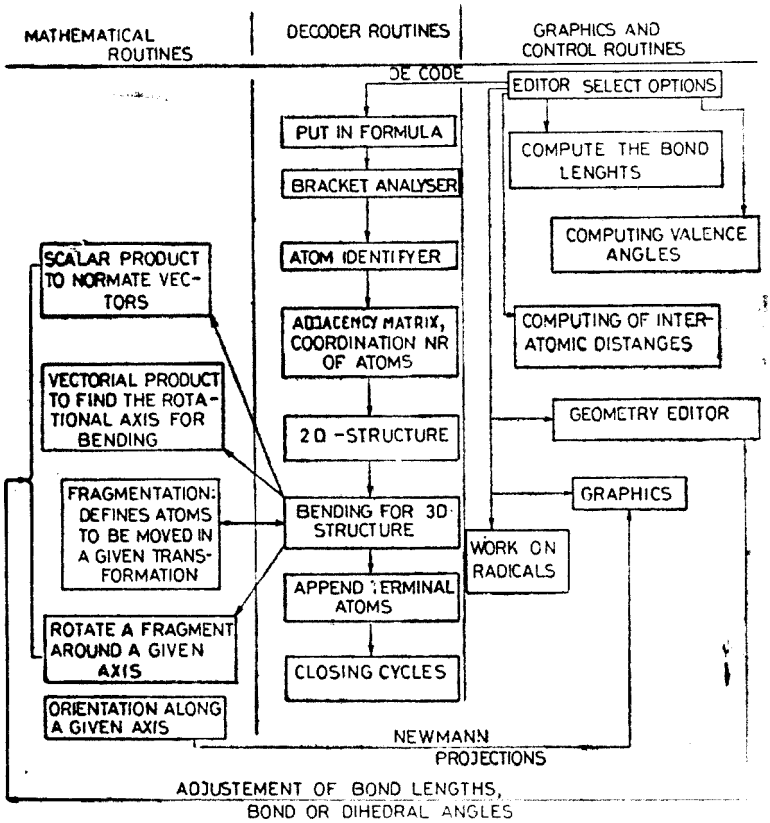

— The adjacency matrix, automatically obtained during the analysis of ine formula may be used further in calculation of topological indices, useful n QSAR studies.

LITERATURE

. A. J. Stuper, W. E. Brugger, P. C. Jurs, "Computer Assisted Studies of Chemical Structure an Biological Function", John Wiley & Sons, New York, 1979.

. F. H. Allen, D. R. Rogers, *Acta Crystallogr.*, B**25**, 1326 (1969).

. W. E. Brugger, P. C. Jurs, *Anal.yt. Chem.*, **47**, 781 (1978).

. W. E. Brugger, P. C. Jurs, UDRAW (Program No. 300). QCPE, Indiana Univ., Bloomington, Indiana, 47401.

. S. R. Niketic, K. Rasmussen, "The Consistent Force Field. A Documentation", Springer-Verlag, Berlin, 1977.

. A. T. Balaban (Ed.), "Chemical Applications of Graph Theory", Acad. Press New York, 1976.

. C. W. Marshall, "Applied Graph Theory", John Willey & Sons, New York, 1971.

. R. S. Cahn, C. Ingold, V. Prelog, *Angew. Chem.*, **78**, 413 (1966).

STUDIA UNIV. BABEŞ—BOLYAI, CHEMIA, XXXIV, 2, 1989

CONTRIBUTIONS TO THE FORMULATION AND NOMENCLATURE OF HETEROPOLYOXOMETALATE ANIONS

ADRIAN PĂTRUŢ*, GHEORGHE MARCU, ALEXANDRU BOTAR* and ADRIANA NAUMESCU****

Received: July 14 1989

The paper proposes a general formulation and a systematic nomenclature of the heteropolyoxometalate anions. Some relevant examples are presented.

Heteropolyanions represent a distinct class among the coordination compounds generally and the polyions especially; they are characterized by high symmetry, cohesion and stability of the structural pattern.

Heteropolyanions are usually known under the most common and widespread formula that has consacrated them:

$$X_xM_mO_y^{-}, \qquad (1)$$

corresponding to a cage-like structure, that consists of quasioctahedral MO_6 groups, in which a transitional metal M (addendum) is coordinated by oxygen atoms (oxo ligands), and which are condensed around one or more heteroatoms X (actually, primary group(s) XO_n, n = 4; 6; 8; 12). The MO_6 groups share edges, corners and edges or corners and faces with one another.

In the last few years, for the traditional term of heteropolyanions, that shows only the existence of a polyanion containing one or more heteroatoms, some alternative terms have been proposed, such as polyoxoanions, which underlines the unic or majoritary ligand nature, or heteropolyoxometalate anions, which also specifies the addenda nature. In the present paper, we propose to use the term heteropolyoxometalate anions (HPOM—A), which we considere to be more appropiate and suggestive.

In spite of the fact that numerous articles are dedicated to HPOM—A, only a restricted number of systematic works, such as general monographs [1—3] or extended studies [4—14], of which few are recent, are mentioned in the litterature.

Formulation of HPOM—A. In the last twenty years, numerous research has led to the synthesis of more and more complicated heteropolyoxoanionic structures, that got farther and farther from the traditional formula (1). HPOM—A with mixed addenda, HPOM—A "ligands" and "complexes", HPOM—A with organic or organometallic groups are conclusive examples in this sense. The aspects presented explain the diversity of classifications and formulations used for HPOM—A by various authors.

* *Institute of Chemistry, 3400 Cluj-Napoca, Romania*
** *University of Cluj-Napoca, Faculty of Chemical Technology, 3400 Cluj-Napoca, Romania.*

In our view, a general formula, includnig the HPOM—A known up to the resent, is of the type:

$$H_hE_eX_x \ldots Z_z \ldots M_m \ldots O_yL_l \ldots ^{q-}, \quad (2)$$

here H = non-substitutable hydrogen, E = encripted cation, X = primary eteroatom, Z = secondary heteroatom, M = addendum, O = oxygen (oxo), = ligand different from oxo, and ... may indicate the existence of more hemical species with the respective function.

According to the general formula (2), the heteroatoms are placed before ıe addenda. In the case of HPOM—A with heteroatoms in non-equivalent tes (primary and secondary), the primary heteroatom (or the primary hete- ɔatoms, noted in alphabetical order of the symbol) is always placed before the econdary heteroatom (or the secondary heteroatoms, noted in alphabetical order f the symbol).

In the case of HPOM—A with mixed addenda, the addenda are noted ı alphabetical order of the symbol. In the case of the presence of one or more gands other than oxo, which coordinate either the primary heteroatom or ıe secondary heteroatom, or are introduced by substitution reactions, these gands are placed after oxygen in alphabetical order. The non-substitutable ydrogens are placed at the beginning of the formula, while those belonging to polyatomic ligand are included in the respective ligand (ex. OH, H_2O). Finally, ıe encripted cation in HPOM—A cryptates is placed before the heteroatoms. he anion can be preceded by a symbol indicating the isomer. The inclusion the anion in square brackets is optional. Square brackets are obligatory only hen the HPOM—A is noted with the external cation(s) in case of an acid HPOM acid) or a salt (HPOM compound) formula.

An alternative formula, with a modified sequence of the constituents, is lmitted in the case of HPOM—A "complexes", which are formed by the ɔordination of a cation Z as a secondary heteroatom by a HPOM—A "ligand", ıe latter being in a proportion higher than 1. In the alternative formula, of ıe type Z_z (HPOM—A "ligand")$^{r-}_n$, where $n > 1$, the secondary heteroatom placed before the HPOM—A "ligand".

Nomenclature of HPOM—A. The current nomenclature of heteropolyanions, commended by IUPAC in 1970 [15], is far too simple to be applied to com- icated structures. On the other hand, the nomenclature of polyanions sug- ɛsted by Jeannin and Fournier [3] and recommended by IUPAC in 1987 [16], hich offers structural information and allows isomer differentiation, is too aborate for routine names. Therefore, HPOM—A with complex structures are dinarily presented under a certain formula without being named.

To name the anions that represent the subject of this paper, we shall use systematic nomenclature, which can be properly applied to the known HPOM -A, unless particular structural data are in view:

1. Indication of Constituents

1.1. The following order and rules are recommended for general constituents:

1.1.1. The groups containing addendum are indicated by naming the cha- ɛcteristic element (usually, by the Latin name, with the elision of the -(i)um

termination, except for tungsten, which has the specific English name, witl the elision of the -en termination), with the -o termination (ex. molybdo, va nado, niobio, tantalo, respectively tungsto). In the case with more than on chemical species as addendum, the different groups are indicated in alphabe tical order. In the case with more ionic species of the same element as adden dum, the corresponding groups are indicated in decreasing order of the oxidatio number.

1.1.2. The primary group(s) containing the primary heteroatom(s) is(are indicated by naming it (them) as anion, with -- ate termination (ex. phos phate, silicate, antimonate, ferrate). In the case with more than one chemica species as primary heteroatom, the different primary groups are indicated i alphabetical order.

1.2. The following order and rules are recommended in the case with on or more particular constituents:

1.2.1. The group(s) containing the secondary heteroatom(s) is (are) indicate by naming the characteristic element (usually, by the Latin name, identical witl or different from the English name, with the elision of the -(i)um termination except some cases, which have the specific English name, with the elision o final letters), with the -o termination (ex. chromo, mangano, ferro, cupro, res pectively tungsto, nickelo, antimono), just before the groups containing adden dum. In the case with more than one chemical species as secondary heteroa tom, the different groups are indicated in alphabetical order.

1.2.2. The encripted cation is indicated by the English name in two brac kets: round inside and square outside, before the group(s) containing primary heteroatom.

1.2.3. The non-substitutable hydrogen(s) is(are) indicated in round brackets before the other constituents.

1.3. The following rules are recommended for ligands:

1.3.1. Oxo ligands (oxygen atoms) are not indicated as such.

1.3.2. Ligands different from oxo are indicated in square brackets, direc tly after the groups they are part of. For non-terminal ligands that simulta neously coordinate atoms with different functions, the following coordinatio priority is considered: primary heteroatom, secondary heteroatom, addendum

2. Notations, Prefixes and Graphical Signs

2.1. General and particular constituents are separated by hyphen.

2.2. The stoichiometric proportions of the constituents different from ox are indicated by an Arabic numeral that precedes their name. Numerical Greel prefixes should be avoided, as they are considered inadequate for large propor tions. The hyphen placed after the numeral is optional.

If the Arabic numeral which indicates the stoichiometric proportion ma generate confusions with reference to the name of a constituent, supplementar round brackets are used to include its name.

2.3. The HPOM—A charge is optionally indicated at the end of the name in the Ewens-Bassett system (by an Arabic numeral, followed by the charg sign, placed in round brackets).

2.4. If necessary, the oxidation number of primary heteroatom(s) and/o secondary heteroatom(s) and/or addendum (addenda) and/or encripted catio

is indicated in the Stock system (by a Roman number, placed in round brackets, directly after the name of the corresponding constituent).

2.5. If necessary, the isomer is indicated at the beginning of the name, by a characteristic symbol, simple or complex, followed by hyphen (ex. α—, β_1—, α—A—).

3. Particular Cases

3.1. For HPOM—A with heteroatoms in non-equivalent sites, formed by the coordination of one or more cations as secondary heteroatom(s) by a HPOM —A as ligand, the latter in a higher proportion than 1, an alternative name is admitted, according to the following order and rules:

3.1.1. The group(s) containing secondary heteroatom is(are) indicated as such, preceded by an Arabic numeral, which indicates the proportion, and followed by hyphen.

3.1.2. The HPOM—A with the role of ligand is indicated with the complete name (exception the charge), according to the above mentioned rules, points 1 and 2, in round brackets, square brackets or braces, preceded outside by a multiplicative numeral, which indicates the proportion (ex. bis, tris, tetrakis).

3.1.3. The charge of the whole HPOM—A is optionally indicated, in the Ewens-Basset system.

A systematic nomenclature in Rumanian was also proposed [17].

Exemplifications. Finally, we present some relevant examples for the proposed formulation and nomenclature:

A) Common HPOM—A

a) with primary heteroatom(s) and identical addenda

$TeMo_6O_{24}^{6-}$	6-molybdo-1-tellurate (6—)
$Ni^{II}W_6O_{18}(OH)_6^{4-}$	6-tungsto-1-nickelato(II) [6-hydroxo] (4—)
$SiMo_{12}O_{40}^{4-}$	12-molybdo-1-silicate (4—)
α-$PW_{12}O_{40}^{3-}$	α-12-tungsto-1-phosphate (3—)
β-$SiW_{11}O_{39}^{8-}$	β-11-tungsto-1-phosphate (8—)
α-A—$PW_9O_{34}^{9-}$	α-A-9-tungsto-1-phopshate (9—)
$HSiW_9O_{34}^{9-}$	(1-hydrogen)-9-tungsto-1-silicate (9—)
$P_2W_{18}O_{62}^{6-}$	18-tungsto-2-phosphate (6—)
α_2-$P_2W_{17}O_{61}^{10-}$	α_2-17-tungsto-2-phosphate (10—)

b) with different primary heteroatoms

$As^{V}PW_{18}O_{62}^{6-}$	18-tungsto-1-arsenate(V)-1-phosphate (6—)

c) with mixed addenda

$SiV_2W_{10}O_{40}^{6-}$	10-tungsto-2-vanado-1-silicate (6—)
$P_2MoW_{16}O_{61}^{10-}$	1-molybdo-16-tungsto-2-phosphate (10—)

d) with reduced addenda (HPOM—A blues; heteropolyblues)

$SiW_{11}^{VI}W^{V}O_{40}^{5-}$	11-tungsto(VI)-1-tungsto(V)-1-silicate (5—)
$P_2V^{V}V^{IV}W_{16}O_{62}^{9-}$	16-tungsto-2-vanado(V)-1-vanado(IV)-2-phosphate (9—)

B) HPOM—A with primary and secondary heteroatoms
(HPOM—A with heteroatoms in non-equivalent sites)

$PMn^{II}Mo_2W_9O_{39}(H_2O)^{5-}$ 1-mangano(II)[1-aqua]-2-molybdo-9-tungsto-1-phosphate (5—)

$Co^{III}Co^{II}W_{11}O_{39}(H_2O)^{7-}$ 1-cobalto(II)[1-aqua]-11-tungsto-1-cobaltate(III) (7—)

$SiCo^{II}W_{11}O_{39}(O_2)^{6-}$ 1-cobalto(II)[1-dioxygen]-11-tungsto-1-silicate (6—)

$SiCo_3^{II}W_9O_{39}(H_2O)_3^{10-}$ 3-colbalto(II)[3-aqua]-9-tungsto-1-silicate (10—)

$PNi^{II}W_{11}O_{39}(C_5H_5N)^{5-}$ 1-nickelo(II)[1-pyridine]-11-tungsto-1-phosphate (5—)

$PCo^{II}W_{11}O_{39}(CH_3—C_5H_4N)^{5-}$
(the CH_3 — group is located at position 2)
1-cobalto(II)[1-(2-methylpyridine)]-11-tungsto-1-phosphate (5—)

$U^{IV}(PW_{11}O_{39})_2^{10-}$ 1-urano(IV)-bis(11-tungsto-1-phosphate) (10—)

$Ce^{IV}(\alpha_2—P_2W_{17}O_{61})_2^{16-}$ 1-cero(IV)-bis(α_2-17-tungsto-2-phosphate) (16—)

C) HPOM—A cryptands and cryptates

a) HPOM—A cryptands

$Sb_9^{III}W_{21}O_{86}^{16-}$ 21-tungsto-9-antimonate(III) (19—)

$As_4^{III}W_{40}O_{140}^{28-}$ 40-tungsto-4-arsenate(III) (28—)

b) HPOM—A cryptates

$NaSb_9^{III}W_{21}O_{86}^{18-}$ [(1-sodium)]-21-tungsto-9-antimonate(III) (18—)

$KAs_4^{III}W_{40}O_{140}^{27-}$ [(1-potassium)]-40-tungsto-4-arsenate(III) (27—)

$(NH_4)As_4^{III}Co_2^{II}W_{40}O_{140}(H_2O)_2^{23-}$
[(1-amonium)]-2-cobalto(II)[2-aqua]-40-tungsto-4-arsenate(III) (23—)

REFERENCES

1. P. Souchay, "Polyanions et polycations", Gauthiers-Villars, Paris, 1963.
2. P. Souchay, "Ions minéraux condensés", Masson, Paris, 1969.
3. M. T. Pope, "Heteropoly and Isopoly Oxometalates", Springer, Berlin, Heidelberg, New York, Tokyo, 1983.
4. L. C. W. Baker, "Advances in the Chemistry of the Coordination Compounds" (S. Kirschner, ed.), MacMillan, New York, 1961, p. 604.
5. H. T. Evans, jr, *Perspect Struct. Chem*, **4**, 1 (1971).
6. D. L. Kepert, "The Early Transition Elements", Academic Press, New York, 1972, pp. 46—60, 288—304.
7. D. L. Kepert, "Comprehensive Inorganic Chemistry" (A. F. Trotman-Dickerson et al., eds.), Vol. 4, Pergamon Press, Oxford, 1973, pp. 607—672.
8. T. J. R. Weakley, *Struct. Bonding (Berlin)*, **18**, 131 (1974).
9. L. P. Kazanskii, E. A. Torchenkova, V. I. Spitsyn, *Russ. Chem. Rev.*, **43**, 525 (1974).
10. G. A. Tsigdinos, *Topics Current Chem.*, **76**, 1(1978).

11. V. I. Spitsyn, L. P. Kazanskii, E. A. Torchenkova, *Sov. Sci. Rev. B., Chem. Rev.*, **3**, 111 (1981).
12. S. Schönherr, H. Görz, W. Gessner, R. Bertram, *Z. Chem.*, **23**, 429 (1983).
13. Gh. Marcu, "Chimia compuşilor coordinativi", Ed. Academiei RSR, Bucureşti, 1984, pp. 347—364.
14. H. J. Lunk, S. Schönherr, *Z. Chem.*, **27**, 157 (1987).
15. I.U.P.A.C., "Nomenclature of Inorganic Chemistry-Definitive Rules 1970", Second Edition, Buttherworths, London, 1971.
16. Comission on Nomenclature of Inorganic Chemistry (Y. Jeannin, M. Fournier), *Pure Appl. Chem.*, **59**, 1529 (1987).
17. A. Pătruţ, Gh. Marcu, Al. Botar, *Rev. Chim. (Bucureşti)*, in **40 (9—10)**, 775 (1989.)

STUDIA UNIV. BABEŞ—BOLYAI, CHEMIA, XXXIV, 2, 1989

NEW HETEROPOLYOXOMETALATE ANIONS WITH HETEROATOMS IN NON-EQUIVALENT SITES

1. Synthesis of anions

ADRIAN PĂTRUŢ*, GHEORGHE MARCU, ALEXANDRU BOTAR***

Received: July 14 1989

The synthesis of some heteropolyoxometalate anions containing heteroatoms in non-equivalent sites of the types $PZMo_2W_9O_{39}(H_2O)^{6-}$ and $P_2ZMoW_{16}O_{61}(H_2O)^{8-}$ (where Z = Mn^{II}, Ni^{II}, Cu^{II}), with modified Keggin and modified Dawson structure respectively, is presented.

Introduction. Some heteropolyoxometalate anions (HPOM—A) may act as multidentate ligands towards metal cations, with formation of complexes, according to a general reaction:

$$mZ^{z+} + nHPOM{-}A_{ligand}^{q-} \rightleftharpoons Z_m(HPOM{-}A_{ligand})_n^{(nq-mz)-} \quad (1)$$

The reaction product is in its turn a HPOM—A containing primary and secondary heteroatoms in the structural pattern.

The most well-known and studied ligands are the unsaturated monolacunary Keggin and monolacunary Dawson HPOM—A of the types $XM_{11}O_3^{b-}$ and $X_2M_{17}O_{61}^{d-}$ respectively (where X = primary heteroatom, M = addendum, O = = oxygen). These monovacant anions formally result from the saturated complete Keggin and complete Dawson HPOM—A of the types $XM_{12}O_{40}^{a-}$ and $X_2M_{18}O_{62}^{c-}$ respectively, by the elimination of a MO^{x+} unit., i.e. an addendum M and its terminal oxygen. Monolacunary Keggin and monolacunary Dawson HPOM—A, with defect-structure, which are deficient in a single MO_6 octahedron, contain a cavity delimited by five oxygen atoms. Metal cation binding occurs at the vacant site.

Towards transitional cations, the cavity O_5 acts as a pentadentate ligand, forming complexes of stoichiometry m : n = 1 : 1. The transitional cation is coordinated as a secondary heteroatom in the centre of the octahedral cavity, in the site corresponding to the absent addendum M. The sixth coordination site, which is terminal, is occupied by another ligand, frequently H_2O, satisfying the coordination number 6 of the secondary heteroatom. The structure of the HPOM—A thus formed is called sometimes modified Keggin and modified Dawson respectively.

The cations of lanthanides and actinides have the coordination number 8 and are too large to enter inside the cavity O_5. With the above mentioned

* *Institute of Chemystry, 3400 Cluj-Napoca, Romania*
** *University of Cluj-Napoca, Faculty of Chemical Technology, 3400 Cluj-Napoca, Romania*

monolacunary HPOM—A, they form complexes of stoichiometry m : n = 1:2, In this case, the cation is coordinated externally as a secondary heteroatom in the centre of a square antiprism, belonging to two monolacunary HPOM—A, each functioning as a tetradentate ligand (the oxygen also belonging to the primary group XO_4 takes no part in the coordination).

The first 1 : 1 HPOM—A "complexes" where synthetized in 1956 by Baker and McCutcheon [1], but they where characterized and correctly formulated as complexes of Co^{2+} with monolacunary Keggin HPOM—A only in 1966 [2]. Malik and Weakley have extended these studies on monolacunary Dawson HPOM —A, obtaining and characterizing 1 : 1 complexes with transitional cations [3, 4].

Peacock and Weakley have synthetized the first 1 : 2 complexes of lanthanide and actinide cations, with monolacunary Keggin and monolacunary Dawson HPOM—A [5].

Further research has demonstrated that other lacunary HPOM—A, usually multivacant, like $PW_9O_{34}^{9-}$, $P_2W_{19}O_{69}^{14-}$, $Sb_9W_{21}O_{86}^{19-}$ or $As_4W_{40}O_{140}^{28-}$, may form complexes of different stoichiometries with metal cations [6].

The different terms used by various authors for complexes of metal cations with HPOM—A as ligands are more or less ambigous. We consider the term HPOM—A with heteroatoms in non-equivalent sites, which makes a clear difference between primary and secondary heteroatoms, to express adequately the definite characteristic of the studied complexes. We also admit the simplified term of HPOM—A "complexes", although obviously improper, since HPOM —A as such are complex combinations, this being the traditional name for coordination compounds. All the same, pleonastic terms, like HPOM—A "ligand" or HPOM—A "complex" distinguish effectively the role of the reactant and the reaction product respectively, in reactions of the type described by the equation (1).

Results and Discussion. The aim of the present work is the study of the formation reactions, properties and possible practical applications of 1 : 1 complexes of some transitional cations with unsaturated lacunary HPOM—A. The resulting complexes are HPOM—A with heteroatoms in non-equivalent sites. The first paper is devoted to the synthesis of the HPOM—A.

The reported HPOM—A are formulated and namee according tot he formulation and nomenclature proposed in previous papers [7, 8].

As ligands have been selected HPOM—A with mixed addenda, with monolacunary Keggin and monolacunary Dawson structure respectively, of higher stability within the corresponding series:

$PMo_2W_9O_{39}^{7-}$	2-molybdo-9-tungsto-1-phosphate
$P_2MoW_{16}O_{61}^{10-}$	1-molybdo-16-tungsto-2-phosphate

The unsaturated character of the ligands, due to their defect-structure, gives them a particular reactivity towards metal cations $Z^{(z+)}$, such as some divalent transitional cations: Mn^{2+}, Ni^{2+}, Cu^{2+}.

By the rapid reaction of the lacunary HPOM—A with the mentioned transitional cations, 1 : 1 complexes are formed, representing HPOM—A with heteroatoms in non-equivalent sites.

The preparative method consists in direct mixing of the aqueous solution of a soluble slat (potassium, ammonium) of the monolacunery HPOM—A and a soluble salt of the $Z^{(z+)}$ cation, at pH values in the optimum formation range (for orientation, this range is situated between pH = 3—5). A corresponding soluble salt (potassium, ammonium) of the HPOM—A with heteroatoms in non-equivalent sites is obtained.

The developing reactions may be resumed in the following equations:

$$PMo_2W_9O_{39}^{7-} + Mn_{aq}^{2+} \rightarrow PMn^{II}Mo_2W_9O_{39}(H_2O)^{5-} \quad (2)$$
1-mangano(II)[1-aqua]-2-molybdo-9-tungsto-1-phosphate

$$PMo_2W_9O_{39}^{7-} + Ni_{aq}^{2+} \rightarrow PNi^{II}Mo_2W_9O_{39}(H_2O)^{5-} \quad (3)$$
1-nickelo(II)[1-aqua]-2-molybdo-9-tungsto-1-phosphate

$$PMo_2W_9O_{39}^{7-} + Cu_{aq}^{2+} \rightarrow PCu^{II}Mo_2W_9O_{39}(H_2O)^{5-} \quad (4)$$
1-cupro(II)[1-aqua]-2-molybdo-9-tungsto-1-phosphate

and

$$P_2MoW_{16}O_{61}^{10-} + Mn_{aq}^{2+} \rightarrow P_2Mn^{II}MoW_{16}O_{61}(H_2O)^{8-} \quad (5)$$
1-mangano(II)[1-aqua]-1-molybdo-16-tungsto-2-phosphate

$$P_2MoW_{16}O_{61}^{10-} + Ni_{aq}^{2+} \rightarrow P_2Ni^{II}MoW_{16}O_{61}(H_2O)^{8-}$$
1-nickelo(II)[1-aqua]-1-molybdo-16-tungsto-2-phosphate

$$P_2MoW_{16}O_{61}^{10-} + Cu_{aq}^{2+} \rightarrow P_2Cu^{II}MoW_{16}(H_2O)^{8-}$$
1-cupro(II) [1-aqua]-1-molybdo-16-tungsto-2-phosphate

The cation $Z^{(z+)}$ ($Z = Mn^{2+}$, Ni^{2+}, Cu^{2+}) is coordinated as a secondary heteroatom inside the cavity delimited by five oxygen atoms of the monolacunary HPOM—A "ligand". The sixth coordination position on the secondary heteroatom Z is occupied by a constitutional water molecule. The saturated HPOM—A obtained exhibit a modified Keggin and modified Dawson structure respectively.

The potassium salts of the synthetized HPOM—A have been analyzed by chemical and physical-chemical methods. The results obtained are presented in Table 1.

Experimental. Synthesis. The synthesis of the potassium salts of the studied HPOM—A has been made in two steps.

In the first step, the potassium salts of the HPOM—A with ligand role, $K_7[PMo_2W_9O_{39}] \cdot 13H_2O$ and $K_{10}[P_2MoW_{16}O_{61}] \cdot 19H_2O$ respectively, have been prepared by the methods described in the litterature [9—11].

In the second step, the potassium salts of the HPOM—A with heteroatoms in non-equivalent sites have been prepared according to the following procedures:

a) Synthesis of $K_5[PMnMo_2W_9O_{39}(H_2O)] \cdot 14H_2O$. $K_7[PMo_2W_9O_{39}] \cdot 13H_2O$ (15 g) is dissolved in water (500 ml) and the pH adjusted to 4 with HCl 6N. The solution obtained is heated to 60—70 °C, then a second solution containing $MnCl_2 \cdot 4H_2O$ (1 g) dissolved in water (25 ml) is added dropwise, with stirring.

Table 1

Analytical results for HPOM potassium salts

HPOM compound	Molecular weight	K (%)	P (%)	Z (Mn, Ni or Cu) (%)	Mo (%)	W (%)	H_2O (%)
$K_5[PMnMo_2W_9O_{39}(H_2O)]$ $14H_2O$	3022.16	6.70 (6.47)	1.04 (1.02)	1.95 (1.82)	6.28 (6.35)	55.90 (54.75)	8.84 (8.94)
$K_5[PNiMo_2W_9O_{39}(H_2O)]$ $13H_2O$	3007.92	6.78 (6.50)	1.01 (1.03)	1.99 (1.95)	6.30 (6.38)	55.80 (55.01)	8.57 (8.39)
$K_5[PCuMo_2W_9O_{39}(H_2O)]$ $14H_2O$	3030.76	6.60 (6.45)	1.04 (1.02)	2.11 (2.10)	6.42 (6.33)	53.85 (54.60)	8.96 (8.92)
$K_8[P_2MnMoW_{16}O_{61}(H_2O)]$ $18H_2O$	4785.50	6.97 (6.54)	1.32 (1.29)	1.22 (1.14)	2.05 (2.01)	63.02 (61.47)	7.08 (7.15)
$K_8[P_2NiMoW_{16}O_{61}(H_2O)]$ $18H_2O$	4789.27	6.66 (6.53)	1.30 (1.29)	1.20 (1.23)	1.97 (2.00)	63.53 (61.42)	7.05 (7.15)
$K_8[P_2CuMoW_{16}O_{61}(H_2O)]$ $19H_2O$	4812.12	6.80 (6.50)	1.32 (1.29)	1.28 (1.32)	2.02 (1.99)	62.85 (61.13)	7.46 (7.49)

* calculated values in brackets

Yellow-orange crystals separate on cooling, are filtered after 48—72 hours and recrystallised from hot water acidulated to pH 4.

b) Synthesis of $K_5[PNiMo_2W_9O_{39}(H_2O)] \cdot 13H_2O$. The preparation is made as in the case of a), with the difference that the second solution contains $NiCl_2 \cdot 6H_2O$ (1,2 g) dissolved in water (25 ml). Paler green crystals are obtained.

c) Synthesis of $K_5[PCuMo_2W_9O_{39}(H_2O) \cdot 14\ H_2O$. The preparation is made as in the case of a), with the difference that the second solution contains $CuCl_2 \cdot 2H_2O$ (0,85 g) dissolved in water (25 ml). Paler light green crystals are obtained.

d) Synthesis of $K_8[P_2MnM_0W_{16}O_{61}(H_2O)] \cdot 18H_2O$. $K_{10}[P_2MoW_{16}O_{61}] \cdot$ $\cdot 19H_2O$ (24 g) is dissolved in water (500 ml) and the pH adjusted to 4 with HCl 6N. The solution obtained is heated to 60—70 °C, then a second solution containing $MnCl_2 \cdot 4H_2O$ (1 g) dissolved in water (25 ml) is added dropwise, with stirring. Brown-reddish crystals separate on cooling, are filtered after 48—72 hours and recrystallised from hot water acidulated to pH 4.

e) Synthesis of $K_8[P_2NiMoW_{16}O_{61}(H_2O)] \cdot 18H_2O$. The preparation is made as in the case of d), with the difference that the second solution contains $NiCl_2 \cdot 6H_2O$ (1,2 g) dissolved in water (25 ml). Light green yellowish crystals are obtained.

f) Synthesis of $K_8[P_2CuMoW_{16}O_{61}(H_2O)] \cdot 19H_2O$. The preparation is made as in the case of d), with the difference that the second solution contains

$CuCl_2 \cdot 2H_2O$ (0,85 g) dissolved in water (25 ml). Very pale green crystals are obtained.

Analysis. Potassium was precipitated and weighed as $K[B(C_6H_5)_4]$.

Phosphorus, molybdenum and tungsten were estimated after alkaline degradation to boiling with NaOH 6N and separation of $Mn(OH)_2$, $Ni(OH)_2$ or $Cu(OH)_2$.

Phosphorus was estimated by gravimetry after precipitation with NH_4MgPO_4 and igntiion to MgP_2O_7.

In order to estimate tungsten and molybdenum, the alkalinized sample was treated with HCl 6N to pH < 1, boiled, precipitated with α-benzoinoxime and ignited to WO_3 and MoO_3. Tungsten was extracted from the precipitation with ammonium solution, acidulated to boiling with HCl 6N, precipitated with cinconine and ignited again to WO_3. Molybdenum was calculated by difference.

Manganese, nickel and copper were estimated after decomposition with HCl 6N of the corresponding hydroxide, formed by alkaline degradation.

Manganese was estimated as MnO_4^- by spectrophotometry, after a preliminary oxidation with $K_2I_2O_7$.

Nickel was precipitated and weighed as nickel salicylaldoxime.

Copper was precipitated and weighed as copper salicylaldoxime.

Water was estimated by thermogravimetry.

Conclusion. HPOM—A with heteroatoms in non-equivalent sites, of the types $PZMo_2W_9O_{39}(H_2O)^{5-}$ and $P_2ZMoW_{16}O_{61}(H_2O)^{8-}$ ($Z = Mn^{II}$, Ni^{II}, Cu^{II}), with modified Keggin and modified Dawson structure respectively, have been synthetized.

The chemical analysis of potassium salts of anhydrous HPOM—A has been achieved.

REFERNCES

1. L. C. Baker, T. P. McCutcheon, *J. Amer. Chem. Soc.*, **72,** 4503 (1956).
2. L. C. W. Baker, V. E. S. Baker, K. Eriks, M. T. Pope, M. Shibata, O. W. Rollins, J. H. Fang, L. L. Koh, *J. Amer. Chem. Soc.*, **88,** 2329 (1966).
3. S. A. Malik, T. J. R. Weakley, *J. Chem. Soc., Chem. Comm.*, 1094 (1967).
4. T. J. R. Weakley, S. A. Malik, *J. Inorg. Nucl. Chem.*, **29,** 2935 (1967).
5. R. D. Peacock, T. J. R. Weakley, *J. Chem. Soc. A.*, 1836 (1971).
6. M. T. Pope, "Heteropoly and Isopoly Oxometalates", Springer, Berlin, Heidelberg, New York, Tokyo, 1983.
7. A. Pătruț, Gh. Marcu, Al. Botar, *Rev. Chim. (București)* **40 (9—10), 775** (1989).
8. A. Pătruț, Gh. Marcu, Al. Botar, A. Naumescu, *Stud. Univ. Babeș—Bolyai, Chem* **34(2),46** (1989).
9. R. Contant, J. M. Fruchart, G. Hervé, A. Tezé, *C. r. hebd. Séanc. Acad. Sci. Paris,* C **278,** 199 (1974).
10. R. Massart, R. Contant, J. M. Fruchart, J. P. Ciabrini, M. Fournier, *Inorg. Chem.*, **16,** 2916 (1977).
11. R. Contant, J. P. Ciabrini, *J. Chem. Res.*, (S)222, 2601 (1977).

STUDIA UNIV. BABEŞ—BOLYAI, CHEMIA, XXXIV, 2, 1989

THIOCYANATO-CHROM(III) — KOMPLEXE IN DER CHEMISCHEN ANALYSE. 44. Mitt. Bestimmung von Pyramidon mit Thiocyanato-chrom(III) — Komplexen

ION GĂNESCU, MIRCEA PREDA and MARGARETA BOROS

Eingegangen am 10 August 1988

Thiocyanato chromium (III) complexes in the Chemical Analysis, 44. Part. Determination of pyramidone with thiocyanato-chromium(III) Complexes
A number of 6 new complex salts of Pyramidon with Reinecke acid analogous thiocyanato-chromium(III) complexes: Pyr. H $Cr(NCS)_4(amine)_2$ were obtained. These slightly soluble salts have been used forvolumetric (oxidimetric and complexometric) and spectrophotometric determination of the mentionedp yrazolone derivative in various pharmaceuticals.

Die heterocyclischen N-Basen bilden mit Thiocyanato-chrom(III)-säuren, wie $H_3 Cr(NCS)_6$, H $Cr(NCS)_4(NH_3)_2$, usw. im Wasser sehr schwer lösliche Salze. Diese Verbindungen können zur quantitativen Bestimmung der N-Basen in reinen Arzneimittelpräparaten verwendet werden.

In früheren Mitteilungen 1—4 haben wir einige gravimetrische, oxidimetrische und spektrophotometrische Methoden für Alkaloide und heterocyclische Amine mit pharamazeutischer Bedeutung beschrieben.

In Fortsetzung dieser analytischer Arbeit beschreiben wir volumetrische und spektrophotometrische Methoden für die Bestimmung des Pyramidons mit einer N-heterocyclischer Struktur.

Experimenteller Teil. *Reagenzien:* Die Reineckesalzanaloge Verbindungen : Amin. $Cr(NCS)_4(Amin)_2$ wurden durch Substitutionsreaktionen aus K_3 $[Cr(NCS)_6]$ mit aromatischen und heterocyclischen Aminen ohne Lösungsmitteln erhalten. Für die Fällungsreaktionen wurden 2 proz.[1] verd. alkoholische Lösungen verwendet. 5.

Pyramidon.H $(Cr(NCS)_4(Amin)_2$ — Salze — wurden durch doppelte Umsetzungsreaktionen aus der salzsaurer Lösung von Pyramidon mit überschüssiger 2% — iger Amin. H $Cr(NCS)_4(Amin)_2$ — Lösung erhalten. Die neuen Salze sind in der Tabelle 1 charakterisiert.

Oxidimetrische Bessimmung als Pyr.H Cr.$(NCS_4)(Anilin_2)$ 2—24 mg Pyramidon in 20—25 ml 2—3%-iger Salzsäurelösung werden mit überschüssiger 2 proz. NH_4 $Cr(NCS)_4(Anilin)_2$ — Lösung bis zur bleibenden Rotfärbung behandelt. Der entstehende rotviolette Niederschlag wird abfiltriert, mit 20 ml 5%-iger NaOH—Lösung gekocht, das dabei entstehende $Cr(OH)_3$ in HCl gelöst und der NCS^- Gehalt mit N 0,1 Oxidationsmittel (KIO_3, $KBrO_3$, $KMnO_4$) in Anwesenheit von ICl-titriert. 1 ml 0,1 N Oxidationsmittellösung entspricht zu 0,9637 mg Pyramidon. Einige Ergebnissed sîn in den Tabellen 2—3 zusammengestellt.

---

[1] *Lehrstuhl für anorganische und analytische Chemie der Universität, Craiova, Rumänien*

Tabelle 1

Neue Komplexsalze des Typs Pyramidon.H [Cr(NCS)$_4$(Amin)$_2$]

Nr.	Verbindung	Mol.Gew.	Ausb.(%)	Analyse	Ber.	Gef.
1	Pyramidon H. [Cr(NCS)$_4$(Anilin)$_2$]	702,81	97	Cr S	7,40 18,24	7,36 18,14
2	Pyramidon H. [Cr(NCS)$_4$(Morfolin)$_2$]	690,91	95	Cr S	7,52 18,50	7,43 18,42
3	Pyramidon H. [Cr(NCS)$_4$(p-Toluidin)$_2$]	730,93	93	Cr S	7,11 17,54	7,05 17,44
4	Pyramidon H. [Cr(NCS)$_4$(Benzilamin)$_2$]	730,83	94	Cr S	7,11 17,54	7,02 17,39
5	Pyramidon H. [Cr(NCS)$_4$(Chinaldin)$_2$]	803,01	96	Cr S	6,47 15,96	6,40 15,83
6	Pyramidon H. [Cr(NCS)$_4$(Imidazol)$_2$]	652,81	96	Cr S	7,96 19,64	7,91 19,53

Analyse: %Cr als Cr_2O_3; %S als $BaSO_4$

Tabelle 2

Permanganometrische Bestimmung als Pyramidon H. [Cr(NCS)$_4$(Anilin)$_2$]

Nr	Pyramidon mg Eingew.	Pyramidon mg Gef.	Abweichung mg	Abweichung %	Statistische* Daten
1	1,20	1,21	0,01	0,83	$\bar{X} = 9{,}58$
2	2,40	2,39	−0,01	0,41	$S^2 = 71{,}33 \cdot 10^{-4}$
3	4,80	4,81	0,01	0,20	$S = 8{,}44 \cdot 10^{-2}$
4	7,20	7,22	0,02	0,27	„t" = 0,237
5	9,60	9,61	0,01	0,10	$t_{n-1,\,\alpha} = 2{,}26$
6	12,00	12,02	0,02	0,16	$\alpha = 95\%$
7	18,00	18,02	0,02	0,11	$9{,}55 < 9{,}60 \leqslant 9{,}60$
8	24,00	24,03	0,03	0,12	$\bar{X} - t.\ S < A < \bar{X} + t.\ S$

* aus je 10 Bestimmungen, Einwaage 9,60 mg

Tabelle 3

Iodatometrische Bestimmung als Pyramidon H[Cr(NCS)$_4$(Anilin)$_2$]

Nr	Pyramidon mg Eingew.	Pyramidon mg Gef.	Abweichung mg	Abweichung %	Statistische* Daten
1	1,20	1,21	0,01	0,83	$\bar{X} = 9{,}614$
2	2,40	2,39	−0,01	0,41	$S^2 = 59{,}37.\ 10^{-4}$
3	4,80	4,79	−0,01	0,20	$S = 7{,}70.\ 10^{-2}$
4	7,20	7,21	0,01	0,13	„t" = 0,182
5	9,60	9,59	−0,01	0,10	$t_{n-1,\,\alpha} = 2{,}26$
6	12,00	11,98	−0,02	0,16	$\alpha = 95\%$
7	18,00	17,97	−0,03	0,16	$9{,}59 < 9{,}60 < 9{,}62$
8	24,00	24,03	0,03	0,12	

* aus Je 10 Bestimmungen, Einwaage 9,60 mg

Tabelle 4

Die Resultate der Komplexometrische Bestimung des Pyramidon als Pyr.H[Cr(NCS)$_4$(Anilin)$_2$]

Pyr. genommen mg	Zahl der Bestimmungen	Mittelwert $\bar{X}$ mg	Mittlere quadratische Abweichung einer Bestimmung, S	t_a 0,0336	t_b 0,0143	$t_{n-1,\,\alpha}$ 2,26 $\alpha = 95\%$
9,60	10	9,608	$3{,}95\ 10^{-2}$			

Komplexometrische Bestimmung als Pyr.H Cr(NCS$_4$(Anilin)$_2$

2—15 mg Pyramidon in 20—25 ml Probelösung werden, wie oben ausgefällt, in Aceton gelöst, in überschüssiger 0,01 M EDTA—Lösung (60—80 ml) behandelt und zum Sieden erhitzt. Die überschüssige EDTA-Menge wird mit 0,01 M Zinkacetat-Lösung (NH_3—NH_4Cl Pufferlösung, Eriochrom — T — Indikator) zurücktitriert. (Siehe Tabelle 4)

Spektrophotometrische Bestimmung als Pyr.H Cr(NCS)$_4$(Anilin)$_2$

2—10 mg Pyramidon werden, wie oben ausgefällt auf einem Glasfilter abgesaugt in Aceton gelöst, in einem Messkolben von 25 ml zur Marke aufgefüllt und die Extinktion der Lösung bei $\lambda max = 540$ nm gemessen.

Die Ergebnisse der Analysen wurden auch statistisch verarbeitet 6. Die Eichkurve für die spektrophotometrische Bestimmung ist in Abb. 1. wiedergegeben.

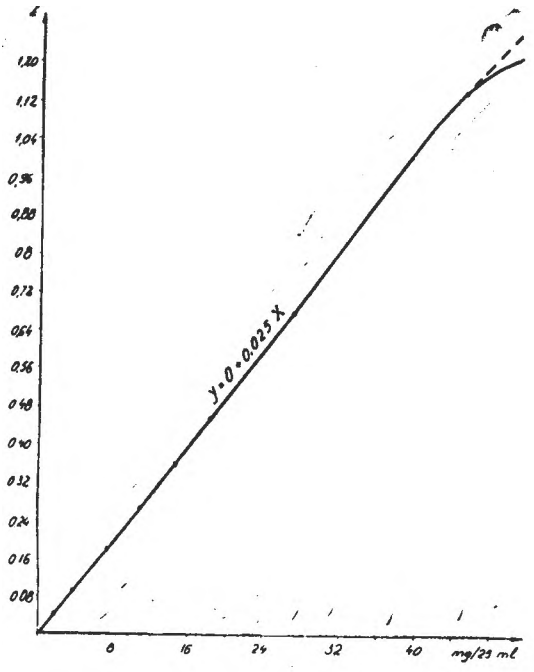

Fig. 1

Erklärung der Abbildung

Abb. 1. Abhängigkeit der Extinktion von der Konzentration des Komplexsalzese Pyr. $[H[Cr(NCS)_4(Anilin)_2]$
λ_{max} = 540 nm; Küvette: 1 cm.

LITERATUR

1. I. Gănescu, Stud. Univ. Babeş—Bolyai, Chem., **12,** 103 (1967).
2. I. Gănescu, Cs. Várhelyi, G. Brînzan, L. Boboc, Monatsh, **106,** 1081 (1975).
3. I. Gănescu, Cs. Várhelyi, I. Papa, Pharmazie (Berlin), **38,** 563 (1983).
4. I. Gănescu, Cs. Várhelyi, G. Brînzan, M. Proteasa, Z. anorg. Chem., **423,** 259 (1976).
5. I. Gănescu, Cs. Várhelyi, Archiv der Pharmazie, **309,** 251 (1976).
6. W. Youden: "Statistical Methods for Chemists", J. Wiley Sons, Inc. New York, 1955, S. 40.

STUDIA UNIV. BABEŞ—BOLYAI, CHEMIA, XXXIV, 2, 1989

ÜBER DIOXIMINKOMPLEXE DER ÜBERGANGSMETALLE

LXXXI. Mitt. Neue Kobalt(III)-chelate mit 1, 2, 3-Cyclohexantriontrioxim

CSABA VÁRHELYI*, BOTOND BURUS* und FERENC MAKKAY*

Eingegangen am August 31 1989

On the Dioximine Complexes of Transition Metals. Part LXXXI. A number of 34 new mixed chelates of cobalt(III) of the type $[Co(Triox.H_2)_{1.5}(Am)X] \cdot nH_2O$ ($Triox.H_3$-trioxime · (1, 2, 3-cyclohexanetrione trioxime, Am-primary and tertiary aromatic and heterocyclic amine or phosphine, X — Cl, Br, I, NCS, NO_2) were obtained by air oxidation of the components in the presence of ammonium acetate. Some thermal stability and structural problems, as compared with those of 1,2-cyclohexanedione dioxime ($Niox.H_2$) derivatives ($[Co(Niox.H)_2(Am)_2]X$) were discussed on the basis of derivatographic and IR spectral measurements.

Einleitung. Wie aus unseren vorhergehenden potentiometrischen und spektrophotometrischen Untersuchungen [1] hervorgeht, ist das 1, 2, 3-Cyclohexantrion trioxim (Trioxim: $Trioxim.H_3$) eine dreibasische, schwache Säure ($pK_1 = 8{,}16$; $pK_2 = 11{,}1$).

Wegen des Vorhandenseins von vicinalen Oximgruppen im Molekül, ist diese Verbindung auch ein Chelatbildner, wie die wohlbekannten α-Dioximen. Im Gegensatz zu den α-Dioximen, bildet das Trioxim keine kristalline Fällungen mit Nickel(II) — und Palladium(II) — salzlösungen. Die dritte vicinale Oximgruppe begünstigt die Bildung von grösseren kettenförmigen oder dreidimensionalen Raumanordnung. Die rotviolette, gelatinöse Nickel(II)—chelat—verbindung mit diesem Reagenz wurde zur kolorimetrischen und amperometrischen Bestimmung des Nickels verwendet [2—4]. Dieser Komplexbildner ist auch für die kolorimetrische Bestimmung des Kobalts geeignet [5].

Wir haben beobachtet, daß die Wechselwirkung von Kobalt(II) salzlösungen mit Trioxim in Anwesenheit von Oxydationsmitteln (Luftsauerstoff, Perhydrol) und einzähnigen neutralen Liganden (primäre und tertiäre aromatische und heterocyclische Amine und Phosphine) und einwertigen Anionen (Halogenen, bzw. Pseudohalogenen) führt zur Bildung von im Wasser unlöslichen Produkten, wahrscheinlich, mit makromolekularer Struktur.

Die chemischen Analysen bestätigen einem $[Co(Triox.H_2)_{1.5}(Am)X]_m \cdot nH_2O$ Bruttoformel.

34 neue chelate von diesem Typ sind in Tabellen 1 und 2 charakterisiert.

* *Babeş—Bolyai Universität Cluj, Fakultät für Chemische Technologie, 3400 Cluj, Räumnien*

Tabelle 1

Neue Chelate vom [Co(Triox.H) (Am) X]nH O Typ mit aromatischen und heterocyclischen Aminen

No.	Verbindung	Mol. Gew. ber.	Charakteristik		Analyse (%) Ber.	Gef.
1	$[Co(Triox.H_2)_{1,5}(Pyridin)Cl] \cdot 4H_2O$	500,6	braune Tafeln	Co	11,77	12,10
				N	15,40	15,10
				H_2O	14,38	14,55
2	$[Co(Triox.H_2)_{1,5}(Pyridin)(NO_2)] \cdot 3H_2O$	493,3	dunkelgelbe Tafeln	Co	11,94	12,20
				C	34,08	33,63
				H	4,69	4,37
				N	18,45	18,08
				H_2O	10,95	10,80
3	$[Co(Triox.H_2)_{1,5}(\gamma\text{-Picolin})Cl] \cdot 3H_2O$	496,8	dunkelbraune mikrocryst.	Co	11,86	12,15
				N	15,50	15,40
				H_2O	10,88	10,60
4	$[Co(Triox.H_2)_{1,5}(\gamma\text{-Picolin})Br] \cdot 3H_2O$	541,2	dunkelbraune mikrocryst.	Co	10,88	11,15
				N	14,23	14,40
				H_2O	9,98	10,10
5	$[Co(Triox.H_2)_{1.5}(\gamma\text{-Picolin})I] \cdot H_2O$	552,2	dunkelbraune mikrocryst.	Co	10,85	10,40
				N	13,95	14,13
				H_2O	3,70	3,90
6	$[Co(Triox.H_2)(_{1.5}\gamma\text{-Picolin})\text{-}(NCS)] \cdot H_2O$	483,4	hellbraune Tafeln	Co	12,19	11,87
				N	18,84	18,75
				S	6,62	6,34
				H_2O	3,72	3,90
7	$[Co(Triox.H_2)_{1.5}(\gamma\text{-Picolin})(NO_2)] \cdot 3H_2O$	507,3	gelbbraune Tafeln	Co	11,61	11,90
				N	17,95	17,73
				H_2O	10,65	10,30
8	$[Co(Triox.H_2)_{1.5}(Imidazol)\text{-}Cl] \cdot 3H_2O$	471,7	gelbbraune Tafeln	Co	12,49	12,74
				N	19,30	19,45
				H_2O	11,45	11,60
9	$[Co(Triox.H_2)_{1,5}(Imidazol)\text{-}Br)] \cdot H_2O$	480,2	dunkelbraune Tafeln	Co	12,27	12,08
				N	18,96	18,80
				H_2O	3,75	4,00
10	$[Co(Triox.H_2)_{1,5}(Imidazol)\text{-}I] \cdot 4H_2O$	581,2	braune mikrocryst	Co	10,14	9,95
				N	15,67	15,55
				H_2O	12,39	12,16
11	$[Co(Triox.H_2)_{1,5}(Imidazol)\text{-}(NCS)] \cdot 3H_2O$	494,4	hellbraune mikrocryst.	Co	11,92	11,77
				N	21,25	21,33
				H_2O	10,93	11,00
12	$[Co(Triox.H_2)_{1,5}(Imidazol)\text{-}(NO_2)] \cdot 3H_2O$	482,3	gelbbraune mikrocryst.	Co	12,22	12,46
				N	21,78	21,60
				H_2O	11,20	11,45
13	$[Co(Triox.H_2)_{1,5}(Anilin)\text{-}(NO_2)] \cdot H_2O$	471,3	gelbbraune Tafeln	Co	12,50	12,18
				C	38,22	39,10
				H	4,49	4,60
				N	19,32	19,40

Tabelle 1 (Fortsetzung)

14	$[Co(Triox.H_2)_{1,5}(\alpha\text{-Naphtylamin})Cl]\cdot H_2O$	510,8	braune mikrocryst.	Co C H N H_2O	11,53 44,67 4,53 15,08 3,52	11,30 44,54 4,43 14,60 13,80
15	$[Co(Triox.H_2)_{1,5}(\alpha\text{-Naphtylamin})Br]\cdot H_2O$	552,3	braune mikrocryst.	Co N H_2O	10,61 13,88 3,24	10,50 13,59 13,30
16	$[Co(Triox.H_2)_{1,5}(\alpha\text{-Naphtylamin})I]\cdot 2H_2O$	620,3	dunkelbraune Tafeln	Co C H N H_2O	9,50 36,79 4,06 12,42 5,80	9,15 37,50 4,30 12,64 5,50
17	$[Co(Triox.H_2)_{1,5}(\alpha\text{-Naphtylamin})(NCS)]\cdot H_2O$	533,4	hellbraune mikrocryst.	Co C H N S	11,04 45,03 4,34 17,07 6,01	10,85 45,50 4,90 17,76 5,70
18	$[Co(Triox.H_2)_{1,5}(\alpha\text{-Naphtylamin})(NO_2)]\cdot H_2O$	521,36	dunkelgelbe Tafeln	Co N H_2O	11,30 17,46 3,45	11,17 17,50 3,60
19	$[Co(Triox.H_2)_{1,5}(\beta\text{-Naphtylamin})Cl)]\cdot 3H_2O$	546,8	hellbraune mikrocryst.	Co C H N H_2O	10,77 41,72 4,97 14,09 9,88	10,37 42,27 5,11 14,37 10,05
20	$[Co(Triox.H_2)_{1,5}(\beta\text{-Naphtylamin})Br]\cdot H_2O$	553,3	braune mikrocryst.	Co C H N H_2O	10,61 41,09 4,17 13,87 3,24	10,88 41,90 4,66 14,15 3,50
21	$[Co(Triox.H_2)_{1,5}(\beta\text{-Naphtylamin})I]\cdot H_2O$	602,2	dunkelbraune kleine unregelmäss. Krist.	Co N H_2O	9,78 12,80 2,99	9,50 12,98 3,30
22	$[Co(Triox.H_2)_{1,5}(\beta\text{-Naphtylamin})(NO_2)]\cdot 3H_2O$	557,4	dunkelgelbe Tafeln	Co C H N H_2O	10,57 40,93 4,88 16,33 9,69	10,19 40,20 4,77 16,02 9,90
23	$[Co(Triox.H_2)_{1,5}(\beta\text{-Naphtylamin})(NCS)]\cdot H_2O$	533,4	rotbraune unregelmäss. Krist.	Co N S	11,04 17,07 6,00	10,70 16,60 5,45

Tabelle 2

Neue Chelate vom $[Co(T\,ox.H_2)_{1,5}(Am)X].n\,H_2O$ Typ mit tertiären Phosphinen

No.	Verbindung	Mol. Gew. ber.	Charakteristik	Analyse (%)	Ber.	Gef.
24	$[Co(Triox.H_2)_{1,5}(Et_2PhP)\cdot Cl]\cdot H_2O$	533,8	braune mikrocryst.	Co N	11,04 11,81	11,40 11,60
25	$[Co(Triox.H_2)_{1,5}(Et_2PhP)Br]\cdot 3H_2O$	614,3	braune mikrocryst.	Co N H_2O	9,59 10,26 8,80	9,10 10,10 8,70
26	$[Co(Triox.H_2)_{1,5}(Et_2PhP)I]$	607,3	dunkelbraune Tafeln	Co N	9,70 10,38	9,50 10,19
27	$[Co(Triox.H_2)_{1,5}(Et_2PhP)(NCS)]$	538,4	rotbraune Tafeln	Co S	10,94 5,90	10,56 5,50
28	$[Co(Triox.H_2)_{1,5}(EtPhP)(NO_2)]\cdot 3H_2O$	580,4	dunkelgelbe unregelmäss. Krist.	Co N H_2O	10,15 13,26 9,31	10,35 13,60 9,50
29	$[Co(Triox.H_2)_{1,5}(Ph_3P)\text{-}Cl]\cdot 2H_2O$	647,9	braune, kleine unregelmäss. Krist.	Co C H N H_2O	9,09 50,04 4,82 9,73 5,56	9,30 49,20 4,62 10,03 5,70
30	$[Co(Triox.H_2)_{1,5}(Ph_3P)\text{-}Br]\cdot 2H_2O$	692,4	braune, kleine unregelmäss. Krist.	Co N H_2O	8,51 9,10 5,20	8,90 9,40 5,50
31	$[Co(Triox.H_2)_{1,5}(Ph_3P)I]\cdot H_2O$	721,4	dunkelbraune, kleine, unregelmäss. Krist.	Co N	8,17 8,74	7,90 8,60
32	$[Co(Triox.H_2)_{1,5}(Ph_3P)(NCS)]$	634,5	grünbraune, kleine unregelmäss. Krist.	Co S	9,29 5,05	8,99 4,78
33	$[Co(Triox.H_2)_{1,5}(Ph_3P)(NO_2)]$	622,4	orangebraune Tafeln	Co N	9,46 12,38	9,75 12,60
34	$[Co(Triox.H_2)_{1,5}(H_2O)(NCS)]\cdot H_2O$	408,3	dunkelbraune Tafeln	Co S	14,44 7,85	14,80 7,20

Et_2PhP — Diäthylphenyl-phosphin; Ph_3P — Triphenylphosphin

Diese Substanzen mit nichtelektrolytischen Charakter sind in Alkohol und in wässrigen-alkoholischen Lösungen unlöslich. Einige Derivate lösen sich ein wenig in Aceton und in Acetonitril und, insbesonders in Dimethylformamid, auf.

Die analoge Reaktion mit 1,2-Cyclohexandiondioxim (Nioxim) führt zur Bildung von wohl krystallisierenden, in wässrige alkoholischen Mischungen

löslichen, umkrystallisierbarea Produkten, wie z. B. $H[Co(Niox.H)_2X_2]$, $[Co(Niox.H)_2(Am)_2]X$, $[Co(Niox.H)_2(Am)X]$.

Es ist bemerkenswert, daß die Oxydation der Kobalt(II)-salze in Anwesenheit von Trioxim und NaX zur Bildung von Aquo-acido-nichtelektrolyte: $[Co(Triox.H_2)_{1,5}(H_2O)X]_m \cdot nH_2O$ führt.

Wegen der Unlöslichkeit der Reaktionsprodukte erhielten wir keine einheitliche Produkte aus $Na_3[Co(NO_2)_6]$, $NH_4[Co(NH_3)_2(NO_2)_4]$, $Na_3[Co(CO_3)_3]$, usw. durch Substitutionsreaktionen mit Trioxim. (Unterschied von den analogen Reaktionen mit Nioxim!).

Die thermische Stabilität der $[Co(Triox.H_2)_{1,5}(Am)X]_m \cdot nH_2O$-Komplexe ist kleiner als diejenige der Nioximin-chelate. z.B. Im Falle der $[Co(Niox.H)_2(Am)_2]X$-Chelate findet eine partiälle Dezaminierungsreaktion beim Erwärmen auf 160—200 °C statt. [6—9]

$$[Co(Niox.H)_2(Am)_2]X = [Co(Niox.H)_2(Am)X] + Am$$

Über 240—260 °C zerfällt sich die Verbindung ohne Bildung von stöchiometrischen Abbauzwischenprodukten.

Die thermische Untersuchung der $[Co(Triox.H_2)_{1,5}(Am)X] \cdot nH_2O$ Verbindungen zeigt, daß eine schnelle, oft explosionsartige Zersetzung (140—200 °C), nach der Entwässerung (70—120 °C), beobachten werden kann.

Einige Verbindungen von diesem Typ wurden, im Vergleich mit den $[Co(Niox.H)_2(Am)_2]X$ binären Elektrolyten, derivatographisch untersucht. In Abb. 1. sind die TG and DTA-Kurven der $[Co(Niox.H)_2(\gamma\text{-Picolin})_2]I$ und $[Co(Triox.H_2)_{1,5}(\gamma\text{-Picolin})I] \cdot H_2O$ als typisches Beispiel, dargestellt.

Wie es ersichtlich, sind die Entwässerung und der Dezaminierungsprozess endotherische Vorgänge. Die Massive Zersetzung der Komplexe im Luftathosphäre ist eine Überlagerung vom mehreren exothermischen, nichtstöchiometrischen Prozessen.

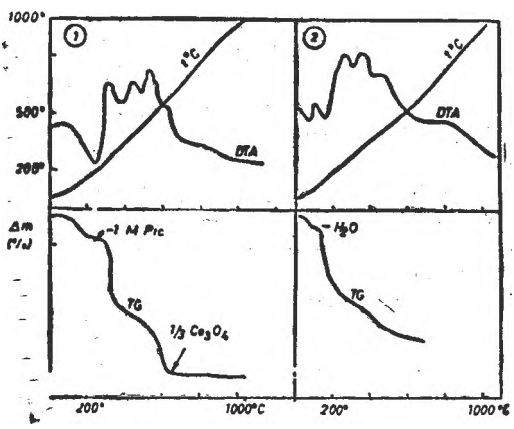

Abb. 1. Thermogravimetrische — und thermodiferentielle Kurven von
1. $[Co(Niox.H_2)(\gamma\text{-Picolin})_2]I$
2. $[Co(Triox.H_2)_{1,5}(\gamma\text{-Picolin})I]$ H_2O

Die Ultrarotspektren einiger $[Co(Triox.H_2)_{1,5}(Am)X]$ - Komplexe mit $X = NO_2$, NCS zeigen daß die koordinative Bindung in beiden Fällen durch das Stickstoffatom verwirklicht ist. (ν_{N-O}: 1418 (s), 1330 (m—s), δ_{ONO}: 825—830 m—s); Nitro-komplexe mit $Co—NO_2$-Bindung; ν_{C-N}: 2080, 2110 (ss), ν_{C-S}: 740, 750 (s): Isothiocyanato-Komplexe mit Co——NCS-Bindung. Die bei 3260——3170 cm^{-1} auftretende breite starke Bande (ν_{O-H}) kann zu der nicht komplex gebundenen, teilweise an Wasserstoffbrückenbindungen beteiligten = N—OH-Gruppe zugeordnet werden. Andere charackteristische Frequenzen dieser freien =C=N—OH Gruppe ($\nu_{C=N}$, γ_{O-H}) erscheinen bei

Tabelle

UR — Spektral Daten einiger $[Co(Niox.H)_2(Am)_2]X$ und $[Co(Triox.H_2)_{1.5}(Am)X]$-Komplexen

Schwingungs-frequenz	VERBINDUNG					
	I	II	III	IV	V	VI
$\nu O-H$	—	—	—	3270—3160 s	3260—3160 s	3270—3160
$\nu N-H$	3220—	3230—	3210—			
	3150 m—s	3150 m—s	3140 m—s			
	3050—60 s	3040 m—s	3050 m—s	3060 m—s	3050 m—s	4070 m—s
$\nu C-H$	2950 ss	2940 ss	2940 ss	2930 ss	2920 s	2920 s
	2870 s	2860 s	2860 m	2860 m—s	2860 s	2850 s
$\nu O-H$	2300—	2300—	2300—	2350—	2350—	2340—
(Brückenbindung)	2350 m—s	2350 m—s	2350 m—s	2280 mr	2250 ms	2260 ms
$\delta O-H\ldots O$	1730—	1740—	1720—	1730—	1740—	1740—
	1800 sch	1800 sch	1810 sch	1820 sch	1830 sch	1830 sch
$\delta C=N-OH$	—	—	—	1630 s	1630 s	1620 s
$\nu C=C$	1605 ss	1605 s	1605 ss	1605 ss	1605 ss	1605 ss
$\nu C=N$	1565 s	1565 ss	1575 ss	1550 s	1550 m	1550 m
δCH_2	1465 ss	1460 s	1465 s	1460 m	1460 m	1460 m
	1350 s	1345 s	1340 s	1380 m	1360 s	1360 s
δNH_2	1525 ss	1525 m	1510 s	1530 s	1520 s	1510 m
δNH_2	1340 m	1345 s	1340 s	1330 m	1330 s	1325 ss
$\nu N-O$(Oxim)	1235 ss	1235 ss	1238 ss	1290 ss	1290 m	1250 m
	1079 ss	1078 ss	1078 ss	1080 m	1075 m	1080 m
$\gamma C=N-OH$	—	—	—	1035 s	1030 m	1035 m
$\gamma O-H$	970 m	970 m	980 s	970 m	980 s	970 m
γNH_2	865 m	360 s	830 m	825 m	825 m	830 s
γCH_2	775 ss	765 ss	765 ss	775 ss	760 ss	770 s

I. $[Co(Niox.H)_2(\alpha\text{-Naphtylamin})_2Br$; II. $[Co(Niox.H)_2(\beta\text{-Naphtylamin})_2]I$, III. $[Co(Niox.H_2)(Anilin)_2]Br$; IV. $[Co(Triox.H_2)_{1,5}(\alpha\text{-Naphtylamin})Cl]$; V. $[Co(Triox.H_2)_{1,5}(\beta\text{-Naphtylamin})Cl]$; $[Co(Triox.H_2)_{1,5}(Anilin)(NO_2)]$; (ss — sehr stark, s — stark, m — mittelstark, sch — schwach

1620—1630 cm^{-1}, bzw. bei 1035 und 985 cm^{-1}. Die Frequenzen der komplexgebundenen Oximgruppen, d.h. $\nu C=N$, $\nu N-OH$ und $\nu N-O$.. sind bei 1550——1560 cm^{-1} (ss), 1240—1280 cm^{-1} 1035—1080 cm^{-1} erkennbar. Für die planare geometrische Konfiguration, d.h. für die starken intramolekularen O—H . . . O Wasserstoffbrückenbindungen charakterischen $\nu O-H$ und $\delta O-H$ . . O Valenz- und Deformations-schwingungsfrequenzen erscheinem bei 2350—2300 cm^{-1} (m und bei 1730—1820 (sch) cm^{-1}. Die verschiedenen Valenz- und Deformationsschwingungsof7quenzen der CH_2 — Gruppen der hydroaromatischen Kerne sind von K—rdinationseffekt nicht beeinflusst.
($\nu C-H$: 29280 40 (s), 2860—70 cm^{-1} (s), δCH_2 1430—1460 (m), 1340—70 cm^{-1} (m) δCH_2 : 760—oor (s) cm^{-1}.

Experimenteller Teil, 1, 2, 3-Cyclohexantriontrioxim wurde durch Izonitrosierung des Cyclohexanons mit Äthylnitrit und nachfolgender Oximierung des intermediären 1, 2, 3-Cyclohexantrion-dioxims (1,3) erhalten. Das Rohprodukt wurde aus Wasser umkristallisiert [1].

$[Co(Triox.H_2)_{1,5}(Am\ X]_m \cdot nH_2O$. Eine Mischung von 10 mMol Kobalt(II)acetat, 20 mMol NaX (X = Cl, Br, I, NCS, NO_2) und 20 mMol Amin (aroma-

tische und heterocyclische Amine, Phosphine) in 100 ml verd. Methanol (1 : 2) wird unter stätigem Umrühren mit 20 mMol Trioxim und 2 g Ammonium acetat in 50 ml Wasser behandelt, und mit einem starken Luftstrom 3—4 Stunden lang oxydiert. Die rasch ausgefallende mikrokristalline Masse wird abgesaugt, mit Wasser gewaschen und an der Luft getrocknet.

$[Co(Triox.H_2)_{1,5}(H_2O)X]_m \cdot nH_2O$ — Derivate können analogerweise ohne Zusatz von Amin-, bzw. Phosphinliganden erhalten werden. (X = Cl, Br, I, NCS, NCSe).

Analyse. Der Kobaltgehalt der Proben wurde komplexometrisch-, C, H and N-Gehalt nach den üblichen mikroanalytischen Methoden bestimmt. Die thermoanalytischen Messungen wurden mit einem Derivatograph MOM (Budapest) ausgeführt. (Probemenge 100 mg, Heizungsgeschwindigkeit : 20°/Min. Die UR-Spektren wurden in Kaliumbromid-Presslingen mit einem UR—20 Spektrophotometer (Carl Zeiss Jena) aufgenommen.

LITERATUR

1. J. Zsakó, A. Benkö, J. Horák, Cs. Várhelyi, *Acta Chim. Acad. Sci. Hung* **103**, 51 (1980).
2. W. J. Frierson, K. Marable, *Analyt. Chem.*, **34**, 210 (1962).
3. F. Mánok, Cs. Várhelyi, A. Benkö, J. Horák, *Mikrochim. Acta*, **1983**, II, 429.
4. F. Mánok, Cs. Várhelyi, M. Tarsoly, "EUROANALYSIS II." Second European Conference on Analytical Chemistry, 25—30 Aug. 1975, Budapest, Vol. II. 82., S. 282—283.
5. W. J. Frierson, N. Patterson, H. Harrill, K. Marable, *Analyt. Chem.*, **33**, 1096 (1961).
6. J. Zsakó, Cs. Várhelyi, E. Kékedy, *Acta Chim. Acad. Sci. Hung.*, **51**, 53 (1967).
7. J. Zsakó, Cs. Várhelyi, E. Kékedy, *Zhur. neorgan. Khim.*, **13**, 3279 (1968).
8. Cs. Várhelyi, L. Szotyori, I. Edler, *Rev. Roumaine Chim.*, **11**, 497 (1966).
R. Ripan, Cs. Várhelyi, L. Szotyori, *Z. anorg. allg. Chem.*, **357**, 149 (1968).

STUDIA UNIV. BABEŞ—BOLYAI, CHEMIA, XXXIV, 2, 1989

ON THE DIOXIMINE COMPLEXES OF TRANSITION METALS

LXXXII. Polarographic behaviour of some $[Rh(Diox.H)_2X_2]^-$ and $[Rh(EDTA)Cl]^{3-}$ type complexes

FERENC MÁNOK*, CSABA VÁRHELYI*, JUDIT FANCSALI* and EUGEN BÓDIS**

Received: September 22 1989

The polarographic behaviour of some anionic chelates of rhodium (III) of the types: $[Rh(Diox.H)_2X_2]^-$ and $[Rh(EDTA)Cl]^{3-}$ (Diox.H_2 = dimethylglyoxime, propoxime, nioxime, heptoxime, and octoxime, X = Cl, Br, I, NO_2, N_3) was studied in different Britton-Robinson's buffer solutions. The simple formation conditions of these complexes and their multielectronic reduction on the dropping mercury electrode at suitable potential values can be used for the polarographic determination of rhodium.

Introduction. The half wave potential of the hydrated $[Rh(H_2O)_6]^{3+}$ appears in the presence of some noncomplexing anions and neutral organic molecules at about O V (vs. SCE). In the presence of NH_3, organic amines, phosphines, amino-acids, oxy-acids and other complexing agents the $E_{1/2}$-value is shifted towards more negative potential values (−0.4—1.3 V (Vs. SCE) [1—5]. The polarographic behaviour of some analogous Co(III), Rh(III) and Ir(III) complexes, especially with NH_3 and amine ligands was also studied and compared on this way [6]. Rhodium(III) chelates with α-dioximes were only a little studied from polarographic point of view. In our previous paper [7] the reduction of $Na[Rh(Octox.H)_2(NO_2)_2]$ at the dropping mercury electrode was reported.

Results and discusson. In continuation of our investigations upon the polarographic reduction of transition metal complexes in the present paper we report on the polarographic behaviour of some chelates of the type $[Rh(Diox.H)_2X_2]^-$ (Diox.H_2-dimethylglyoxime, propoxime, nioxime, heptoxime, and octoxime, X = Cl, Br, I, NO_2, N_3) and of $[Rh(EDTA)Cl]^{3-}$ in a wide pH range in Britton-Robinson's buffer solutions. Some characteristic polarogramms are presented in Fig. 1—3.

The numerical data are shown in Tables 1—3.

It was observed, that in the case of the dioximino-chelates of the type $[Rh(Diox.H)_2X_2]^-$ appear generally three waves. The half waswe potentials of these waves are determined by the pH value of the supporting lectrolyte

* *Babeş—Bolyai University, Faculty of Chemical Technology, 3400 Cluj, Romania*
** *Chemical Institute, 3400 Cluj, Romania*

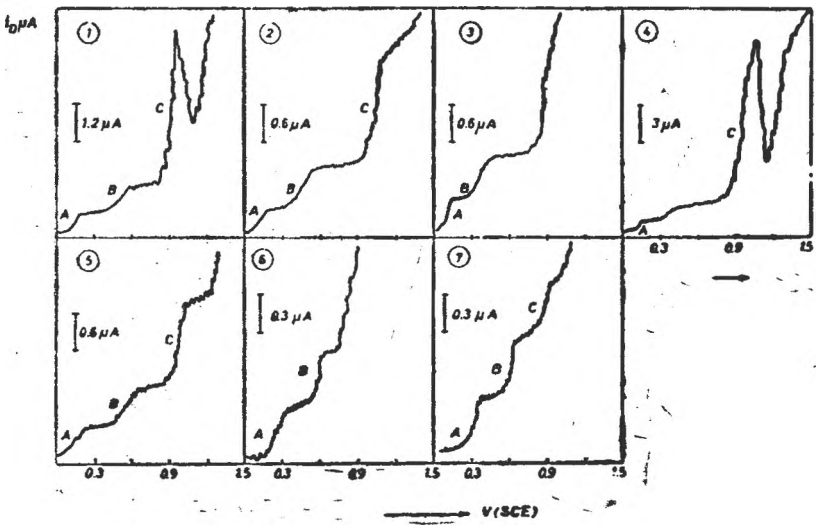

Fig. 1. Polarograms of some HRh(Diox.H)$_2$X$_2$ type complexes with Diox.H$_2$: aliphatic α-dioximes

1. Polarogram of H[Rh(DH)$_2$Cl$_2$] at pH = 3.29
   $C_{compl} = 2.4 \times 10^{-4}$ mole/l
2. Polarogram of H[Rh(DH)$_2$Cl$_2$] at pH = 8.95
   $C_{compl} = 2.4 \times 10^{-4}$ mole/l
3. Polarogram of H[Rh(DH)$_2$Br$_2$] at pH = 3.29
   $C_{compl} = 1.17 \times 10^{-4}$ mole/l
4. Polarogram of H[Rh(DH)$_2$Br$_2$] at pH = 3.29
   $C_{compl} = 1.17 \times 10^{-4}$ mole/l
5. Polarogram of H[Rh(DH)$_2$I$_2$] at pH = 7.96
   $C_{compl} = 0.97 \times 10^{-4}$ mole/l
6. Polarogram of H[Rh(DH)$_2$(N$_3$)$_2$] at pH = 3.29
   $C_{compl} = 4.7 \times 10^{-4}$ mole/l
   ($C_{NaClO_4} = 0.125$ mole/l)
7. Polarogram of H[Rh(Propox.H)$_2$Cl$_2$] at pH = 7.96
   $C_{compl} = 6.9 \times 10^{-4}$ mole/l

(Britton-Robinson's solution and $NaClO_4$) and by the nature of the chelating agent.

The nature of the dioximine ligand influences only a little the $E_{1/2}$ values. The influence of the nature of X is more considerable. In the presence of X = $= N_3^-$, appear, generally, only two reduction steps (A and B). The NO_2-ligand makes the polarogram more complicated and more difficult to explain. Besides the Rh(Diox.H$_2$)-moiety, the co-ordinated NO_2-groups are also reduced at more negative potential values.

The height of the first two waves varies parallel with the concentration of the complex (waves A and B) up to a limiting value. At more higher concentrations the height of the steps remains constant. This behaviour is charac-

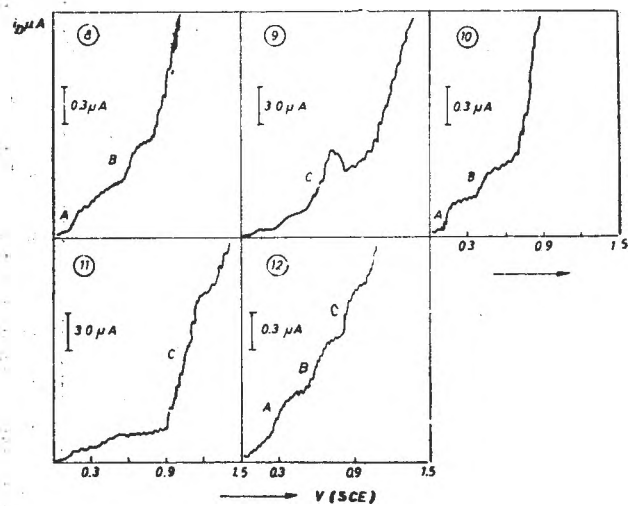

Fig. 2. Polarograms of some $H[Rh(Diox.H)_2X_2]$ type complexes with $Diox.H_2$: alycyclic α-dioximes

8. Polarogram of $H[Rh(Heptox.H)_2Cl_2]$ at pH = 7.69
   $C_{compl} = 1.5 \times 10^{-4}$ mole/l
9. Polarogram of $H[Rh(Heptox.H)_2Cl_2]$ at pH = 7.96
   $C_{compl} = 1.5 \times 10^{-4}$ mole/l
10. Polarogram of $H[Rh(Octox.H)_2Cl_2]$ at pH = 3.29
    $C_{compl} = 1.2 \times 10^{-4}$ mole/l
11. Polarogram of $H[Rh(Octox.H)_2Cl_2]$ at pH = 3.29
    $C_{compl} = 1.2 \times 10^{-4}$ mole/l
12. Polarogram of $H[Rh(Niox.H)_2(N_3)_2]$ at pH = 11.20
    $C_{compl} = 6.9 \times 10^{-4}$ mole/l

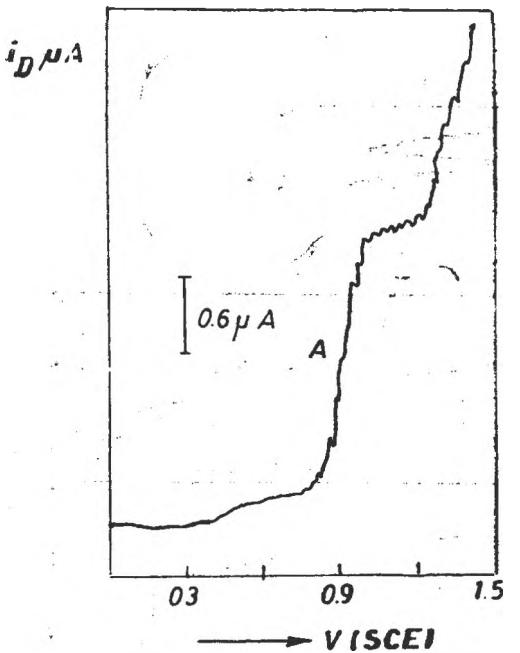

Fig. 3. Polarogram of $Na_2H[Rh(EDTA)Cl]$ at pH = 3.29

$C_{compl} = 2.4 \times 10^{-4}$ mole/l

$C_{NaClO_4} = 0.125$

Table 1

Polarographic data on the H[Rh(DH)$_2$X$_2$] type complexes

Formula	Supporting electrolyte	pH — value	$E_{1/2}$ (vs. SCE) A	B	C	Observation
H[Rh(DH)$_2$Cl$_2$]	Britton-Robinson's	3.29	0.15	0.53	1.30	*
	buffer solution,	4.10	0.15	0.54	1.14	*
	$NaClO_4$	6.80	0.12	0.45	1.05	**
	0.125 M	7.24	0.13	0.52	1.14	**
		7.96	0.15	0.54	1.18	**
		8.95	0.15	0.54	1.30	**
		11.98	0.15	0.54	1.30	**
H[Rh(DH)$_2$Br$_2$]	,,	3.29	0.08	0.38	1.10	*
		11.98	0.16	0.54	1.29	**
H[Rh(DH)$_2$I$_2$]	,,	7.96	0.20	0.60	1.00	**
H[Rh(DH)$_2$(N$_3$)$_2$]	,,	3.29	0.23	0.48	—	***
		7.96	0.28	0.58	—	***
Na[Rh(DH)$_2$(NO$_2$)$_2$]	,,	3.29	0,90	1.30	—	****
		8.95	1.10	1.30	—	****

* wave "C" presents a sharp maximum, which cannot be supressed with addition of gelatine
** the height of the well formed wave "C" is proportional to the concentration of Rh(III)
*** only two wave with no proportional heights to the concentration of Rh(III)
**** badly formed waves without proportionality to the conc. of Rh(III)

Table 2

Polarographic data on the H[Rh(Diox.H)$_2$X$_2$] type complexe

Formula	Supporting electrolyte	pH — value	$E_{1/2}$ (vs. SCE) A	B	C	Observation
H[Rh(Propox.H$_2$)Cl$_2$]	Britton-Robinson's	3.29	0.23	0.52	0.80	*
	buffer solution,	7.96	0.35	0.67	0.85	**
H[Rh(Niox.H)$_2$(N$_3$)$_2$]	$NaClO_4$	3.29	0.20	0.43	—	*****
	0.125 M	7.96	0.29	0.60	—	*****
	,,	11.20	0.33	0.64	0.88	**
H[Rh(Heptox.H)$_2$(N$_3$)$_2$]		3.29	0.21	0.53	—	*****
	,,	7.96	0.33	0.68	—	*****
H[Rh(Heptox.H)$_2$Cl$_2$]	,,	3.29	0.12	0.45	—	*****
		7.96	0.15	0.64	0.80	*
	,,	11.98	0.22	0.78	—	*****
H[Rh(Octox.H)$_2$Cl$_2$]		3.29	0.13	0.50	0.95	**
	,,	7.96	0.14	0.52	1.14	**

***** adsorption wave

Table 3

Polarographic data on the $H_3[Rh(EDTA)Cl]$ complex

Supporting electrolyte	pH — value	$E_{1/2}$ (vs. SCE)	Observation
Britton-Robinson's	3.29	0.96	**
buffer solution,	7.90	1.09	irreversible
$NaClO_4$	11.20	1.12	wave
0·125 M			"

teristic for adsorption waves. At acidic pH — values the third wave (C) presents, generally, a sharp maximum. At higher pH-values disappears this peak and the well defined shape of the wave "C" makes possible the accurate determination of the height of the step and those of the concentration of the complex. As compared with the polarographic waves of the simple rhodium (III) salts (e.g. $RhCl_3$), one can observe, that the height of the third wave ("C") of the dioximine complexes is much higher than in the case of $RhCl_3$. This, means, that simultaneously with the Rh(III) and Rh(I) specia, the chelating aliphatic — or alycyclic — dioxime groups are also reduced on the dropping mercury electrode to the corresponding 1,2-diamines in an eight electronic electrode process:

$$\begin{matrix} R-C=N-OH \\ | \\ R-C=N-OH \end{matrix} + 8H^+ + 8e = \begin{matrix} R-CH-NH_2 \\ | \\ R-CH-NH_2 \end{matrix} + 2H_2O$$

Due to the multielectronic reduction of the dioximino-chelates this form is much more sensible for the determination of rhodium than the reduction of the simple rhodium salts in an analogous way. Calibration curves for $RhCl_3$ can be taken in a conc. range of $1-6 \times 10^{-4}$ mole/l, and in the case of $Rh(Diox.H)_2X_2$-chelates in a conc. range of $1-7 \times 10^{-5}$ mole/l.

The transformation of $[Rh(H_2O)_6]^{3+}$ in bis-dioximino-chelates of the type $[Rh(Diox.H)_2X_2]^-$ is a simple reaction in a single step, phenomenon which support the electroanalytical application of these compounds.

The considerable shift of $E_{1/2}$ of $[Rh(H_2O)]^{3+}$ towards negative potential values by complexation with EDTA (a single, well formed wave of $[Rh(EDTA)Cl]^{3-}$ is also advantageous from analytical point of view for the determination of the above mentioned metal in the presence of some other accompanying elements. In this case the reduction of the Rh(III) at the dropping mercury electrode is however not followed by the reduction of the hexadentate EDTA-ligand.

Experimental. $H[Rh(DH)_2Cl_2]$, $H[Rh(Heptox.H)_2Cl_2]$ and $H[Rh(Octox.H)_2Cl_2]$-solutions were obtained by refluxing 2—2 mmoles $RhCl_3 \cdot 3H_2O$ with 4—4 mmoles α-dioxime (dimethylglyoxime, heptoxime, octoxime) in 25 ml dil. methanol (2 : 1) in the presence of 1 drop hypophosphorous acid (H_3PO_2), catalyst, during 6—8 hours. $H[Rh(DH)_2Br_2]$ was obtained analogously using

$RhBr_3$ for the synthesis. ($RhBr_3$ forms following the scheme: $RhCl_3 \xrightarrow{NaOH} Rh(OH)_3 \xrightarrow{HBr} RhBr_3$). $H[Rh(Diox.H)_2I_2]$ and $H[Rh(Diox.H)_2(N_3)_2]$ were obtained also from $RhCl_3$ by means of the above mentioned methode in the presence of an excess of KI or NaN_3, respectively (2 mmol $RhCl_3$ + 10 mmol KJ (NaN_3). [8]

$Na_3[Rh(EDTA)Cl]$ forms by refluxing 2 mmol $RhCl_3$ with 2 mmol EDTA in 25 ml dil. methanol.

The obtained yellow ... brown solutions were used for the polarographic measurements. The complexes were also separated in crystalline state and characterized. (Results in a fortcomming paper).

The polarograms were taken on a RADELKIS-TYPE-OH-120 polarograph by using a conventional polarographic cell with a saturated calomel reference electrode, connected to the cell by means of an agar-agar bridge (1 M KNO_3). The oxygen was eliminated from the solutions with purified methane.

REFERENCES

1. L. E. Johnston, J. A. Page, *Canad. J. Chem.*, **47**, 4241 (1969).
2. F. Pantani, *J. Electroanal. Chem.*, **5**, 40 (1963).
3. P. W. Alexander, L. E. Hohr Smythe, *J. Electroanal. Chem.*, **80**, 143 (1977).
4. J. B. Willis, *J. Amer. Chem. Soc.*, **66**, 1067 (1944).
5. R. D. Crow, *"Polarography of Metal Complexes"*, Academic Press, London, 1969.
6. A. W. Addison, R. D. Gillard, *J. Chem. Soc., Dalton Trans.*, **1970**, 2523; **1973**, 1187.
7. F. Mánok, Cs. Várhelyi, H. Szakács, *Stud. Univ. Babeş–Bolyai, Chem.*, **33**, (1) 69 (1988).
8. Cs. Várhelyi, F. Mánok, N. Almási, I. Nagy, *Stud. Univ. Babeş – Bolyai, Chem.*, **31**, (1), 32 (1986).

STUDIA UNIV. BABEŞ—BOLYAI, CHEMIA, XXXIV, 2, 1989

INFRARED SPECTROSCOPICAL STUDY ON SOME SALTS OF THE HEXATHIOCYANATO-CHROMIUM(III) COMPLEX ANION

JÁNOS ZSAKÓ*, CSABA VÁRHELYI* and MÁRTA MÁTÉ*

Received: October 4 1989

The infrared spectra of some $M_3[Cr(NCS)_6]$ type complex salts were recorded. Force constants of the N—C and of the C—S bondings were calculated. The nature of the chemical bonds in these complexes is discussed on the base of HMO calculations and IR spectral data.

Introduction. Thiocyanato-chromium(III) complexes were obtained in a considerable number from the monothiocyanato ($[Cr(NH_3)_5(NCS)]^{2+}$), dithiocyanato-(cis- and trans-$[Cr(en)_2(NCS)_2]^+$) derivatives up to the hexathiocyanato-salts. In function of the used neutral ligand (NH_3, H_2O, etc.) complete Werner-Miolati's series of the chromium(III) complexes were described, which played a prominent part in the elaboration of the co-ordination theory by Werner and Pfeiffer [1, 2].

The thiocyanate: NCS^- as ambidentate ligand can be co-ordinated to the chromium(III) through the sulphur atom (Cr—SCN)(thiocyanato-complexes) or through the nitrogen atom (Cr—NCS) (isothiocyanato-derivatives).

The UV spectroscopical investigations of Sutin et al. [3, 4] show, that the sulphur-bonded thiocyanato-derivatives of this metal ion are formed only in special experimental conditions and transform gradually by a linkage isomerism in the corresponding isothiocyanato-derivatives, which are more stable from thermodynamic point of view.

In the present paper a series of metal salts of the tribasic acid: $H_3[Cr(NCS)_6]$ were studied by infrared spectroscopy.

From the NCS infrared frequencies the $\nu C{=}N$, $\nu C{-}S$ and δNCS are the most characteristic. Their position is determined by the co-ordination manner of this atomic group to the metal ion.

In the case of NCS^- ions, e.g. in KCNS the wave number of the νCN valence vibration is equal to 2066 cm^{-1} and that of the νCS to 748 cm^{-1} [5]. The co-ordination of the NCS^- ion to a transition metal atom (ion) modifies the frequency of both νNC and νCS valence vibrations. This modification depends on the atom co-ordinated by M. According to literature data [5—7] νNC frequency values are lower, νCS ones are higher in the case of M—NCS type isothiocyanato complexes, as compared to the M—SCN type thiocyanato ones. These effects are due to the modifications of the bond strenght, which can be correlated with the π bond order variations.

We made an attempt to calculate π — bond orders by using the simple HMO method and to correlate our results with IR data.

* Babeş—Bolyai University, Faculty of Chemical Technology, 3400 Cluj, Romania

Results and Discussions. Bond order calculations. On the basis of IR spectral data neither the free, nor the co-ordinated NCS^- ion corresponds to the "classical" $N \equiv C-S^-$ structure. The characteristic frequency of the $C \equiv N$ bond, corresponding to $2300 \div 2210\ cm^{-1}$ in nitrils [8, § 23.6], is shifted towards lower values, down to $2150 \div 2050\ cm^{-1}$. Reversely, the frequency of the valence vibration, corresponding to the C—S, situated at $700 \div 570\ cm^{-1}$ [8, § 23.6], is shifted towards higher values up to $860 \div 690\ cm^{-1}$. These data plead for the delocalization of π bonds in the NCS^- ion, due to the participation of the unshared electron pair(s) of the S atom. Therefore, the influence of co-ordination can be theoretically studied by means of the MO method.

For this purpose an attempt is made to use the simplest Hückel approximation and the following parameter values in the case of the free NCS^- ion were taken [9]:

$$\alpha_C = 0, \quad \alpha_{\dot{N}} = 0.5, \quad \alpha_{\dot{S}} = 1, \quad \beta_{C\dot{N}} = 1, \quad \beta_{C\ddot{S}} = 0.8$$

The co-ordination of the ion implies the formation of a dative type σ-bond. The donor being either the N or the S atom, (or both of them), the electronegativity of these atoms increases, which is taken into account in our calculations, by introducing a correction of $\Delta\alpha = 0.5$. One obtains the following secular equations:

$$\begin{vmatrix} 0.5-\varepsilon & 1 & 0 \\ 1 & -\varepsilon & 0.8 \\ 0 & 0.8 & 1-\varepsilon \end{vmatrix} = 0 \qquad \begin{vmatrix} 1-\varepsilon & 1 & 0 \\ 1 & -\varepsilon & 0.8 \\ 0 & 0.8 & 1-\varepsilon \end{vmatrix} 0 = \qquad \begin{vmatrix} 0.5-\varepsilon & 1 & 0 \\ 1 & -\varepsilon & 0.8 \\ 0 & 0.8 & 1.5-\varepsilon \end{vmatrix} = 0$$

NCS^- $\qquad$ M — NCS $\qquad$ M — SCN

and if NCS forms a bridge between two M atoms, one has

$$\begin{vmatrix} 1-\varepsilon & 1 & 0 \\ 1 & -\varepsilon & 0.8 \\ 0 & 0.8 & 1.5-\varepsilon \end{vmatrix} = 0$$

M—NCS—M

Solution of these equations yields the energies ε_j of the MO—s and allows the calculation of the coefficients of the atomic orbitals in the expression of the molecular orbital $\varphi_j = C_{N_j} \cdot \psi_N + C_{C_j} \cdot \psi_C + C_{S_j} \cdot \psi_S$. These values are summarized in Table 1.

Table 1

MO energies and Hückel coefficients of the AO for free and co-ordinated NCS^- ion

System	j	ε_j	C_{Nj}	C_{Cj}	C_{Sj}
NCS^-	1	1.716	0.481	0.585	0.653
	2	0.776	0.700	0.193	−0.688
	3	−0.992	0.528	−0.788	0.316
M—NCS	1	1.875	0.645	0.564	0.516
	2	1.000	0.625	0.800	−0.781
	3	−0.875	0.440	−0.826	0.352
NCS—M	1	1.987	0.330	0.491	0.806
	2	0.964	0.769	0.356	−0.531
	3	−0.951	0.548	−0.795	0.260
M—NCS—M′	1	2.067	0.476	0.508	0.717
	2	1.257	0.749	0.193	−0.634
	3	−0.823	0.460	−0.839	0.289

Since the delocalized π-bonds are achieved by 4 electrons, the MO—s φ_1 and φ_2 are occupied and the antibonding MO φ_3 remains empty. Due to the latter, transition metal ions possessing t_{2g} type d electrons, may give retrodative π bonds. In terms of the MO approach, this means that φ_3 is combined with the t_{2g} type AO of the M atom, ψ_M, giving the MO—s φ_4 and φ_5. Let us presume these MO—s to correspond to the following expressions:

$$\varphi_4 = \frac{1}{\sqrt{2}} (\psi_M + \varphi_3); \quad \varphi_5 = \frac{1}{\sqrt{2}} (\psi_M - \varphi_3)$$

In the case of the Cr^{3+} ion, each t_{2g} type orbital has a single d electron, i.e. the electron configuration of the M—NCS and M—SCN systems may be presumed to be $\varphi_1^2\ \varphi_2^2\ \varphi_4^1$. The π bond orders p_{rs} calculated for this electron configuration by means of the coefficients given in Table 1, are presented in Table 2, together with the IR frequencies of the corresponding valence vibrations [5—7].

As seen, the π bond order values obtained plead for the correctness of the izomer configuration assignement on the basis of ν_{NC} and ν_{CS} frequencies.

As for as the bridging NCS moiety is concerned, on the base of our calculation both ν_{NC} and ν_{CS} values are expected to exhibit intermediate values between those characteristic for M—NCS and M—SCN type complexes. Literature data show that if NCS forms a bridge between two Co, two Cr or a Co and a Cr atom, the ν_{NC} frequency becomes with about 50 cm^{-1} larger as compared to the non bridging Co—NCS and Cr—NCS moieties [10]. This result is in agreement with our calculations (see Table 2).

Tabel 2

π bond orders and valence vibration frequencies for M—NCS, M — SCN and M—NCS—M' complexes

	P_{NC}	P_{CS}	$\tilde{\nu}_{NC}$, cm^{-1}	$\tilde{\nu}_{CS}$, cm^{-1}
M—NCS	0.470	0.376	<2100	860÷780
NCS—M	0.563	0.267	>2100	720÷690
M—NCS—M'	0.560	0.314	>2100	

Table 3

Wave numbers of the IR absorption bands of $M_3[Cr(NCS)_6]$ type complexes and force constants for the N—C and C—S bonds

M	$\tilde{\nu}_{CN}$ cm^{-1}	$\tilde{\nu}_{CS}$ cm^{-1}	$\tilde{\nu}_{NCS}$ cm^{-1}	$f_{CN} \times 10^{-5}$ dyne/cm	$f_{CS} \times 10^{-5}$ dyne/cm
K	2115	840	480	10.35	1.23
Tl	2135	822	477	10.55	1.18
Ag	2140	805	470	10.60	1.13
Cu	2145	805	465	10.65	1.13
Pd/2	2150	790	448	10.70	1.09
Hg/2	2165	810	480	10.85	1.14
Bi/3	2150	812	475	10.70	1.15

IR spectral data. The ν_{NC}, ν_{CS} and δ_{NCS} frequencies determined for the complexes studied are presented in Table 3.

From the valence vibration frequencies force constants were calculated by using a very rough approach [8, § 21.4]. According to this "diatomic" approach the R—N—C—S molecule is considered to be formed of two "atoms". These being, e.g. in the case of the N—C bond, the moieties R—N and C—S, respectively, where R stands for $Cr(NCS)_5$. The force constant f_{ij} can be calculated as

$$f_{ij} = 4\pi^2 c^2 \tilde{\nu}_{ij}^2 M_{ij}$$

where c stands for the velocity of light, $\tilde{\nu}_{ij}$, for the wave number of the valence vibration band and the reduced mass M_{ij} has the following expressions for the two bands considered:

$$M_{NR} = \frac{(M_R + M_N)(M_C + M_S)}{M_R + M_N + M_C + M_S}, \quad M_{CS} = \frac{(M_R + M_N + M_C)\, M_S}{M_R + M_N + M_C + M_S}$$

The force constants f_{NC} and f_{CS} calculated in the above given manner are also presented in Table 3.

Inspection of Table 3 shows that on the basis of $\tilde{\nu}_{CN} > 2100$ cm^{-1}, the NCS ion would be co-ordinated to Cr through the S atom (see Table 2), but the high $\tilde{\nu}_{CS}$ values already plead for the isothiocyanate structure: Cr—NCS. We mention that $\tilde{\nu}_{CN} > 2100$ cm^{-1} values have been reported for other Co and Cr complexes, too, in which co-ordination is also performed through the N atom [5].

From Table 3 one can see that substitution of the external sphere cation K^+ with strongly polarizing cations, having not a rare gas configuration, $\tilde{\nu}_{NC}$ values are shifted towards higher, $\tilde{\nu}_{CS}$ values towards lower values. Presumably this phenomenon is due to a partial covalent bond formation between the external sphere cation and the S atom of the NCS ligand. Therefore the NCS ion becomes a bridging one. The shifts observed are in very good agreement with the bond order values presented in Table 2, provided the co-ordination to the Cr atom occurs through the N atom.

On the basis of our IR spectral data and HMO calculations we conclude that in the $[Cr(NCS)]^{3-}$ complex ion the Cr atom co-ordinates the N atoms of the NCS ligands. Between this complex anion and the external sphere K^+ ions the bond has a purely ionic character. In the case of the other cations investigated (Tl^+, Ag^+, Cu^+, Pd^{2+}, Hg^{2+}, Bi^{3+}) this bond has a partial covalent character, i.e. the NCS ligands become bridging ones, which entails in the case of the C—N bond an increase of the bond strength, of the bond order, of the force constant and of the wave number of the absorption band. Reversely, with the C—S bond all these magnitudes exhibit a diminution due to the bridging.

Experimental. $K_3[Cr(NCS)_6]$ was obtained from $KCr(SO_4)_2 \cdot 12H_2O$ and KCNS in aqueous solution using Roessler's method [11]. The metal salts are formed by double decomposition reactions in aqueous solutions with an excess of 1—2% MNO_3, M_2SO_4 (M = Ag, Tl, Bi, Cu, Hg, etc.).

Analysis. The purity of the complex salts was controlled by chromium (iodometrically) and sulphur determination ($BaSO_4$).

Infrared spectra were recorded in kalium bromide pellets with an UR 20 Spectrophotometer (Carl Zeiss Jena).

REFERNCES

1. A. Werner: "Neuere Anschauungen auf dem Gebiete der anorganischen Chemie", Braunschweig, 1924.
2. F. Hein "Chemische Koordinationslehre", Leipzig, Hierzel Verlag, 1950.
3. A. Haim, N. Sutin, *J. Amer. Chem. Soc.*, **87**, 4210 (1965); **88**, 434 (1966).

4. N. Orhanovic, N. Sutin, *J. Amer. Chem. Soc.*, **89**, 722 (1967); **90**, 538, 4286, 7224 (1968).
5. M. Chamberlain, J. C. Bailar, *J. Amer. Chem. Soc.*, **81**, 6412 (1959).
6. D. C. H. Michell, R. J. Williams, *J. Chem. Soc.*, **1960**, 1912.
7. J. Lewis, R. S. Nylholm, P. W. Smith, *J. Chem. Soc.*, **1961**, 4590.
8. M. A. Eliashevich: "Atomnaya i molekularnaya spektroskopia", Gos. Izd. fiz. mat lit., Moscow, 1962.
9. A. Streitwieser, Jr: "Molecular orbital theory for organic chemists", Chapter 5, John Wiley, New York—London, 1961.
10. R. C. Buckley, J. G. Wardeska, *Inorg. Chem.*, **11**, 1723 (1972).
11. J. Roessler, *Liebigs Ann. Chem.*, **141**, 189 (1867).

STUDIA UNIV. BABEŞ—BOLYAI, CHEMIA, XXXIV, 2, 1989

SECONDARY GALVANIC CELLS HAVING ELECTROACTIVE POLYMER ELECTRODES

L. ONICIU*, D. POP** and SIMONA PĂUNESCU***

Received: April 4 1989

The article is a review (27 references) of the researches on the galvanic cells with electroconductive polymers. Some of the polymers which display promising performances are mentioned. The problems which arise during the exploitation and storage and which must be overcome in view of further developments are underlined.

1. Introduction. Secondary lithium batteries using a conductive polymer as positive/negative or positive and negative electrode have attracted considerable attention since the demonstration of the electrochemical doping and undoping of polyacetylene (PA) [1].

The conductive polymers such as polypyrrole (PP), polythiophene (PT) and polyaniline (PAN), which have the same conjugated double bonds as PA, were synthesized by electropolymerization since 1979 [2].

PAN is known to be the most stable of the conductive polymers and was recommended as positive electrode in PAN/$H_2SO_{4,\,aq}$/Pb cell [1] and in a secondary lithium battery [3], because PAN is electrochemically active also in the nonaqueous electrolyte solutions and may be doped with 0.45 ClO_4^-/aniline unit. F. Goto *at al.* [4] investigated the PAN in order to clarity the redox mechanism in nonaqueous electrolyte solution. It has been found that the reaction of PAN is determined by the doping/undoping of ClO_4^- anions, solvated with 3—4 molecules of propylene carbonate (PC); one ClO_4^- anion/aniline unit could be doped into the polymer [4].

Among the most widely studied conductive polymers are polyacetylene, polypyrrole, polyaniline, polyphenylene and data are presented on the performance of oxidized PA, PPy, PAN (as positive electrodes) and of reduced PA, PPh and some other polymers (as negative electrodes) [5]. A conducting polymer can be partially oxidized or reduced electrochemically to *p*-type or *n*-type conductors which can be used as cathodes or anodes, respectively:

$$P + yA^- \rightarrow PAy + ye^-, \quad \text{for exidation or } p\text{-doping and} \qquad (1)$$

$$P + yB^+ + ye^- \rightarrow PBy, \quad \text{for reduction or } n\text{-doping} \qquad (2)$$

A^- and B^+ are the inserted anion and cation, respectively, P the polymer and y the fractional charge por repeat unit (the so-called doping level). The charge which is removed from or injected into the polymeric chains is balanced by a negative/positive counterion of the electrolyte. These operations mav be perfor-

* *University of Cluj, Faculty of Chemical Technology, 3400 Cluj, Romania*
** *I.C.P., 1700 Reşiţa, Romania*
*** *Lic. Industrial nr. 6, 2400 Sibiu, Romania*

med on very thin layers of Au, Pt, SnO_2 or In_2O_3, at constant current density and potential, in various aprotic solvent + electrolytes systems. Pt and Au were used as counter electrodes, SCE as reference and the measurements are carried out in inert gas (Ar, N_2) atmosphere.

In choosing among the existing polymers, or in designing new ones for the use in battery electrodes, priority is given te these which have processibility, controlled morphology, flexibility, porosity, electroactivity, and conductivity. The succes of the battery designing assumes the compatibility of the polymeric electroactive material with the solvent/solvent mixture, electrolyte, current collector, case and spacer, stability against corrosion and wettability of the components (particularly of the spacer and the electroactive polymer) by the solvent/solvent mixture. Many fundamental aspects of conducting polymers (called also organic metals) were treated in [6].

Reactions (1) and (2) are often referred to as doping processes, but they are quite different from those concerning classical semiconductors and, therefore, they are more correctly termed as redox reactions. These redox reactions are generally reversible and that allows the use of the polymers as electrode materials in secondary galvanic cells. To be effective, however, these redox reactions must fulfill the following requirements : fast electron transfer, reversibility (high coulombic efficiency), cyclability and high storage capacity, stability, high energy and power densities. The storage capacity of the polymer electrode (maximum value of y) is one of the most important parameters of the battery. As concerning y (highest doping level and therefore the electrochemically reversible cycling) it must be experimentally determined. It is dependent of the structural and thermodynamic properties of the host polymer and of the guest ion.

As concerning conductive polymers used as cathodes, oxidized forms have advantage over reduced ones, because mid-discharge voltages are superior for the formers (tab. 1 and 2) [5].

Table 1

Polymers that undergo reversible oxidation

	PA	PPy	PAN
Max. nr. of charge/ repeat unit	0.09	0.33	0.5
Mid-discharge voltage (*vs.* Li)	3.5	3.2	3.4
Gravimetric* capacity (Ah/g)	0.12	0.095	0.10
Volumetric capacity (Ah/cm^3)	0.14	0.12	0.13

* including the weight of the BF_4^- anions

Comparing the charge storage capacities for reduced and oxidized polymers the greater values can be observed for the reduced ones because of the smaller size of the inserted cations as compared with the anions, and because of the greater stability of organic anions *vs.* organic cations.

Table 2

Polymers that undergo reversible reduction

	PPhQ	PPh	PA
Max. nr. of charge/ repeat unit	0.7	0.50	0.167
Mid-discharge voltage (*vs.* Li)	1.5	0.7	1.0
Gravimetric* capacity (Ah/g)	0.094	0.19	0.34
Volumetric capacity (Ah/cm³)	0.14	0.24	0.41

* including the weight of Li^+ counterion

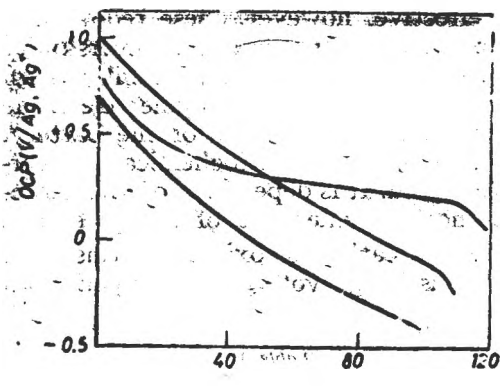

Fig. 1. Discharge curves for some oxidized polymers in 0.2 M $NaPF_6$/BN. Capacities are calculated on polymer weights only.

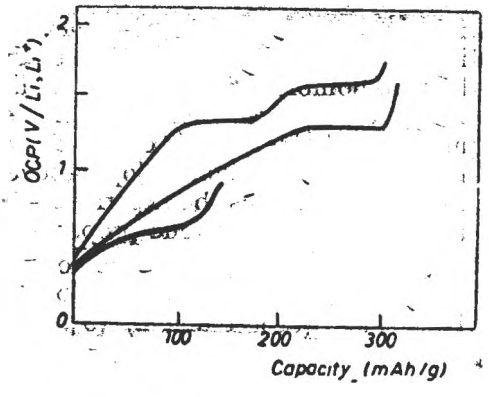

Fig. 2. Discharge curves for some reduced polymers (Na^+ — and K^+ — doped).

Discharge curves for some oxidized polymers are presented in fig. 1 [5]; a general behaviour which can be observed on the figure, is the sloping discharge curves, typical characteristic for nonstoechiometric ion-insertion electrode. Discharge curves for some polymer anodes are shown in fig. 2 [5]. Principially, any polymer from fig. 1 can be combined with polymers from fig. 2, to form an all-polymer cell, but stability restrictions reduce the possibilities.

The task to select a suitable electrolyts solutions for the polymer battery is very difficult, especially because of the high anodic and cathodic voltage at which oxidized and reduced polymers must operate. In adition, these polymers are quite catalytically active. It has been found [5, 7] that the reductive stability of the electrolyte anion is critical. High reduction levels of conductive

polymers can be achieved with alkali metal salts of various organoborates and hexafluorophosphates. On the other hand, propylene carbonate, sulpholane and various nitriles have sufficient oxidation stability for most polymers. A variety of anions (BF_4^-, XF_6^- and $CF_3SO_3^-$, where X = P, As, Sb) have a sufficient oxidative stability [5].

2. *Some secondary galvanic cells with conductive polymers*

Test cells with polymers prepared by electropolymerization from aqueous (PAN) and propylene carbonate (PA, PPy and PT) solutions, containing $HClO_4$ and $LiClO_4$, respectively, were assembled, using nonwoven cellulose separators, two Li-foil anodes and 1 M $LiClO_4$ in propylene carbonate as electrolyte. The charge/discharge experiments were carried out in an inert atmosphere (Ar) and dry box [4].

The charge/discharge characteristics of PAN at 1 mA/cm² are given in fig. 3 [4] and the coulombic efficiencies of PAN, PA, PPy and PT are given in fig. 4 [4]. PAN yields 100% coulombic efficiencis up to about 120 Ah/kg and not far

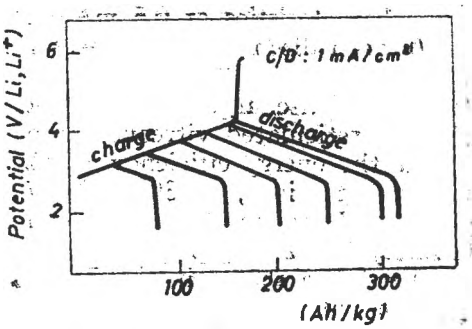

Fig. 3. Charge/discharge potential of PAN electrode in 1 M $LiClO_4$/PC. The quantity of electricity (Ah) is refered to the weight (kg) of fully discharged PAN.

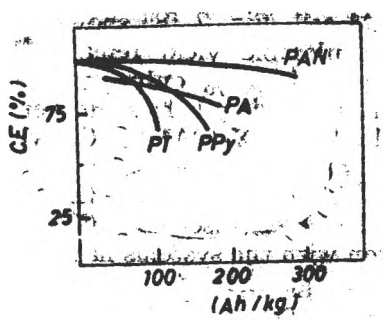

Fig. 4. Coulombic efficiency of PAN and some other conducting polymers.

from this value, at higher charging quantity, while the other polymer electrodes exhibit a sharp decrease of this parameter. The self-discharge rate of PAN (charged up to 120 Ah/kg) and of PA, PPy and PT (charged up to 30 Ah/kg only) are given in fig. 5 [4]. Since the retained capacity after 30 days for PAN was ~93% of the original value, and the self-discharge of the Ni/Cd battery is ~30%/month, PAN appears to be a good cathodic material for storage batteries.

A button-type R 2020 cell was manufactured and tested, using a PAN cathode (synthesized at 30 coulombs/cm²), having a capacity of 2.6 mAh, a surface of 1.77 cm² and a Li (80%)—Al alloy as anode. The cycle life of the

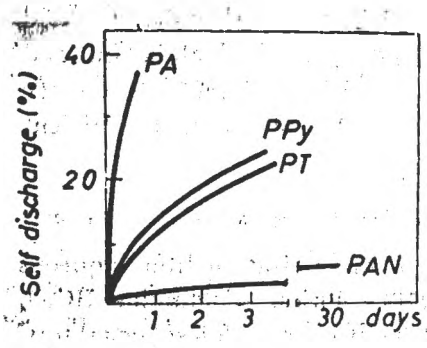

Fig. 5. Self discharge rate of some conducting polymers. Charging quantity: 20 Ah/kg (PAN)and 30 Ah/kg (PA, PPy, PT).

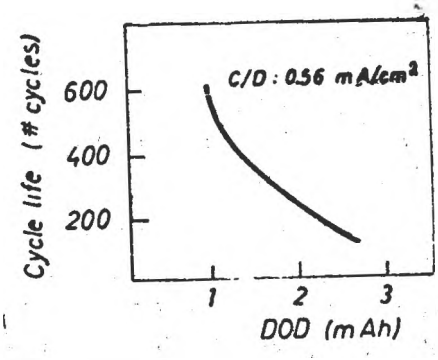

Fig. 6. Cycle life and depth-of-discharge of button-type cell (R2020). C/D current density: 0.56 mA/cm².

battery is shown in fig. 6 [4]; it is strongly dependent of depth-of-discharge (DOD), at a constant current density (0.56 mA/cm²). At 100% DOD the life was abont 150 cycles.

A chemically prepared PAN cathode was tested in a PAN/PC, 1 M $LiClO_4$/ /Li, Al cell. Fig. 7 [8] shows charge-discharge characteristics at 0.5 mA/cm². The coulombic yield remains 100% after 400 deep discharge, and the self-discharge is 10% only, after a storage of 120 days [8].

A promising behaviour demonstrated the charge/discharge characteristics of the $Zn/ZnX_2/PAN/RVC$, where X = I, RVC: reticulated vitreous carbon [9]. The storage capacity was 143 Ah/kg, and the energy efficiency >70%. The OCV = 1.2 V, and the charge/discharge polarizations, at 30—120 mA, were low. Self discharge (60% after 12 days in OCV regime is lower in comparison with the systems having as electrolyte $ZnCl_2$ and $ZnBr_2$ [10]. The charge/discharge characteristics at 30, 60 and 120 mA are shown in fig. 8 [10]. The polymer electrods was obtained by oxidation, at +0.8 V/SCE, of 1.5% aniline in 0.5 M aqueous H_2SO_4, on reticulated vitreous carbon.

Table 3 [10] shows the performances of the cell clearlly; after 284 h (≃12 days) the coulombic efficiency decreases to ~60% so it must be concluded that the PAN has a strong interaction with iodine. However, the Zn/ZnI_2/

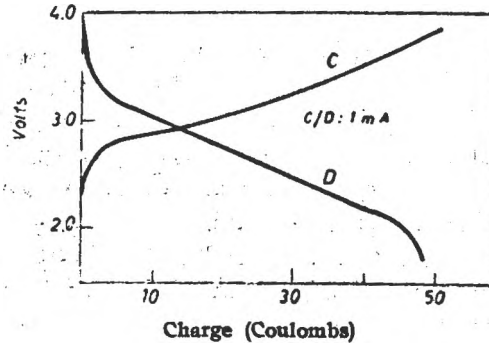

Fig. 7. Charge-discharge characteristic of a PAN/1 M $LiClO_4$, PC/Li, Al battery, at 0.5 mA. Electrode area 1 cm².

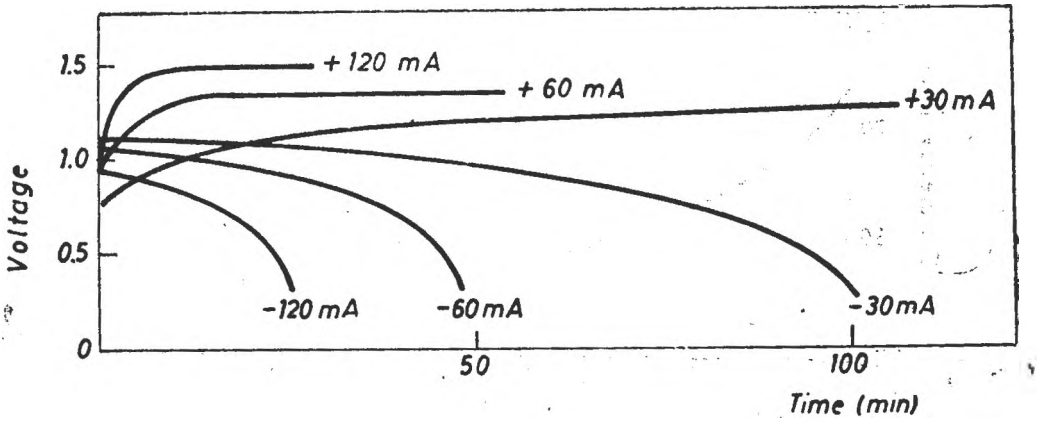

Fig. 8. Charge(+)/discharge(−) characteristics of the Zn/1.5 M ZnI_2 + 1 M NH_4I/PAN, RVC cell.

Table 3

Charge/discharge behaviour of Zn/ZnI_2 + NH_4I/PAN cell. Each charge was 200 C

Charging current (mA)	OCV (V)	Discharging current (mA)	Charge returned (C)	Coulombic efficiency (%)
30	1.20	30	190	95
60	1.21	60	177	88.5
90	1.25	90	185	92.5
120	1.23	120	183	91.5
60	1.21	30	176	88
60	1.21	30	184	92
60	1.16	30	140	70
60	1.18	30	122	61

/PAN secondary galvanic cell shows promising performance, superior to cells having $ZnCl_2$ or $ZnBr_2$ as electrolyte.

Studies of electrochemical behaviour of PA, PPy, PT and PDTT carried out by cyclic voltammetry (CV), impedance measurements, absorption spectra and charge/discharge cycling [11] demonstrated the following features:

— As concerning PA, the oxidation processes in 1 M $LiClO_4$/PC:

$$PA + yClO_4^- \rightleftharpoons PA(ClO_4)_y + ye^-, \quad (3)$$

the repetitive CV indicated that the process is limited by poor cyclability and low coulombic efficiency (fig. 9) [12, 13]. Furthermore, the PA electrodes show a self-discharge upon storage. The low coulombic efficiency and stability limitations may be explained on the basis of the diffusion-controlled transport of ClO_4^- anions from the bulk of the polymer to the interface [14—16]. Kaufman *et al.*, and Will [17—18] have reported values of the diffusivity of ClO_4^-,

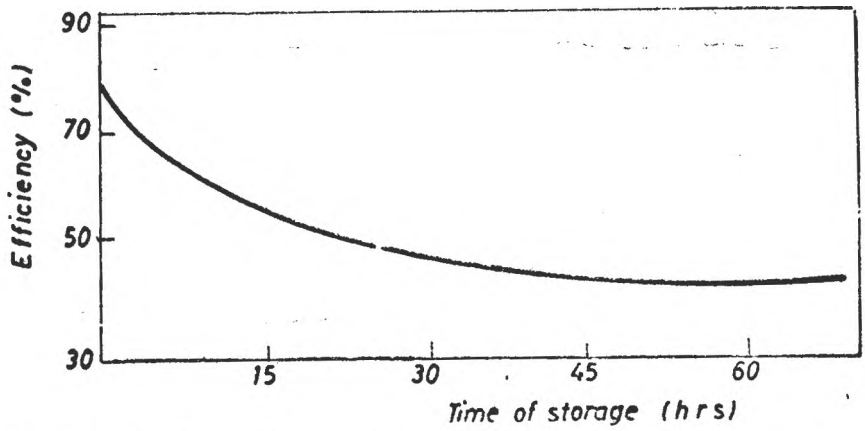

Fig. 9. Charge/discharge efficiency of $PA(ClO_4)y$ electrode *vs.* time of storage, in the charged $LiClO_4/PC$.

BF_4^- ... anions, at room temperature, ranging between 10^{-18} and 10^{-15} cm^2s^{-1}. This seems to limit the kinetics of the electromotive reaction and therefore the possible use of the PA as cathode in high-rate lithium batteries.

The energy density of polymer electrode is directly related to the extent of the oxidation reaction (doping). For PA electrode, y has a maximum value of 10%/CH unit, which corresponds to a theoretical capacity of 78 Ah/kg and, assuming an average discharge voltage of 3 V it amounts to 230 Wh/kg (referred to the weight of active material only).

As concerning the $PA(Li)_y$ anode, the reduction reaction has a slightly faster kinetics and a better reversibility, due to the slightly faster diffusion rate of Li^+ in the host polymer as compared to that of the ClO_4^- anion.

— By the oxidation of PT in $LiClO_4/PC$ + DME:

$$PT + yClO_4^- \rightleftharpoons PT(ClO_4)_y + ye^-, \tag{4}$$

the cyclic voltammogram has a similar shape for both anodic and cathodic hemicycles and the integrated charge under the oxidation and reduction waves respectively, reflect a coulombic efficiency close the 100% [11].

— Good cyclability and a very fast electromotive active reaction has the PDTT [11]:

$$PDTT + y\,ClO_4^- \rightleftharpoons PDTT(ClO_4)_y + ye^-. \tag{5}$$

This is proof that PDTT electrodes are not affected by the very slow diffusion rate, reported at PA electrods (PDTT electrodes have, also, an attractive capacity content; the doping may be extended up to 50%). Unfortunately, PT and PDTT electrodes suffer a self-discharge when stored in charge state, in electrolyte solution. The mechanism of the self-discharge process is still unknown.

— The oxidation of PP in $LiClO_4/PC$ has a reversible cathodic cycle, demonstrated by cyclic voltammetry. The repetitive CV has shown a coulombic efficiency of 88% [11]. Therefore, the kinetics of the $PP(ClO_4)$ electrode indicates

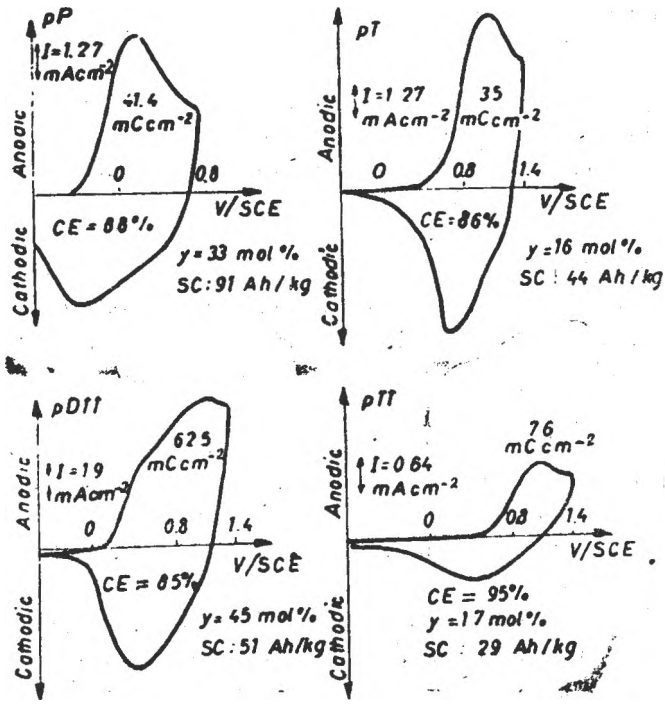

Fig. 10. Cyclic voltammograms of PPy, PT, PDTT and PTT electrodes, in 1 M $LiClO_4$/PC, at 0.1 V/s.
SC: specific capacity; y: doping level; CE: coulombic efficiency.

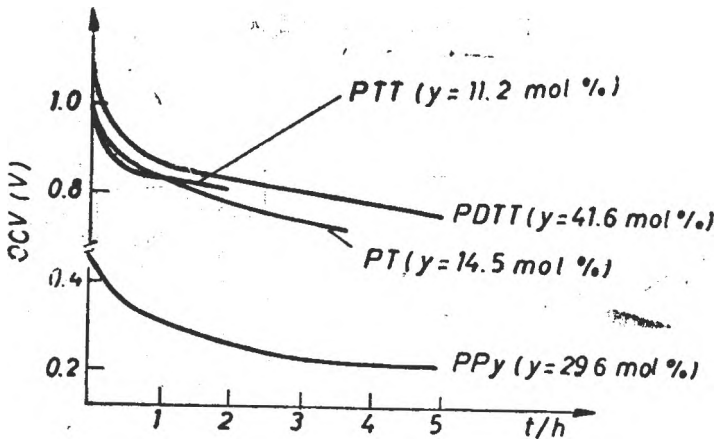

Fig. 11. Open circuit voltage *vs.* storage time in 1 M $LiClO_4$/PC solution.

a slight dependance of the diffusion control. However, the impedance measurements reveal, under extreme conditions, the presence of the slow diffusion of the ClO_4^- anions within the bulk of the polymer.

— Figure 10 shows the cyclic voltametry of PPy, PT, PDTT, and PTT films on PT electrodes in $LiClO_4$/PC solution [19]. Galvanostatic charge/discharge characteristics of PPy, PT, PDTT, and PTT electrodes at different times after the charging demonstrated that the coulombic efficiencies of the C/D cycles become lower, as the time between the end of the charge and the begining of the discharge increases. These results, and the decrease of the OCV *v.s.* storage time of the same electrodes (fig. 11) show their poor electrochemical stability when left standing in 1 M $LiClO_4$/PC solution.

The polyacetylene, the simplest conjugated polymer, may be used as cathodic active material, in long-lasting secondary galvanic cells with high performances [20]. The PA synthesized after Shirakawa *et al.*, [21] in the form of silvery films by direct polymerization of C_2H_2 on the surface of concentrated soluble catalyst solution consists of an interwoven network of ca. 200 Å $(CH)_x$ fibrils. The electrical conductivity can be varied over 12 orders of magnitude by suitable doping (oxidation/reduction). The film is very stable chemically and has an absorption coefficient over $10^5\ cm^{-1}$ (visible).

The oxidation/reduction (doping) reactions are: at the anode: $(CH)_x + xy\ ClO_4^- \rightarrow [(CH)^{y+}(ClO_4)_y]_x + xye^-$ and the cathode: $(CH)_x + xyLi^+ + xye^- \rightarrow [Li_y^+(CH)^{-y}]_x$. The extent of doping is calculated by taking into account the weight of the PA film and the number of coulombs used.

The battery is shown in fig. 12 [20] and the variations of the conductivities and the activation energy of the conductivity of the PA doped films are presented in fig. 13 [20]. The effect of the charge/discharge cycles number upon the cell voltage is shown in fig. 14 [20]. The discharge capacity and coulombic efficiency of *n*-PA/1 M $LiClO_4$, PC/*p*-PA battery charged at various

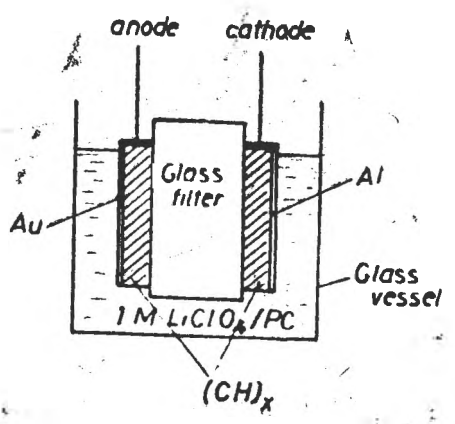

Fig. 12. Scheme of the *n*-$(CH)_x$/1 M $LiClO_4$ + + PC/*p*-$(CH)_x$ battery.

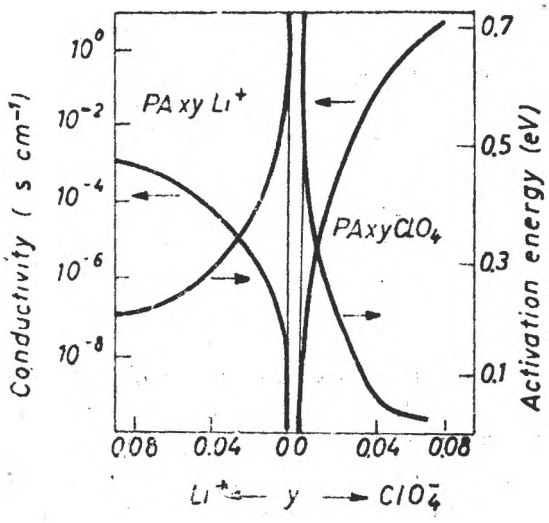

Fig. 13. Variation of the conductivity and of the activation energy for electric conduction of doped PA films, as a function of the dopant concentration.

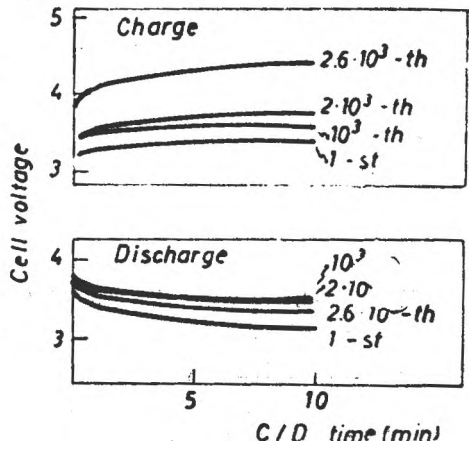

Fig. 14. Charge/discharge cycles of *n*-PA/1 M $LiClO_4$ — PC/*p*-PA battery. Charge conditions: 0.1 mA, 10 min, 0.06 C; discharge conditions: 50 kΩ, 10 min, 0.042 C.

charge capacities si represented in fig. 15 [20]. The operation temperature of PA battery depends on the solvent employed (fig. 16 [20]). Because the permitivity of the mixture 20% PC + EC is larger than that of the PC, the conductivity of the electrolyte solution (1 M $LiClO_4$) is higher in the mixture than in PC alone and thus the mixture is superior.

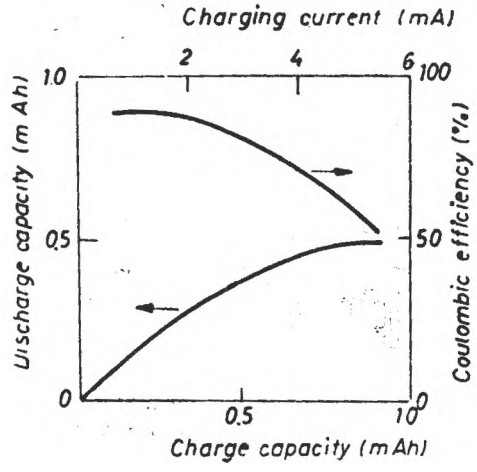

Fig. 15. Discharge capacity and coulombic efficiency of *n*-*pa*/1 M $LiClO_4$ — PC/*p*-PA battery; charging time: 10 min; discharge: constant resistance load: 560 Ω.

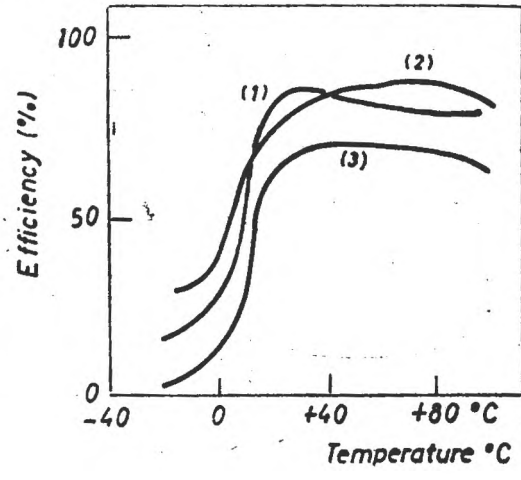

Fig. 16. Temperature dependence of current efficiency (1) voltage efficiency (2) and power efficiency (3) of *n*-PA/1 M $LiClO_4$, 20% PC+EC/*p*-PA; current density of charge: 50 μA/cm², time of charge: 10 min, discharge resistance: 33 kΩ.

Table 4

Physical properties of some nitriles

Nitrile	Boiling point (°C)	Melting point (°C)	DC(25°C)
Acetonitrile	81.6	−43.8	37.5
Benzonitrile	190.7	−12.9	75.2
m-Tolunitrile	200	−23	—

Kobayashi *et al.* [22] found that acetonitrile (AN) and benzenitrile (BN) are suitable solvents for the non-aqueous PA/PA battery, because of their capacity to solve tetraalkylammonium salts (TAAS) thereby ensuring a high ionic conductivity of the solutions, and a wide electrochemical stability range. AN has a better dielectric constant, but BN exhibited a better chemical stability with polyacetylene, and thus better performances. The table 4 [22] shows some physical characteristics of AN and BN, and fig. 17 presents the variation of the ionic conductivity of the various TAAS solutions used in the test battery (fig. 18) [22]. The battery performances for 3 types of PA (film, gel and powder) were compared (table 5 [22]).

The effect of concentration of the electrolyte solution, of the operation temperature and of the conductivity of electrolyte solutions on cell performance are shown in table 5, 6 and 7, respectively [22]. Figure 19 [22] shows the effect of the kinds of electrolyte solution on battery performance.

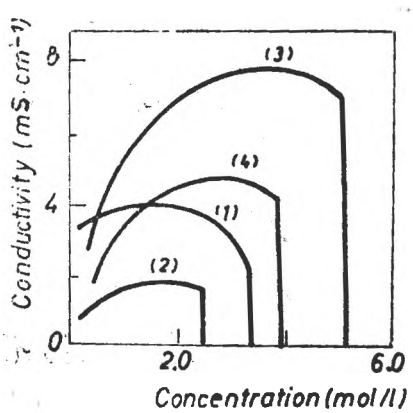

Fig. 17. Concentration of various TAAS *vs.* conductivity.
(1): Bu_4NBF_4 in BN; (2): Bu_4NBF_4 in *m*-TN; (3): Et_3BuNBF_4 in BN; (4): Et_3BuNBF_4 in *m*-TN.

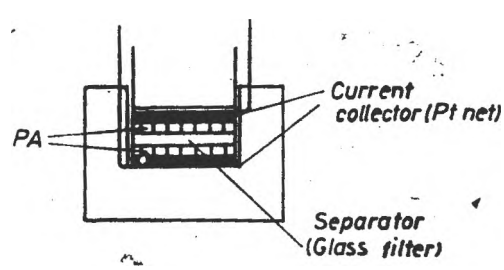

Fig. 18. Cyclindrical test cell (inner Ø = 9 mm).

Table 5

Effect of type of PA on battery performance (electrolyte: 1 M Bu_4NBF_4 in BN)

PA type	Bulk density (g/cm^3)	Thickness (μm)	Cycle life (nr.)	Self discharge (%, 15 hrs)
Film	0.35	180	118	38.2
Gel	0.36	220	158	21.3
Powder	0.33	250	133	22.8

Table 6

Effect of concentration of salt in electrolyte solution on battery performance

Electrolyte	Conductivity (mS/cm)	Cycle life (nr.)	Self discharge (%, 15 hrs)
1 M Et_3BuNBF_4/BN	5.1	107	36.5
3 M Et_3BuNBF_4/BN	7.5	123	26.1
5 M Et_3BuNBF_4/BN	7.2	119	23.8

Table 7

Effect of temperature on battery performance

Electrolyte	Cycle life (nr.)		Self discharge (%, 15 hrs)	
	20	−28 °C	20	−28 °C
1 M Et_4NBF_4/AN	66	106	52.1	18.0
1 M Bu_4NBF_4/BN	130	186	38.4	19.9
1 M Et_3BuNBF_4/BN	107	620	36.5	9.5

An all-plastic battery with polyacetylene and polymeric solid electrolyte (fig. 20) was studied by T. Nagatomo *et al.* [23, 24]. The polymeric solid electrolyte was prepared from PVDF, with $LiClO_4$ dispersed at molecular level. PVDF and $LiClO_4$ are dissolved in PC at 120 °C and the solution is poured into a metallic dish. The solid was obtained by evaporating a determined amount of PC, at 120 °C, in vacuum. The conductivity of the polymeric solid is dependent of the $LiClO_4$ content (fig. 21) [23]; the solid electrolyte used in the experiments of Nagatomo *et al.*, was of $\sim 3 \cdot 10^{-4}$ S cm^{-1} (20 mol% $LiClO_4$ in PVDF). The dopings of the PA film electrodes with ClO_4^- and Li^+, respectively, were performed by attaching the film to the positive and negative terminal, respectively, of a d.c. power source. All experiments were carried out in

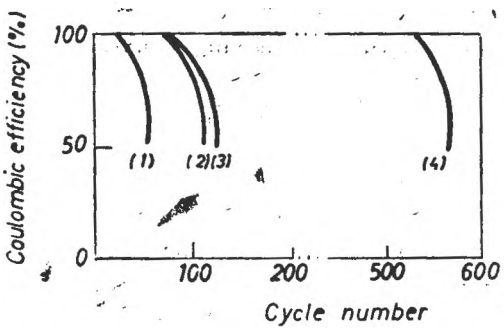

Fig. 19. Effect of kinds of electrolytes on battery performance.
(1): Me_3BuNBF_4/AN; (2): Et_3BuNBF_4/BN; (3): $Me_3(Hep)NBF_4$/BN; (4): Et_3BuNBF_4/BN. Cut-off voltage: O V.

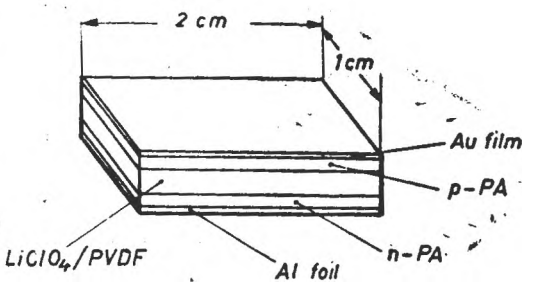

Fig. 20. Schematic diagram of rechargeable polyacetylene battery using as electrolyte a polymeric solid film of polyvinylidene fluoride which incorporates $LiClO_4$/PC.

argon atmosphere (absence of air and moisture). The charge/discharge characteristics are shown in fig. 22 [23] and the variation of coulombic efficiencies with the number of the cycles is represented in fig. 23 [23]; the very low value, down to ~30 cycles, may be attributed to the insufficient doping of the PA-film and the low (~50%) coulombic efficiency may have several origins: the solid electrolyte has an insufficient doping level (this was shallow: $y = 0.001$, even after 50 succesive charge/discharge cycles); the adhesion between PA and the polymeric solid electrolyte is not very good.

The experimental energy density of 6.5 Wh/kg (at a stored charge of 0.12 C, doping level $y = 0.004$), and the maximum power density of ~1.1 kW/kg (cell voltage of 3.4 V short-circuit current of ~10 mA) make this battery slightly superior to the PA/PEO, NaI/PA all plastic battery [25].

The PA/PVDF, $LiClO_4$, PC/PA, all plastic battery may serve as a small power source for low current electronic devices, but its development involves some problems to be solved (conductivity of the solid electrolyte, the adhesion between PA film and solid electrolyte etc.).

Table 8

Effect of conductivity of electrolyte on performance of gel-PA-cell

Electrolyte	Conductivity (mS/cm)	Cycle life (nr.)	Self discharge (%, 15 hrs)
1 M Bu_4NBF_4/BN	2.9	118	21.3
2 M Bu_4NBF_4/BN	4.0	132	16.9
1 M Et_3BuNBF_4/BN	5.1	143	16.0
5 M Et_3BuNBF_4/BN	7.2	165	12.1

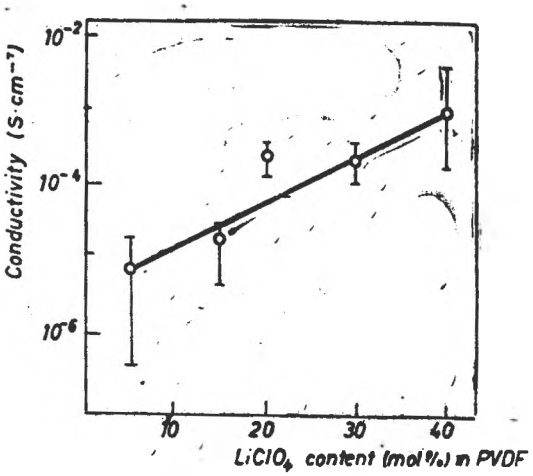

Fig. 21. The conductivity of polymeric solid electrolyte (PVDF—$LiClO_4$—PC) as a function of $LiClO_4$ content.

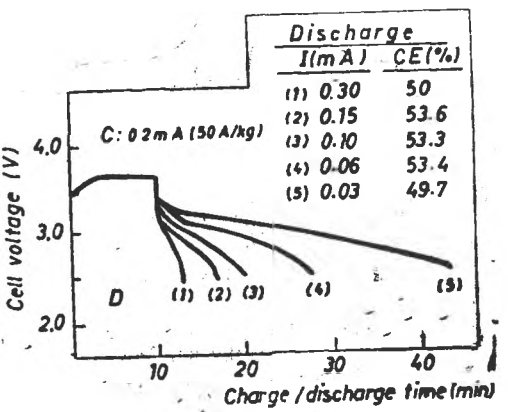

Fig. 22. Charge/discharge characteristics for *n*-PA/PVDF, $LiClO_4$, PC/*p*-PA cell. CE: coulombic efficiency.

Nagatomo *et al.* [26] found significant differences hetween the charge/discharge (C/D) characteristics of the large-scale PA battery (having 27 cm² area of electrode) and that of 2 cm² battery; a *n*-PA/$LiClO_4$, PC/*p*-PA galvanic cell was investigated. The number of the C/D cycles was 2600, with a low doping level (y = 0.002) and a maximum energy density of 424 Wh/kg was obtained. Those performances were observed with both electrodes, having a weight of ~8 mg and small surface electrode: 2 cm².

Fig. 24 [26] shows the scheme of the stacked type PA battery; the PA film had the thickness of 50—100 μm and area the of 27 cm² (3 cm × 9 cm).

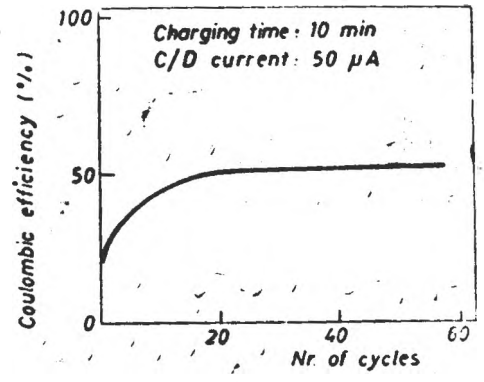

Fig. 23. Coulombic efficiencies of the C/D cycle of *n*-PA/PVDF, $LiClO_4$, PC/*p*-PA cell.

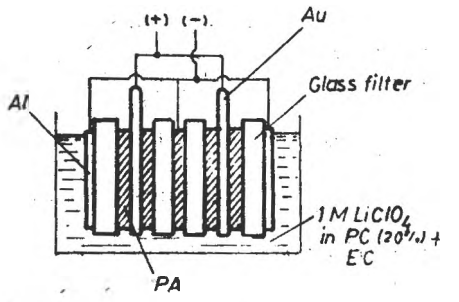

Fig. 24. Scheme of stacked-type polyacetylene battery *p*-PA/$LiClO_4$ + PC (20%) + + EC/Al. (Au (thickness ~ 10^3 Å) had been evaporated on one side of PA.

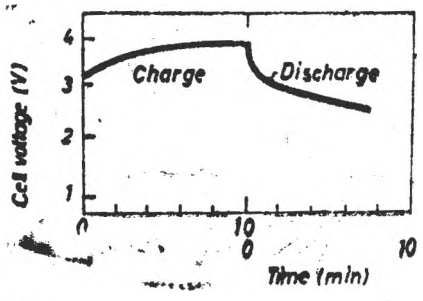

Fig. 25. Charge/discharge characteristics of stacked-type p-PA/$LiClO_4$ + PC (20%) + EC/Al battery (cathode area 27 cm^2).
$I_C = I_D = 40$ mA (212 Ah/kg for 10 min; doping level: 1,7%).

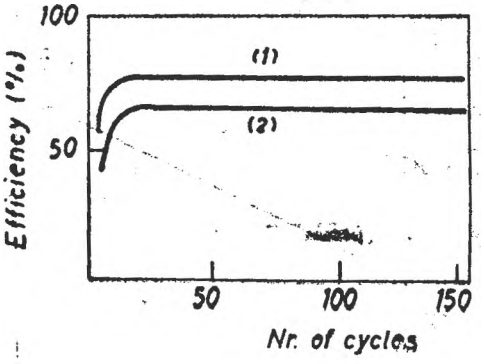

Fig. 26. Coulombic (1) and power (2) efficiencies of the C/D cycles of the stacked-type (4 cells) p-PA/$LiClO_4$ + PC (20%) + EC/Al battery (cathode area 27 cm^2). $I_C = I_D = 20$ mA (106 Ah/kg); $T_C = 10$ min.

The battery has 4 PA cathodes and 3 Al anodes, arranged in an alternating fashion. When attaching the PA film and the Al foil electrodes to the positive and negative poles, respectively, of a d.c. source (~3.8 V), the ClO_4^- ions penetrate the positive polarized electrode, and Li^+ ions are deposited on the negative one. The extent of doping (y) was calculated by taking into account the weight of the PA film and the number of coulombs passed. All experiments were varried out in the argon atmosphere (absence of moisture and air) and by using a 1 M $LiClO_4$ solution in a mixture of DC (20%) and EC. The C/D characteristics for the high electrode area (27 cm^2) battery (fig. 25 [26]) is not very different from that of the small electrode area (2 cm^2) battery. The coulombic and power efficiencies show for both lower values in the initial cycles (fig. 26 [26]), in the case of the stacked battery. The higher coulombic efficiency (~92%) for small area battery can be explained by the doping inhomogenity and the non-uniformity of the film thickness in the larger area electrode.

The most serious shortcoming of these batteries is the pronounced self-discharge (fig. 27) [26]. During the storage, the doped film becomes spontaneously undoped. The dopant diffuses into the interior of the PA fibrils and therefore its concentration decreases at the PA/electrolyte solution interface. Also, the dopant reacts with impurities from PA film and from the electrolyte solution. The conductivity is effected more in the low level doped film and less in higher doping level ones (fig. 27) [26].

The high voltage leads to the degradation of organic solvents used in polymeric batteries. Unfortunately, there is no proper organic solvent which is resistant against these high potentials; it has been proved that the decomposition of propylene carbonate occurs above 3.5 V. Another serious problems is the loss of mechanical stability in doped PA films. These films become very brittle upon doping and handling and the applying of stable electrical contacts to the polymer is quite difficult.

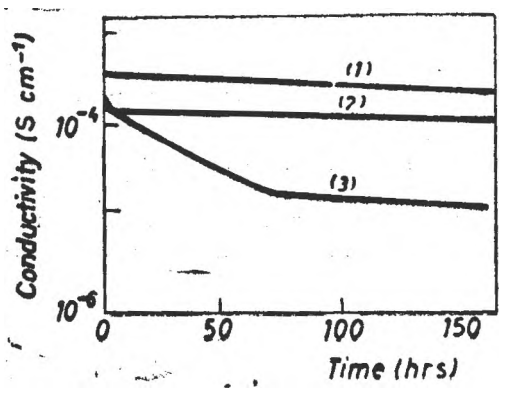

Fig. 27. Conductivity variation with time, for ClO_4^- ion doped PA film, in argon atmosphere. Doping level (1): 6%; (2): 4%; (3): 2%.

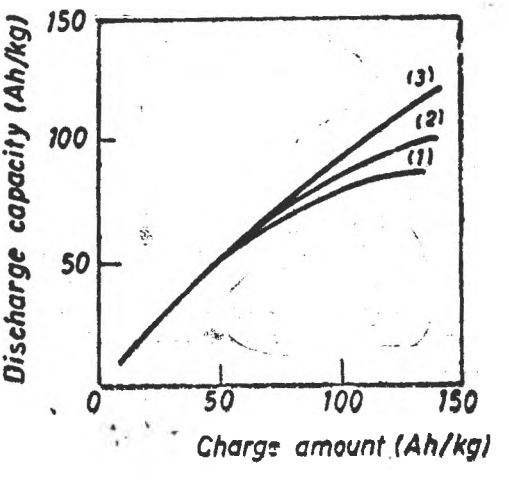

Fig. 28. Discharge capacity in various charge amounts as a parameter of polymerization current (i_p). (1): $i_p = 1$ mA/cm²; (2): $i_p = 5$ mA/cm²; (3): $i_p = 10$ mA/cm².

Studies carried out on PA films showed not only the oxidative, but also the thermal instability and the special handling conditions requires with this polymer. As an alternative to PA, the electrochemically polymerized poly(3-methylthiophene) (P3MT) was used as cathode in a secondary galvanic cell, having as electrolyte an 1 M $LiBF_4$/PC solution and as counter electrode a foil of aluminium [27]. Experimental energy densities of 326 Wh/kg, at a doping

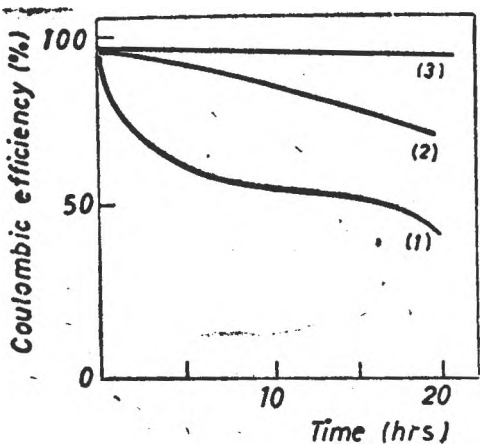

Fig. 29. Self discharge of 3 kinds of bat teries.
(1): PA/$LiClO_4$ + PC + EC/Al (2% doped);
(2): PT/$LiBF_4$ + PC/Al (7,6% doped);
(3): P3MT/$LiBF_4$ + PC + EC/Al (8% doped).

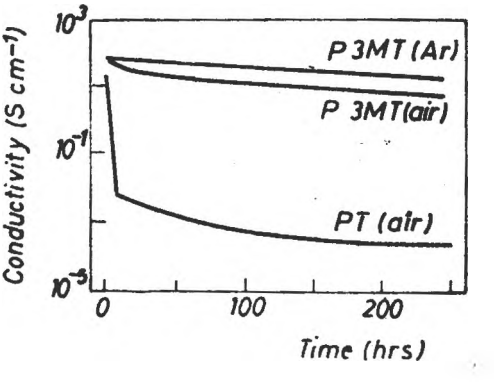

Fig. 30. Conductivity modifications of BF_4^- ion doped poly (3-methylthiophene) and polythiophene films in air and Ar atmosphere.

level of 38%, a discharge capacity of 97.3 Ah/kg and an average discharge voltage of 3.3 V were obtained. The coulombic efficiency was >96%, even after 1200 cycles, at a doping of 9%. The discharge characteristics (at charge amount >60 Ah/kg) depend on the polymerization current (fig. 28) and the self discharge is very small, in comparison with polythiophene and polyacetylene batteries (fig. 29) [27].

The small variation of the conductivity of the BF_4^- ions deped films (doping level ~30%) in air and in the Ar atmosphere, indicates the good stability of the electrochemically synthesized P3MT in the film structure (fig. 30) [27]. The study has shown the dependence of the surface morphology and physical properties of the polymerization current density; the most suitable was 10 mA/cm^2. These batteries have very good performance and a relatively small self-discharge.

3. *Conclusions*

A large variety of conductive polymers were studied in order to be used in secondary galvanic cells. Some of them have promising characteristics, but other require further developments for making them suitable for practical applications.

REFERENCES

1. A. G. Mac Diarmid, S. L. Mu, N. L. D. Somasivi, W. Wu, Ext. abstr., Electrochem. Soc. Fall Meeting, New Orleans, 1984, p. 906.
2. A. Diaz, K. K. Kanazawa, G. P. Gardini, *Chem. Commun*, **1979**, 635.
3. A. Kitani, M. Kaya, Y. Hiromoto, K. Sasaki; *Denki Kagaku*, **53**, 592, 1985.
4. F. Goto, K. Abe, K. Okabayashi, T. Yoshida, H. Morimoto, *J. Power Sources*, **20**, 243, 1987.
5. L. W. Shacklette, M. Maxfield, S. Gould, J. F. Wolf, T. R. Jow, R. H. Baughman, *Synthetic Metals*, **18**, 611, 1987.
6. H. Kuzmany, M. Mehring, S. Roth, eds., *Electronic Properties of Polymers and Related Compounds*, Springer, Berlin—Heidelberg—New York—Tokyo, 1985.
7. L. W. Shacklette, I. E. Toth, N. S. Murthy, R. H. Baughman, *J. Electrochem. Soc.*, **132**, 1529, 1985.
8. E. M. Genies, M. Lapkowski, C. Santier, E. Vieil, *Synthetic Metals*, **18**, 631, 1987.
9. G. Mengoli, M. M. Musiani, D. Pletcher, S. Valcher, *J. Appl. Electrochemystry*, **17**, 523, 1987.
10. G. Mengoli, M. M. Musiani, D. Pletcher, S. Valcher, *J. Appl. Electrochemistry*, **17**, 515, 1987.
11. B. Scrosati, S. Panero, P. Prosperi, *J. Power Sources*, **19**, 27, 1987.
12. A. Padula, B. Scrosati, *J. Power Sources*, **14**, 65, 1985.
13. G. C. Farington, B. Scrosati, D. Frydrych, J. De Nuzzio, *J. Electrochem. Soc.*, **131**, 7, 1984.
14. S. Marzilli, M. Patriarca, B. Scrosati, *J. Electrochem. Chem. Interfacial Electrochem.*, **191**, 147, 1985.
15. F. G. Will, *J. Electrochem. Soc.*, **132**, 2093, 1985.
16. F. G. *J. Electrochem. Soc.*, **132**, 2351, 1985.
17. J. H. Kaufmann, E. J. Mele, A. J. Heeger, H. Kaber, A. G. Mac Diarmid, *J. Electrochem. Soc.*, **130**, 571, 1983.
18. F. G. Will, *J. Electrochem. Soc.*, **132**, 743, 1985.
19. A. Corradini, M. Mastragostine, *Synthetic Metals*, **18**, 625, 1987.

20. T. Nagamoto, K. Negishi, H. Kakehata, O. Omoto, Proceedings Symp. Adv. Battery Mater. Processes, 164-th Meeting of Electrochem. Soc., Washington DC., Oct., 1983, p. 1.
21. T. Ito, H. Shirakawa, S. Ikeda, *J. Polym. Sci., Polym. Chem. Ed.*, **12**, 11, 1974.
22. Y. Kobayashi, T. Shishikura, H. Nakamura, H. Konuma. *Synthetic Metals*, **18**, 619, 1987.
23. T. Nagatome, H. Kakehata, C. Ichikawa, O. Omoto, *Jap. J. Appl. Physics*, **24**, (6), 1397, 1985.
24. T. Nagatomo, C. Ichikawa, O. Omoto, *J. Electrochem. Soc.*, **134**, (2), 1987.
25. C. K. Chiang, *Polymer*, **22**, 1454, 1981.
26. T. Nagatomo, C. Ichikawa, O. Omoto, *Synthetoc Metals*, **18**, 649, 1987.
27. T. Nagatomo, M. Mitsui, K. Matsutani, O. Omoto, *Trans. IECE, E* **70** (4) 346, 1987.

ABRBERVIATIONS

AN	: acetenitrile
BN	: benzonitrile
Bu	: butyl
C	: charge
C/D	: charge/discharge
CE	: coulombic efficiency (%)
CV	: cyclic voltymetry
D	: discharge
DC	: dielectric constant
DME	: dimethoxyethane
DOD	: depth-of-discharge
EC	: ethylene carbonate
Et	: ethyl
Hep	: heptyl
HNE	: hydrogen normal electrode
Me	: methyl
OCP/OCV	: open circuit potential/open circuit voltage
PA	: polyacetylene
PAN	: polyaniline
PC	: propylene carbonate
PDTT	: polydithienothiophene
PEO	: polyethyleneoxide
P3MT	: poly (3-methylthiophene)
PPh	: polyphenylene
PPhQ	: poly (phenylquinoline)
PPy	: polypyrrole
PT	: polythiophene
PTT	: polythienothiophene
PVDF	: polyvinylidene fluoride
QAS	: quaternary ammonium salt
RVC	: reticulated vitreous carbon
SC	: specific capacity (Ah/kg)
SCE	: saturated calomel electrode
TAAS	: tetraalkylammonium salt
m-TN	: m-tolunitrile
y	: oxidation/reduction (doping) degree (%); nr. of charge/repeat unit

RECENZII

S. Petrescu V. Petrescu, **Metode şi modele în termodinamica tehnică**, Ed. Tehnică, Bucureşti, 1988, 268 p.

Lucrarea constituie o abordare originală a Termodinamicii Tehnice, ştiinţă de bază cu implicaţii de incontestabilă valoare în activitatea practică omenească, în general şi în cea de conversie a energiei, în particular. METODE ŞI MODELE ÎN TERMODINAMICA TEHNICĂ conţine 9 secţiuni şi o bogată listă bibliografică.

În *Introducere* (secţiunea întîi) se fixează contextul şi se motivează conţinutul cărţii, care se ocupă de metodele şi modelele termodinamicii tehnice. Astfel, cartea este continuarea altei lucrări aparţinînd soţilor Petrescu (Principiile Termodinamicii, Ed. Tehnică, Bucureşti, 1983) şi, la elaborarea ei, s-au urmărit sorgintea metodelor/modelelor, justificarea lor logică şi epistemologică şi validarea lor practică.

Secţiunea a 2-a este consacrată aspectelor metodice în termodinamică, prezentîndu-se diverse scheme, cu comentarii pertinente, referitoare la destinaţia (localizarea), extinderea şi utilizarea unei metode sau a alteia.

Procesul de cunoaştere în termodinamica fenomenologică se tratează în secţiunea a 3-a. Pornind de la faptul că ştiinţa are o structură de tip reţea şi de la schema de abordare interacţională a sistemelor mecanice, subliniind rolul modelelor în termodinamică, legăturile lor cu metodele termodinamicii şi valoarea axiomatizării, se ajunge la examinarea structurii termodinamicii, la clasificarea metodelor ei şi la sfera de cuprindere a termodinamicii.

În secţiunea a 4-a se subliniază (sesizează) abordarea sistemic interacţională în termodinamica fenomenologică, menţionîndu-se că apariţia lucrării în discuţie este asociată cu încercarea de utilizare sistematică a noţiunilor de bază din termodinamica fizică, chimică şi tehnică cu concepţia care le leagă între ele.

Secţiunea a 5-a conţine consideraţii referitoare la termodinamica fundamentală şi la ramurile ei practice (termodinamica fizică, termodinamica chimică şi termodinamica tehnică), precum şi la metodele proprii de cercetare, de tratare şi de aplicare ale acestora. În centrul discuţiei se plasează cele 3 principii ale termodinamicii, formulările acestora şi o serie de consecinţe avînd interes teoretic şi practic.

Modelele utilizate pentru deducerea şi explicarea ecuaţiilor de stare sînt tratate în secţiunea a 6-a. Principalele concluzii care se degajă din considerarea ecuaţiilor termice de stare sînt următoarele: ecuaţiile de stare derivă din principiul zero al termodinamicii; modelul fizic utilizat la ecuaţia de stare a gazelor perfecte este ideal, reflectînd o stare limită a gazelor reale; inexistenţa vreunei ecuaţii de stare termice pentru un gaz real, capabilă să acopere un domeniu mai larg de presiuni şi temperaturi: ecuaţiile propuse reprezintă modele matematice aproximative; tehnica de calcul contemporană permite exprimarea şi calcularea ecuaţiilor de stare sub formă de serii de puteri, avînd pînă la 100 de termeni, obţinîndu-se precizii foarte bune.

În secţiunea a 7-a metodele de tratare şi metodele aferente principiului conservării şi transformării energiei se judecă prin prisma semnificaţiei noţiunilor de entalpie şi de lucru mecanic tehnic. Conţinutul secţiunii şi modul mai puţin convenţional de tratare a lucrurilor se justifică prin „implicaţiile conceptuale şi cantitative ale principiului întîi în întreaga termodinamică (fizică, chimică şi tehnică)". Autorii consideră esenţial principiul întîi pentru tot ceea ce este legat de modele şi metode în termodinamică.

În secţiunea a 8-a principiul întîi se prezintă pentru tipurile de sisteme închise, lărgite (deschise/închise/deschise) şi deschise, într-o concepţie sistemic-interacţional-cauzală, unitară. Se comentează cele 4 tipuri de metode de analiză energetică (metode de abordare pentru găsirea expresiilor „generale" ale principiului I; metode pentru particularizarea expresiilor generale ale principiului I şi metode de cercetare teoretică şi metode de cercetare experimentală, acordîndu-se atenţie primelor două.

Cea din urmă secţiune, a 9-a, trece în revistă, succint, rolul şi esenţa metodelor utilizate în termodinamică.

METODE ŞI MODELE ÎN TERMODINAMICA TEHNICĂ este o lucrare originală, nemaiîntîlnită în literatura de specialitate din ţara noastră şi poate fi de folos atît cadrelor didactice din învăţămîntul superior, profilurile Chimie, Fizică şi Termotehnică, cît şi specialiştilor din cercetare şi producţie. Poate fi consultată şi de cadrele didactice din învăţămîntul liceal, deoarece oferă imagini şi interpretări preţioase pentru înţelegerea fenomenelor co-

mentate în manualul de chimie al clasei a XI-şi în cel de fizică predat în clasa a X-a.

Materialul informativ consultat este bogat (289 surse bibliografice), reprezentativ, critic preluat şi minuţios analizat. Sursele bibliografice acoperă o perioadă de timp extrem de întinsă, aparţinînd începuturilor termodinamicii, dar şi perioadei contemporane. Sînt deosebit de sugestive, judicios întocmite şi deci foarte funcţionale diversele scheme referitoare la legăturile dintre teorie şi experiment, la aplicarea metodelor utilizate în termodinamica moleculară şi fenomenologică, la obiectul termodinamicii, domeniile termodinamicii şi interacţiunea cu alte discipline, la corelarea principiilor cu metodele termodinamicii fenomenologice etc.

Este vrednică de menţiune specială, evidenţierea contribuţiilor româneşti la întregirea conţinutului teoretic şi experimental al sferei termodinamicii (chimice, fizice şi tehnice). De asemenea, merită atenţie surprinderea momentului istoric în care a pătruns în literatura de specialitate din România, noţiunea de entalpie.

Comentariile care însoţesc fiecare secţiune a cărţii, concluziile trase şi mulţinea corelărilor cresc valoarea lucrării, argumentînd convingător originalitatea ei. Imaginile sînt clare, iar evocările diverselor etape istorice în evoluţia termodinamicii sînt pertinente şi au legătură cu contextul. Legătura dintre teorie şi practică este pregnantă, una fiind justificarea celeilalte. Se subliniază stimularea reciprocă a teoriei şi a practicii în dezvoltarea generală a termodinamici şi efectele esenţiale înregistrate în perfecţionarea tehnologică a activităţii creatoare omeneşti.

Rod al unor frămîntări de aproape 3 decenii, lucrarea în discuţie marchează un eveniment demn de remarcat în activitatea ştiinţifică românească, constituind un valoros ghid pentru „ieşirea din labirintul termodinamicii".

Stilul îngrijit şi fluent, în bun acord cu conţinutul, fac lectura cărţii agreabilă, pe alocuri de-a dreptul captivantă. Consider reuşită şi pe deplin onorată tentativa autorilor de-a pune la îndemîna specialiştilor o lucrare conţinînd interpretări şi precizări într-o disciplină de bază extrem de importantă pentru multe domenii de activitatea creatoare.

L. ONICIU

CRONICA

Participări la manifestări științifice internaționale

● La a 6-a Conferință Internațională de ința Coloizilor și a Suprafețelor ce a avut între 5—10 iunie 1988 la Hakone în Japo-, Maria Tomoaia—Cotișel, J. Zsakó, E. Chi- M. Nakagaki au trimis lucrarea *Molecular semblies in Lipid Carotenoid Monolayers* (pre-ıtată de M. Nakagaki)

● La cea de-a 8-a Conferință de Spectros-pie a R. S. Cehoslovacia care a avut loc în- 6—14 iunie 1988 la Česke Budějovice, Emil rdoș a prezentat lucrarea *Un spectrometru venţial cu plasmă cuplată inductiv.*

● La al 4-lea Simpozion Internațional „E-ctul staniului asupra celulei tumorale" din iulie—3 august 1988 de la Scranton, Penn-lvania, SUA, Ionel Haiduc a prezentat con-rința plenară *Compuși anorganici cu acțiune ıtitumorală.*

I. Haiduc, Carmen Socaciu și C. Silvestru au ırticipat cu comunicarea *Ditiofosfinați organo-ınici, sinteză, structură, activitate biologică.*

● La al 5-lea Simpozion Internațional de ıimia Ciclurilor Anorganice din 5—7 august 88 de la Amherst, Massachusetts, SUA, a ırticipat Ionel Haiduc.

● La Simpozionul National de Biofizică u participare internațională) de la București— ırtea de Argeș din 20—25 august 1988, E. Chi-, Maria Tomoaia-Cotișel, J. Zsakó, M. Sălă-n, Aurora Mocanu și P. T. Frangopol au par-cipat cu lucrarea *The Interaction of Gerovital ith the Monolayers of Stearic Acid and Cho-sterol at the Air/Water Interface.*

● La a 39-a Întîlnire a Societății Internațio-ale de Electrochimie de la Glasgow, Marea ritanie, din 9—15 septembrie 1988 au fost imise lucrările: *Saving Energy through Con-ol at Brine Electrolysis Cell* de L. Oniciu, S. gachi, P. Dobra (publicat în Extended Abs-acts of the 39th Meeting of ISE, p. 216)

Synergetic Effects in the Electroreduction of crylonitrile-Pyridine Systems, de L. Oniciu, Flo-ıntina Ciomoș, I. A. Silberg, și O. H. Oprea ibid. p. 112).

Propionitrile Electrosynthesis on F. c. c. Crys-ılline Structure Metals, de L. Oniciu, Maria itaru, D. A. Löwy și B. C. Toma (ibid p. 114).

● La al 6-lea Seminar privind studiul mate-ialelor și tehnologiile cosmice din programul *„Intercosmos"*, Brașov, 14—19 noiembrie 1988 . Chifu, I. Stan, Eugenia Gavrilă și Maria Tomoaia-Cortișel au prezentat lucrarea *Marangoni Motion and Mass Transfer on a Spherical Liquid-liquid Inerface in Microgravity Conditions.*

Participări la manifestări științifice naționale

Membrii Facultății de tehnologie chimică au participat cu lucrări la următoarele manifestări:

● A 8-a Consfătuire pe țară: Chimia Analitică și Controlul de Calitate, Craiova, 19—20 mai 1988.

● Al 3-lea Congres National de Chimie, București, 21—24 septembrie, 1988.

● A 4-a ediție a Simpozionului National de Inginerie Proceselor Chimice, Piatra-Neamț, 21—22 octombrie 1988.

● Sesiunea de comunicări științifice, Călimănești, octombrie 1988.

● Sesiunea jubiliară de comunicări științifice „Contribuția învățămîntului politehnic la dezvoltarea ramurilor de vîrf ale industriei din România", Iași, 10—12 noiembrie 1988.

● A 3-a Conferință Națională de Metalurgia Pulberilor, Cluj-Napoca, 10—12 noiembrie 1988.

● Zilele Academice Clujene, Cluj-Napoca, 21—26 noiembrie 1988.

● Săptămîna științei și tehnicii pentru tineret, Cluj-Napoca, 24—30 noiembrie 1988.

Publicări de tratate, cărți și cursuri universitare

N. Dulămiță, M. Fodoreanu, *Lucrări practice la Bazele tehnologiei chimice*, vol. I, ed. 2-a, Lito Univ. Cluj-Napoca, 1988.

Eugenia Gavrilă, I. Bâldea, V. A. Topan, S. Agachi, *Ingineria reactiilor chimice. Utilaje specifice.*, Lito Univ. Cluj-Napoca, 1988.

L. Oniciu, contribuții la *Enciclopedia de chimie* vol. 5 (DEU—DY), Ed. Științ. și enciclop. București, 1988.

Lucrări ştiinţifice apărute în reviste de specialitate din ţară şi străinătate

Maria Curtui, I. Haiduc, „Extracţia toriului şi a pământurilor rare cu acizi dialchilditiofosforici", *Rev. Chim (Bucureşti)*, **39**, 1099 (1988)

M. V. Diudea, B. Pârv, „Molecular Topology 3. A New Centric Connectivity Index (CCI), *Math. Chem.*, **23**, 65 (1988).

N. Dulămiţă, I. Hopârtean, L. Dulămiţă, „Reacţii redox în chimia organică II. Calculul coeficienţilor în ecuaţiile reacţiilor redox.", *Rev. fiz. chim.*, **25**, 375 (1988).

M. Sălăjan, J. Demeter-Vodnar, Eugenia Gavrilă, E. Chifu, „Studiul coalescenţei unei picături la o interfaţă lichid-lichid plană II. Drenajul şi ruperea filmului", *Rev. chim. (Bucureşti)*, **39**, 138 (1988).

V. Hurgoi, S. David-Mark, S. Mucichescu, S. Gocan, Simona Gocan, „Raţia optimă de proteine la prematur", *Pediatria (Bucureşti)*, **37**, 365 (1988).

Iovanca Haiduc, C. Crişan, S. Gocan, T. Hodişan, „Determinarea vitaminei K_3 prin metode cromatografice şi spectrofotometrice", *Rev. chim. (Bucureşti)*, **39**, 623 (1988) .

I. Hopârtean, N. Dulămiţă, „Reacţii redox în chimia organică I. Determinarea numerelor de oxidare ale atomilor în compuşii organici *Rev. fiz. chim.*, **25**, 299 (1988).

M. Horn, S. Mager, A. Orban, „Models for Tetrahedra of All Possible Point Group Symmetries", *J. Chem. Ed.*, **65**, 1073 (1988).

L. Literat, „Microstructura, compoziţia şi textura unor betoane uşoare cu granulit" (The Microstructure, Composition and Texture of Some Light Concretes with Granulite), *Materiale de Construcţii (Bucureşti)*, **18**, 89 (1988)

L. Literat, D. Vasilescu, „Suporturi de catalizatori pentru anhidridă ftalică", *Materiale de Construcţii (Bucureşti)*, **18**, 204 (1988)

Gh. Marcu, Livia Crivei, N. Pascu, „Recuperarea cuprului, zincului şi cadmiului din unele resurse secundare de materii prime", *Rev. chim. (Bucureşti)*, **39**, 133 (1088).

Gh. Marcu, Teodora Panea, Teodora Marcu, „Contribuţii în domeniul regulatorilor de creştere a plantelor", *Rev. chim. (Bucureşti)*, **39**, 1108 (1988).

L. Oniciu, „Deschideri ale tehnologiei electrochimice spre secolul al XXI-lea", *Rev. chim (Bucureşti)*, **39**, 616 (1988).

L. Oniciu, D. A. Löwy, Maria Jitaru, B. C. Toma, I. Bâldea, „Electrosinteza propionitrilului III. Aspecte cinetice ale reducerii electrochimice nedimerizante a acrilonitrilului la propionitril", *Rev. chim. (Bucureşti)*, **39**, 219 (1988).

L. Oniciu, D. A. Löwy, Maria Jitaru, „Electr synthesis of Propionitrile", *Bull. Electroche* **4**, 104 (1988).

L. Oniciu, D. A. Löwy, O. H. Oprea, I. A. S berg, „Studii structurale asupra membran lor schimbătoare de ioni obţinute prin fun ţionalizarea unor folii de polimer", *Mate le plastice (Bucureşti)*, **25**, 186 (1988).

O. Cozar, R. Semeniuc, V. Znamirovschi, I. H duc, „ESR and IR Studies of some Ox vanadium Dithiophosphonates", *Rev. Ro maine Phys.* **33**, 1131 (1988).

I. Silaghi-Dumitrescu, I. Haiduc, „Linear Ve sus Bent Bis (diphenylphosphine) iminiu Cations. A Molecular Orbital Discussion the Bonding in $[H_3PNH_3]^+$ and Relat Species.", *Rev. Roumanine Chim.* **33**, 1 (1988).

I. Silaghi-Dumitrescu, I. Haiduc, „Electron Structure and Bonding in Diamidoboro Cations. A Molecular Orbital Study $[H_3NBNH_2]^+$, *Rev. Roumaine Chim.*, **3** 851 (1988).

Maria Tomoaia-Cotişel, J. Zsako, A. Mocan E. Chifu, P. J. Quinn, „Monolayer Prope ties of Membrane Lipids of the Extrem Halophile Halobacterium Cutiruburm at th Air/Water Interface", *Biochim. Biophy. Acta.* **942**, 295 (1988).

Maria Tomoaia-Cotişel, E. Chifu, Aurora Moca nu, J. Zsako, M. Sălăjan, P. T. Fragopo „Srearic Acid Monolayers on Procaine Con taining Subphases", *Rev. Roumaine Biochem.* **25**, 227 (1988)

Cs. Juhos, E. Grünwald, Cs. Várhely, M. Har sanyi, J. Harsanyi, „Beobachtungen zum Verhalten von Zink bei der Abscheidun und Auflösung in schwach sauren Elektro lyten", *Galvanotechnik*, **79**, 99 (1988)

Cs. Juhos, E. Grünwald, Cs. Várhelyi, „Ein fluss der Temperatur auf die Löslichkei von Kupferanoden in cyanidischen Kup ferelektrolyten",*Galvanotechnik*, **79**, 1829 (1988

Z. Finta, J. Zsakó, Cs. Várhelyi, „Kinetics and Mechanism of Substitution Reactions o Complexes LIX. Influence of pH upon the Aquation Kinetics of Iodo-aquo-bis-dimethylglyoximato-Cobalt (III)", *Rev. Roumaine Chim.*, **33**, 263 (1988)

J. Zsakó, „Remarks on A New Equation for Modelling Nonisothermal Reactions" *J. Thermal. Anal.*, **43**, 1489 (1988).

V. Chioreanu, I. Panea, A. Donea, I. Cristea. I. Olteanu, B. Tserejamtsiin, M. Diudea, I. Hopârtean, V. Fărcăşan, „Aplicarea metodei difuzimetrice la testarea activităţii microbiostatice a unor compuşi organici", în *Contribuţii ale concepţiilor şi metodelor biochimi-*

ce în progresul științei", editat de Academia R.S.R., Filiala Cluj-Napoca, Cluj-Napoca, 1988, pag. 132.

Brevete

. Glück, Gh. Raita, Gh. Marcu, Iudita Glück, Marie Brie, Z. Paloșanu, I. Hircega, C. Vîrzob, Compoziție pentru curățarea suprafețelor sticloase, Brevet R.S.R. nr. 95.813 din 19. 05. 1988.

irginia Danciu, I. A. Silberg, O. H. Oprea, L. Oniciu, Metodă electrochimică de obținere a p,p'-diaminodibenzilului, Brevet R.S.R. nr. 94.517 din 1987 (acordat în 1988).

. Oniciu, Anca Pantea, Liana Mureșan, V. A. Topan, D. Gherțoiu, Procedeu de obținere a unor membrane schimbătoare de ioni, Brevet R.S.R. nr. 94943 din 1988.

Susțineri de teze de doctorat

zégeni Árpád-Attila, *Contribuții la studiul combinațiilor complexe ale reniului*, conducător științific: prof. dr. Gheorghe Marcu (14 ianuarie 1988).

Câmpean Eugen, *Contribuții la elucidarea mecanismelor reacțiilor ce au loc prin transfer de Co catalizate de carbonili metalici* conducător științific: prof. dr. doc. Maria Ionescu (22 aprilie 1988).

Feneșan Ioan, *Sinteza, structura și proprietățile fizico-chimice ale unor noi derivați ai acizilor amido-tiofosfinici, tiofosfonici, tiofosforici. Contribuții la elaborarea tehnologiei de sinteză a insecticidului Disulfoton*, conducător științific: prof. dr. doc. Maria Ionescu (8 iunie 1988)

Stănescu Liviu, *Studiul unor sisteme oxidice pe bază de* V_2O_5, conducător științific: prof. dr. doc. Ion Cădariu (2. iulie 1988).

Majdic Cornelia, *Valorificarea sintetică a unor acetofenonoxime, produși secundari la fabricarea de medicamente*, conducător științific: prof. dr. doc. Maria Ionescu (9 decembrie 1988).

ÎNTREPRINDEREA POLIGRAFICĂ CLUJ,
Municipiul Cluj, C-da nr. 601/1989

În cel de al XXXIV-lea an (1989), *Studia Universitatis Babes-Bolyai* apare în specialităţile

matematică
fizică
chimie
geologie-geografie
biologie
filosofie
ştiinţe economice
ştiinţe juridice
istorie
filologie

In the XXXIV-th year of its publication (1989) *Studia Universitatis Babes—Bolyai* is issued as follows:

mathematics
physics
chemistry
geology-geography
biology
philosophy
economic sciences
juridical sciences
history
philology

Dans sa XXXIV-e année (1989), *Studia Universitatis Babeş—Bolyai* paraît dans les spécialités

mathématiques
physique
chimie
géologie-géographie
biologie
philosophie
sciences économiques
sciences juridiques
histoire
philologie

Abonamentele se fac la oficiile poştale, prin factorii poştali şi prin difuzorii de presă, iar pentru străinătate prin „ROMPRESFILATELIA", sectorul export-import presă, P. O. Box 12—201, telex. 10 376 prsfir, Bucureşti, Calea Griviţei nr. 64—66.

Lei 35